

Study on durability and practicability of concrete bridge using carbon fiber reinforced plastic tendon

著者	グエン テ フエ
著者別表示	NGUYEN THI HUE
journal or publication title	博士論文本文Full
学位授与番号	13301甲第5131号
学位名	博士（工学）
学位授与年月日	2020-03-22
URL	http://hdl.handle.net/2297/00059762

doi: <https://doi.org/10.3151/jact.16.317>



Dissertation

Study on durability and practicability
of concrete bridge using carbon fiber
reinforced plastic tendon

炭素繊維強化プラスチック tendon を用いた
コンクリート橋梁の耐久性と実用性に関する研究

Graduate School of
Natural Science & Technology
Kanazawa University

Division of Environmental Design

Student ID No. 1724052004

Name: NGUYEN THI HUE

Chief advisor: Professor. HIROSHI MASUYA

Date of Submission: January 2020

Contents

Abstract.....	9
Chapter 1. Introduction.....	11
1.1 General introduction	11
1.2 Carbon fiber reinforced plastic	15
1.3 Literature review regarding the application of CFRP in bridge construction	18
1.4 Research Objective	20
1.5 The structure of the dissertation.....	22
References.....	24
Chapter 2. Load-carrying capacity and durability of prestressed concrete girder using CFRP tendons under long-term exposure in corrosive salt environment .	26
2.1 Introduction.....	26
2.2 Description of Shinmiya Bridge	28
2.3 Experimental method	31
2.4 Estimate of effective stress	32
2.4.1 Test method	32
2.4.2 Estimation results	33
2.5 Loading test.....	34
2.5.1 Test method	34
2.5.2 Results and discussion.....	35
2.6 Transfer length test	39
2.6.1 Test method	39
2.6.2 Results and discussions	41

2.7 Measurement of salt content	42
2.7.1 Test method	42
2.7.2 Results and discussion	43
2.8 Compression test of concrete	45
2.8.1 Collected the samples	45
2.8.2 Experimental result	45
2.9 Tensile test of CFRP	46
2.9.1 Collected the samples	46
2.9.2 Experimental results	47
2.10 Chemical analysis of CFRP tendon	47
2.10.1 FE-SEM observation	47
2.10.2 Fourier Transform Infrared Spectroscopy (FT-IR) Analysis	48
2.11 Conclusions	49
References	50
Chapter 3. Numerical analysis on the flexural behavior of the prestressed concrete girder using CFRP tendons	51
3.1 Introduction	51
3.2 Finite element model using LS-DYNA software	52
3.2.1 Overview of analysis	52
3.2.2 Method for prestressed in tendon	53
3.2.3 Material modelling	53
3.2.4 Contact and boundary conditions	57
3.2.5 The analysis method	57
3.2.6 Comparison between analytical and experimental results	57
3.2.7 Parametric study	59
3.3 Finite element model using DIANA software	61

3.3.1 Overview of this model	61
3.3.2 Material properties of concrete and steel	62
3.3.3 The analytical method	64
3.3.4 Comparison between analytical and experimental results	64
3.3.5 Parametric study	65
3.4 Conclusion	72
3.5 References	73
Chapter 4. Fundamental pull-out experiment for cast-in-place joint of precast concrete slabs reinforced by CFRP	74
4.1 Introduction	74
4.2 The outline of fundamental pull-out experiment	76
4.3 The material of experiment	76
4.3.1 Concrete	77
4.3.2 CFRP diameter	78
4.3.3 The fixation length	78
4.3.4 The method using CFRP in joint part	79
4.4 The first experiment	80
4.4.1 The set-up of experiment	80
4.4.2 The result of the first experiment	80
4.5 The second experiment	82
4.5.1 The set-up of experiment	82
4.5.2 The result of the second experiment	83
4.5.3 Bond stress	86
4.6 The third experiment	88
4.6.1 The set-up of experiment	88
4.6.2 The result of the third experiment	90

4.7 Conclusions.....	92
4.8 References.....	93
Chapter 5. Conclusion and Recommendations.....	95
5.1 Introduction.....	95
5.2 Summary	95
5.3 Conclusions and Observations	97
5.4 Recommendations for future work	99
ACKNOWLEDGEMENTS	101

List of Figures

Figure 1.1 Relationship between stress and strain of FRP and steel [3]	13
Figure 1.2 Amount of using FRP reinforcement in Japan	15
Figure 1.3 CFRP strand (top) and steel (bottom)	16
Figure 1.4 Cross section of steel (left) and CFRP strand (right) [19]	16
Figure 1.5 Structure of this dissertation	23
Figure 2.1 Shinmiya Bridge - October 2017	27
Figure 2.2 Side view (mountain side) of Shinmiya Bridge	29
Figure 2.3 Cross-section of Shinmiya Bridge (unit: mm)	29
Figure 2.4 Cross-section of main girder (unit: mm)	29
Figure 2.5 The mountain girder after removing from the site	30
Figure 2.6 The flow chart of research	31
Figure 2.7 Measurement position	33
Figure 2.8 The setup of experiment	35
Figure 2.9 The setup of loading test	35
Figure 2.10 Measurement positions (unit: mm)	35
Figure 2.11 Girder specimen before test	34
Figure 2.12 Girder specimen at failure	36
Figure 2.13 Crack pattern after loading test	36
Figure 2.14 Load-displacement relationship at the center of the girder	37
Figure 2.15 Status of CFRP in compression and tension zone at failure	36
Figure 2.16 Load-strain relationship of concrete	38
Figure 2.17 The neutral axis depth	38
Figure 2.18 Setup of transfer length test	40
Figure 2.19 The ½ girder before and after cutting flanges	40
Figure 2.20 Changes in transfer length in web	41
Figure 2.21 The method collecting the cores	42
Figure 2.22 Chloride ion concentration on web of main girder	43
Figure 2.23 Chloride ion concentration on the lower flange of main girder	43
Figure 2.24 Setup the compressive experiment	45

Figure 2.25 CFRP after removed from the girder and prepare for the tensile test	46
Figure 2.26 Setup the tensile experiment of CFRP	46
Figure 2.27 CFRP surface and carbon fiber surface.....	48
Figure 2.28 Analysis result by FT-IR.....	48
Figure 3.1 Three-dimensional analysis model for mountainside girder in LS-DYNA.....	52
Figure 3.2 Stress-strain concrete behavior in LS-DYNA.....	55
Figure 3.3 Relationship between applied load and displacement.....	58
Figure 3.4 Deformation and strain situation in several stages of simulation	59
Figure 3.5 Relationship between applied load and middle-span deflection in case of prestressing decrease	60
Figure 3.6 Relationship between applied load and middle-span deflection in case of middle-span deflection in case of decrease of concrete strength	61
Figure 3.7 Three-dimensional (3D) analysis model for the CFRP girder in DIANA	62
Figure 3.8 Stress-strain curve for concrete in DIANA.....	63
Figure 3.9 Load-displacement relationship at the middle of span.....	64
Figure 3.10 Crack pattern due to loading test and DIANA predicted	65
Figure 3.11 Bond stress-slip relationship	68
Figure 3.12 FE-predicted the load-displacement relationships.....	68
Figure 4.1 Salt damage due to flying salinity in Hokuriku region	74
Figure 4.2 The cast- in-situ joint o precast concrete slabs reinforced by CFRP	75
Figure 4.3 The set-up of pull-out experiment.....	76
Figure 4.4 Cross-section size of the first, second, and third experiment.....	77
Figure 4.5 Three types of CFRP used at joint	79
Figure 4.6 Situation of specimens after the first experiment.....	81
Figure 4.7 Relationship between load and displacement of 10Ø group in the first experiment	81
Figure 4.8 Relationship between load and displacement of 15Ø group in the first experiment	82

Figure 4.9 Relationship between load and displacement of 20Ø group in the first experiment	82
Figure 4.10 Situation of specimens after the second experiment	83
Figure 4.11 Relationship between load and displacement of 10Ø group in the second experiment	84
Figure 4.12 Relationship between load and displacement of 15Ø group in the second experiment	84
Figure 4.13 Relationship between load and displacement of 20Ø group in the second experiment	84
Figure 4.14 Specimen of (Ø15.2-20Ø-F2) after test	86
Figure 4.15 Bond stress of specimens in the second experiment	87
Figure 4.16 Three lengths of tuft body	89
Figure 4.17 Polymer cement mortar filled inside tuft body (Fb-type)	89
Figure 4.18 The relationship between the pull-out load and the length of tuft body corresponding with Fa-type and Fb-type	90
Figure 4.19 Three lengths of tuft body	91
Figure 4.20 The relationship between the pull-out load and displacement corresponding with Fa-type and Fb-type	92

List of Tables

Table 1.1 New standard sepecification of CFCC.....	17
Table 1.2 Standard characteristics of CFCC	17
Table 2.1 Comparison of effective stress of design value and estimated value .	34
Table 2.2 Comparison of crack initiation load and ultimate load	37
Table 2.3 Results of compressive strength test of concrete.....	45
Table 2.4 Results of CFRP tensile test	47
Table 3.1 Material properties of numerical model	56
Table 3.2 Concrete properties for FE analyse	63
Table 3.3 Cases to parametric study	66
Table 4.1 Standard specification of compounding of concrete	77
Table 4.2 Standard specification of CFRP	78
Table 4.3 Size of specimens	79
Table 4.4 List of specimen number	80
Table 4.5 Summary of experimental results of the second experiment.....	85
Table 4.6 Summary of experimental results of the third experiment	85

Abstract

The history of Fiber Reinforced Plastics (FRP) application is about 40 years at most. Among the methods against the corrosion of steel reinforcement, FRP is considered a suitable as a new material that can replace conventional reinforcement, mitigate resists the steel corrosion, and improves the durability and serviceability. FRP has outstanding properties in comparing with conventional steel such as light weight, high tensile strength, high corrosion resistance, high fatigue characteristic, and low linear expansion. Carbon Fiber Reinforced Plastic (CFRP) has been studied as an alternative to steel in construction engineering to limit the deterioration due to salt damage. CFRP was applied in various constructions in the world including reinforcing construction, precast concrete, and bridge structures. The aim of this present study is to contribute more studies regarding the durability and practicability of concrete bridge using Carbon Fiber Reinforced Plastic (CFRP) tendon. With this purpose, this study focused on the experiments and numerical simulation for using CFRP in the girder and the cast-in-place joint of precast concrete slabs. One full-scale girder of Shinmiya Bridge, the first prestressed concrete bridge in Japan and the world used CFRP tendons in the main girders against salt damage, was brought to the laboratory after nearly 30 years of service in a corrosive environment. A series of experiments were conducted on this prestressed concrete girder. First, the effective stress was estimated using the stress release technique with a core incision, and the obtained value was compared with the design value. Next, the bending fracture experiment was carried out on the girder; the load-bearing capacity, the relationship between applied load and displacement, failure model, strain distribution and crack pattern were considered and evaluated. The transfer length of the prestressed girder, which obtained by recording a relationship between strains on the concrete girder surface versus the distance to the end of the girder before and after cutting the upper and lower flanges, was examined by using half of the girder after the flexural experiment. On the other half of the girder, the concrete cores were collected, the compressive strength test was conducted, and salt content was measured. Finally, the mechanical and chemical characteristics of the CFRP removed from the main girder were determined. From the results, the serviceability and durability of the girder were been confirmed, the suitability of using CFRP in the structural bridge was also clarified.

In addition, a numerical model was proposed to observe the behavior of a main prestressed concrete girder using a finite element analysis program called LS-DYNA and DIANA. The first model was built in LS-DYNA software. The accuracy of the model was evaluated by comparing the analysis result and experimental result including the load-bearing capacity, the relationship between applied load and displacement. Then, a parametric study considered the loss of prestress force and the decrease of the compressive concrete strength to the change of structural behavior. The second model was built by the commercial finite element software, DIANA. The method, which created directly the prestress force, and load control were used in this model to surmise the behavior of a prestressed concrete girder using the CFRP tendons. Moreover, parametric studies were conducted with the following objectives: to investigate the influence of the input data from the results of the CFRP tensile test and concrete compressive test on the results on the accuracy of the simulation; to determine the change in structural behavior with the modification of the material properties; and finally to study the model with or without the bond-slip model for contact between the CFRP and concrete.

The final work of this study is conducted three series of fundamental pull-out test for the cast-in-place joint of precast concrete slabs reinforced by CFRP. Experiments were performed with the difference in setup of specimens. Two diameters of CFRP were selected including Ø12.5 mm and Ø15.2 mm. Three types of fixation length were chosen in the relationship with CFRP diameter namely 10Ø, 15Ø, and 20Ø. In addition, straight type (S-type), no filling inside tuft body in non-twisted type (N-type) and filling inside tuft body in non-twisted type (F-type) also known as three methods using CFRP in joint. Final, the method using CFRP with a diameter of Ø15.2 mm, the fixation length of 15Ø, and F-type (filling inside tuft body) was proposed to apply in the precast concrete slabs and the cast-in-place joint to enhance the durability and shortest the width of joint.

Chapter 1. Introduction

1.1 General introduction

Corrosion of steel reinforcement caused by exposed the natural environment, especially the aggressive environmental conditions. The phenomenon is considered to be one of the main reason for the degradation of concrete structures. In the world, this problem consumes a larger amount of money to solve by repair method, maintenance and even new construction. The number was estimated approximately \$128 billion to repair and replace 54007 bridges (9.1% the total bridges) in the United States in 2006 due to structural degrading [1]. Therefore, it is a current required challenge that motivates scientist to study a new method, new material in term of more efficient, durable construction regarding cost, technical, serviceable life and long-term performance.

Epoxy-coated steel, stainless steel, cathode protection, and improved concrete quality have been studied. They are the methods for making the corrosion process slow. However, there are limits regarding efficiency, complexity and long-term durability.

Another approach is to find a new material that can replace the steel and bring the expected effectiveness. Fiber Reinforced Plastics (FRP), which is a composite material made of polymer matrix reinforced with fibers, have attracted the attention of scientists to research for addressing steel corrosion owing to their non-corrosive properties. In structural engineering, the lightweight of FRP not only reduces the weight of construction but also make convenience in transport and installation. In addition, FRP has a higher tensile strength in comparing with conventional steel. Therefore, the application FRP in construction engineering has an increasing trend from the late of 80's. Three commonly FRP are Aramid (AFRP), Glass (GFRP) and Carbon (CFRP). They can be fabricated in the various size and used in the concrete structure in plates, laminates, bars, cables and wraps form. However, FRP has some drawback in use, for example high cost, lack of design code, which are focusing on by researchers to solve in the applying FRP in civil engineering field. The detail of the main advantages and main disadvantage of using FRP in comparing with normal steel as follows.

Advantages of FRP in comparison with traditional steel

- High ratio of strength and high ratio of stiffness to mass density

The previous studies show that FRP has the higher strength in comparing with convention steel and the weight of FRP is lighter than steel [2]. Therefore, the strength-to-weight ratio improves remarkably, it is around 10 to 15 times larger than that of steel [3].

- High corrosion resistance

Because this characteristic, FRP is selected to replace conventional steel in structures or external application to upgrade the strength, especially the structures exposed in the salt damage environment. The serviceably of these structures using FRP was confirmed after long-term without maintenance request [4] [5].

- High electromagnetic transparency

FRP is a composite material so that FRP does not conduct electricity, it can be used for constructions located in areas obtained the risk of electric shock like footbridges in railway area [6].

- Light weight

FRP is lightweight, it is about 20% the density of steel in case of CFRP [7]. This feature can support the transport process to become convenient. In addition, the installation of structures using FRP becomes easier, the requirements related to machines or equipment are reduced. Furthermore, using FRP makes a significant decrease in the weight of structures that bring the benefits for construction, especially bridge construction.

- High fatigue characteristic

FRP has excellent fatigue performance, especially CFRP that the fatigue characteristic is superior to the steel strands [7] [8].

- Low linear expansion

Among three types of fiber, CFRP has lowest coefficient of linear expansion, it is about 1/20 of the steel [9] [10].

- Flexibility

The various in dimension, shape and type of FRP make it possible for FRP application in many different structures.

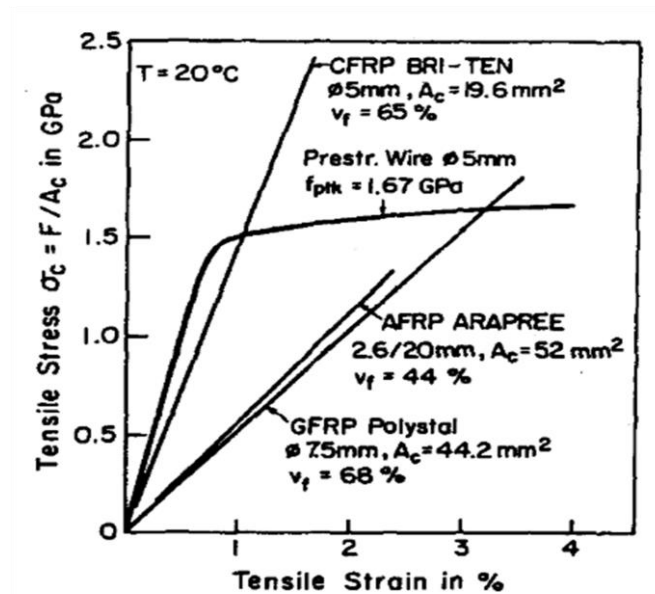


Figure 1.1 Relationship between stress and strain of FRP and steel [3]

Disadvantages of FRP in comparison with traditional steel

- Higher initial cost and uncertain long-term cost

FRP has the lightweight and high corrosion resistance; it can help a decrease in construction cost or a decrease in cost of transport and installation. However, the cost for material using FRP is higher of 5 to 50 times [3] than the cost of conventional steel. In addition, this is a new material that requires knowledge, training and new equipment in using, fabrication. Therefore, the initial cost of using FRP is higher than using convention steel.

Regarding the long-term cost, it concluded the maintenance cost, repair cost, replacement cost, etc...It is difficult to estimate accurately this cost because of various unpredictable costs and the lack of previous data.

Nowadays, technical and science is more development, the life-cycle cost including the initial cost and long-term cost becomes more important for construction project and an essential factor to evaluate the effectiveness of project.

- Lack of ductility

FRP is anisotropic whereas steel is isotropic. It lacks of ductility owing to stress-strain behavior is linear up to failure. The yield was not show in stress-strain behavior of FRP, which observed in regular steel. This characteristic creases a concern of a sudden

destruction of structure. The relationship between stress-strain of FRP, and steel were shown in *Figure 1.1*.

However, the researchers found the design method to structures using FRP to achieve a safe mode of failure that involved slow failure and larger deformation [6]

➤ Low fire resistance

Fire resistance is also a requirement for materials in many constructions. In comparing with steel, FRP has the index of fire resistance lower than that of traditional steel. Strength of FRP can begin loss in a low degree, such as 80°C for polyester. If there is a potential danger due to fire, considerable improvement of the behavior can be achieved using phenol matrices instead of polyester.

➤ Lack of design standard

FRP is a new material, and then it requires the investment for more studying regarding behavior of structures with FRP application. Those are fundamental for making codes, design standard that is necessary and support for engineering to design and apply in projects.

Japan, the United States and Canada are the few developed countries that currently have standards and codes for the application of FRP in construction engineering field.

➤ Uncertain durability

The durability of FRP and structures using FRP have been examined by numerous experiments. However, most of experiments were conducted in laboratory; they were not real structures and were not exposed in nature environment. In addition, the design life of a civil engineering structure is between 50 to 100 years. On the other hand, the application history of FRP is about 40 years at most, hence only a few of data are evidence for long-term serviceability and long-term quality of FRP and structure using FRP. This is an important factor for a comprehensive evaluation of the application of materials including technical, quality and cost.

The application of FRP for construction in Japan and in the world

Overall, the FRP application in construction divides two ways. The first way is used FRP to retrofit structures with external application. The second application is the use of FRP reinforcements instead of steel reinforcing bars or prestressing strands in concrete structures. This thesis focuses on the second way of using FRP.

FRP is considered suitable as a new material that can replace conventional reinforcement owing to the outstanding properties [3]. FRP was applied in girder, deck, column and beam of many bridges as well as other structures in develop countries including Japan, USA, Europe, Canada, etc.

Japan has the highest number of construction using FRP. Since 1980's the application of FRP in Japan has a significantly increase. It was applied for seismic construction, upgrading construction, and improving durability. *Figure 1.2* shows the statistics of using FRP reinforcement in Japan.

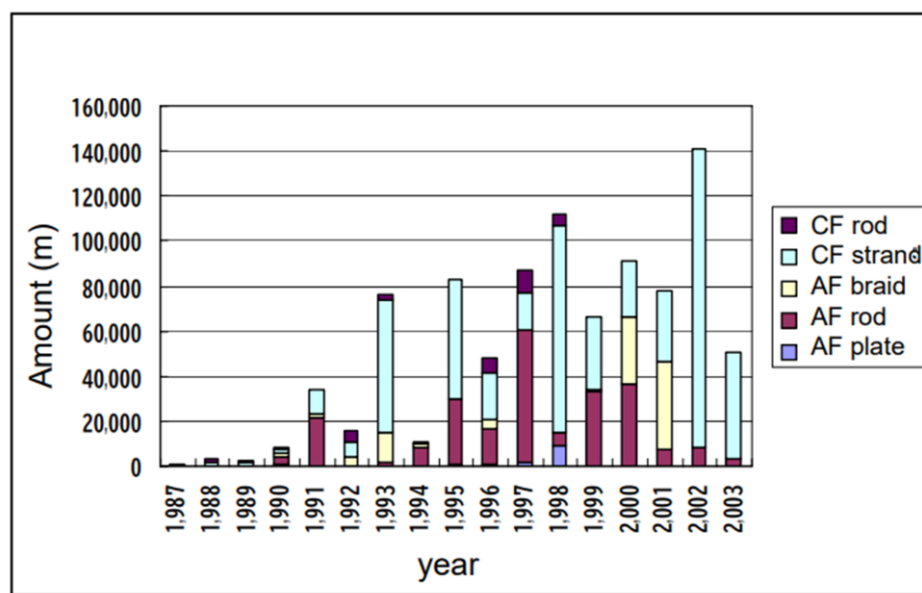


Figure 1.2 Amount of using FRP reinforcement in Japan
(Data source: ACC Club)

1.2 Carbon fiber reinforced plastic

Carbon fiber was made from poly-acrylonitrile (PAN-based) or pitch-based. It is a type of FRP so it fully involves the properties of this composite material. Among three types of FRP reinforcement, CFRP has the highest tensile modulus of elasticity. The form of CFRP reinforcement includes rod, tendon and rope. The modulus of elasticity of CFRP is about 65% or more of that of steel [3]. In addition, CFRP has excellent creep and fatigue resistance, low linear expansion coefficient and low stress relaxation. These characteristics are necessary for reducing the losses of prestressing force in tendons so CFRP was selected and developed to fabricate in the main form of tendon.

Several brands are available for CFRP prestressing tendons, namely Carbon Fiber Composite Cable (CFCC) of Tokyo Rope in Japan, Leadline of Mitsubishi Kasai of Japan, Jitec of Cousin Composites in France and Bri-Ten of British Ropes in England. *Figure 1.3* and *Figure 1.4* show the outside image and cross section of a standard steel strand and CFRP strand (CFCC).



Figure 1.3 CFRP strand (top) and steel (bottom)



Figure 1.4 Cross section of steel (left) and CFRP strand (right) [19]

CFCC of Tokyo Rope was made from carbon fiber of poly-acrylonitrile (PAN-based). The weight of CFCC is around 1/5 weight of steel strands. It contained the outstanding characteristic of high acid resistance, alkali resistance, and non-magnetic interact. The thermal coefficient of linear expansion is $0.6 \times 10^{-6}/^{\circ}\text{C}$, which is about 1/20 of the steel. The tensile strength and tensile elastic modulus of CFCC for type (1x7, $\varnothing 12.5$ mm) were 2.69 kN/mm^2 and 150 kN/mm^2 , respectively. CFCC was fabricated with various diameter from 5 to 50 mm and made from 1, 7, 19, or 37 wires in cross-section.

New standard specification of CFCC and standard characteristics were shown in *Table 1.1* and *Table 1.2*.

Table 1.1 New standard specification of CFCC

(Data source: Tokyo Rope)

New Standard specification of CFCC 標準仕様						
Designation (Configuration diameter) 呼称	Diameter 直径 (mm)	Effective cross sectional area 有効断面積 (mm ²)	Guaranteed capacity 保証破断荷重 (kN)	Nominal mass density* 単位長さ質量 (g/m)	Tensile elastic modulus* 弾性係数 (kN/mm ²)	
● U 5.0φ	5.0	15.2	38	30	167	
● 1×7 7.5φ	7.5	31.1	76	60	155	
	10.5	57.8	141	111	155	
	12.5	76.0	184	145	155	
	15.2	115.6	270	221	155	
	17.2	151.1	350	289	155	
● 1×19 20.5φ	20.5	206.2	316	410	137	
	25.5	304.7	467	606	137	
	28.5	401.0	594	777	137	
● 1×37 35.5φ	35.5	591.2	841	1,185	127	
	40.0	798.7	1,200	1,529	145	

*Reference value

Table 1.2 Standard characteristics of CFCC

(Data source: Tokyo Rope)

Standard characteristics 標準特性				TOKYO ROPE	
Properties 特性	Item 項目		1×7 12.5φ	Standard type 特性値	
General mechanical properties 一般機械特性	Tensile strength 引張強度	kN/mm ²	*1	2.69	
	Tensile elastic modulus 弾性係数	kN/mm ²	*1	155	
	Elongation at break 破断伸び	(%)		1.7	
	Specific gravity 比重			1.6	
Static properties 静的特性	Relaxation リラクセーション率	(%)	*2	1.3	
	Creep strain クリープひずみ		*3	0.07×10 ⁻³	
	Coefficient of linear expansion 線膨張係数	(×10 ⁻⁴ /°C)	*4	0.6	
	Specific resistance 比抵抗	(μΩcm)		3,000	
	Creep failure load ratio クリープ荷重比		*5	0.85	
Others その他	Fatigue capacity (Stress range) 疲労耐力 (応力範囲)	(N/mm ²)	*6	780	
	Bending stiffness 曲げ剛性	kN·cm ²		56.9	
	Heat resistance 耐熱性	(°C)		130	
	Acid resistance 耐酸性			Superior to steel スチールより優れている	
	Alkaline resistance 耐アルカリ性			Almost the same as steel スチールとほぼ同等	

*1: Calculated by Effective cross sections
 *2: 0.7pu, 1000hrs(20±2°C), according to JSCE-E534.
 *3: 0.6pu, 1000hrs(20±2°C)
 *4: 20°C~200°C, according to JSCE-E536.
 *5: Tests of CFCC 1×12.5φ according to JSCE-E533 "Test Method for Creep Failure of Continuous Fiber Reinforcing Materials" gave a load ratio of 0.85 at 1 million hours.
 *6: Average load is 75% of Guaranteed capacity. The number of cycles is 2×10⁶, according to JSCE-E535.
 pu: Guaranteed capacity

*1: 有効断面積で算出した値
 *2: 0.7pu, 1000hrs(20±2°C) JSCE-E534に準ずる
 *3: 0.6pu, 1000hrs(20±2°C)
 *4: 20°C~200°C JSCE-E536に準ずる
 *5: JSCE-E533「連続繊維補強材のクリープ破壊試験方法(案)」による試験結果100万時間後の荷重比
 *6: 平均応力は保証破断荷重の75% 繰返し回数/2×10⁶回 JSCE-E535に準ずる
 pu: 保証破断荷重

With outstanding characteristic, CFRP was applied widely in various constructions in building engineering such as reinforcing structures, using in concrete precast, application for bridge construction and other construction.

1.3 Literature review regarding the application of CFRP in bridge construction

Since the 1980s in Japan, Carbon-Fiber-Reinforced Plastic (CFRP) had been studied as an alternative to steel in civil engineering to combat deterioration due to salt damage [7]. Therefore, CFRP was selected as the tensioning material for the main girders of the new Shinmiya Bridge in October 1988. The new Shinmiya Bridge was the first prestressed concrete bridge in Japan and the world to utilize CFRP tendons against salt damage [11].

Subsequently, researchers across the globe took note of this technique and it began to be applied in a variety of structures in civil engineering. In November 1993, the Beddington Trail Bridge was built in Calgary, Alberta, Canada. CFRP tendons and Leadline strands were selected to prestress two spans of this bridge [12]. In 1997, Abdelrahman and Rizkalla in Canada conducted another study on the flexural behavior of concrete beams prestressed by CFRP reinforcement. In this study, T beams with 6.2 m in length and 0.33 m in depth were used, the CFRP bars had a diameter of 8 mm, and the tensile strength and elastic modulus were 1970 MPa and 147 GPa, respectively. While eight concrete beams were prestressed by CFRP bars, two beams were prestressed by regular steel strands for comparison. The observations of the different failure modes indicated deflection and cracks [13]. In the United States, the Bridge Street Bridge was built in Southfield, Michigan in 2001. It was the first bridge in the USA that used a CFRP tendon in the T beam. The deflections, concrete strains, CFRP and CFRP strains will be monitored until 2020 to record the long-term value [14]. The first CFRP application for a prestressed girder in the road bridge in Belgium was in 2004. Carbon-fiber polymer wires with a diameter of 5 mm, tensile strength of 2450 MPa, and Young's modulus of 160 GPa were chosen for a T beam [15]. In 2012, Enomoto et al. summarized the results of the structural bridges using CFRP and confirmed that CFRP were suitable for prestressed concrete bridges [16].

Furthermore, Grace et al. (2012) conducted a study about comparing the life-cycle cost analysis (LCCA) of the bridges using cathodic method, epoxy-coated method and using CFRP. The results of this study showed that the initial cost of CFRP was higher than the regular steel-reinforced bridges, but the life cycle cost of the prestressed concrete bridge using CFRP bars or strands was not high. The cost will become the least significant obstacle after 20–40 years of service time belong to traffic volume and bridge geometry. [17].

Therefore, recent studies on the usage of CFRP in a prestressed concrete structure focus on standards in design and durability in actual service. The Concrete Committee of the Japan Society of Civil Engineers established Research committee on Continuous Fiber Reinforcing Material (CFRM) in 1898. This organization was study the design method, construction methods, specifications and standard test method from 1993 to 1995. Recommendations for design and construction of concrete structures using continuous fibre reinforcing materials was published in Japanese in 1996 and translated in 1997 [7]. In the same time, one design guidelines has been developed and taken by the AIC Committee 440 in 1996 [18]. In 2015, a study analyzed a concrete beam prestressed with a CFRP tendon according to ACI 440.4R-04 and ISIS design manual No.5. The difference in the structural behavior between both codes was presented [19]. In 2016, Sevil Yaman conducted a series of experiments for CFRP application as a corrosion-resistant material in the prestressed precast concrete bridge for marine environments. T-Beam specimens (length of 3350 mm, height of 304.80 mm, flange width of 914.40mm and 304.80 mm in the web width) were analyzed and compared the results obtained using the ACI 318 Code prediction [20].

However, there were few findings to be confirmed regarding the durability of the bridge prestressed by CFRPs subjected to actual long-term salt damage. In 2017, Mark F.Green presented research on the durability of CFRPs for bridges over a long period in Canada. The strength and durability of a prestressed CFRP sheet and CFRP tendon over 13 years were confirmed [4]. In Shinmiya Bridge, the first prestressed concrete bridge in the world using CFRP tendons in the main girders, investigations to clarify the serviceability and durability of the main girders reinforced by CFRP tendons have been conducted from the time of construction. Three test girders were manufactured with the same size as the main girders in 1988. At the same time, one girder was used to perform

a flexural experiment to determine the ultimate behavior and load carrying capacity of the prestressed concrete girder [21] as well the deflection and the strain behavior of the CFRP [22]. Furthermore, two other girders (mountainside, seaside) were placed next to the main girders in the same conditions for confirming their long-term quality. Six years after the construction time (1994), a destructive test was carried out on the seaside girder, a comparison of load-carrying capacity with the results at the time of construction was done, and the durability of the CFRP tendon was confirmed [23].

1.4 Research Objective

The main object of this study is to study on durability and practicability of concrete bridge using Carbon Fiber Reinforced Plastic (CFRP) tendon.

The first object is to investigate and clarify the quality, durability of CFRP as well as the structure reinforced by CFRP after long-term service. One full-scale girder of Shinmiya Bridge was brought from the site after nearly 30 years of service in a corrosive environment. This girder was prestressed by eight CFRP tendons. A series of experiments were conducted on this prestressed concrete girder. Finally, the serviceability and durability of the girder were confirmed, the suitability of using CFRP in the structural bridge was also clarified.

In addition, an analytical model was developed by finite element method to understand deeply the flexural behavior in the prestressed concrete girder by CFRP tendons. Furthermore, parametric study using this model had been done to evaluate the change in structural behavior.

To develop the application of CFRP for the precast concrete slabs is the thirds object of this study. Series of investigation using CFRP for precast concrete slabs at the cast-in-place joint position were conducted. The aim of this investigation is to find the method to enhance the durability of the joint and reducing the width of the joint as short as possible. A lot of specimens were fabricated and three series of the fundamental pull-out experiment were performed. A method for joints of precast concrete slabs reinforced by CFRP was proposed for the application in a real structure.

The objective of this study can be summarized in the following points:

- To study the serviceability and durability of prestressed concrete girder using CFRP tendons after 30 years in a salt damage environment. This study was examined about the following factors:
 - Effective stress
 - Bending load
 - Transfer length
 - Salinity analysis
 - Compressive strength of concrete
 - Tensile strength of CFRP
 - Chemical analysis of CFRP
- A simulation model was developed for the analysis flexural behavior of the prestressed concrete girder using CFRP tendon via finite element method. The verification of the model was evaluated by comparing numerical result and experimental result including load-bearing capacity, the curve of applied load versus middle span deflection, and crack pattern. After the good agreement was be confirmed, the model is fundamental to consider the variables affected on the structural behavior by LS-DYNA and DIANA software such as:
 - Level of prestress force
 - Compressive strength of concrete
 - The input parameters for material card
 - Change of characteristic of main materials
 - The bond slip model
- To investigate the method for using CFRP in the cast-in-place joint of precast concrete slabs reinforced by CFRP via a series of experiments with the variation difference including:
 - Two types of CFRP diameter
 - Three types of the fixation length
 - Three method using CFRP in joint
 - Method filling inside tuft body

1.5 The structure of the dissertation

The dissertation presented in five chapters, the entire study is described roughly by structure shown in *Figure 1.5*.

Chapter 1 describes the backgrounds, previous studies, motivation and the objectives of this study.

Chapter 2 presents the series of the experiment conducted on the prestressed concrete girder using CFRP after 30 years exposed in the aggressive environment. The durability and serviceability of CFRP and the girder were confirmed. It is evidence for a suitable of application CFRP in bridge construction in long-term

Chapter 3 built the three-dimensional model of the prestressed concrete girder using CFRP tendons in software to bring a deeply understand regarding the flexural behavior of the girder. After the accuracy of the model was confirmed, the parametric study was examined on the fundamental model to evaluate the effect of some factors to the structural behavior that need to consider in future.

Chapter 4 focuses to investigate the method for using CFRP in the cast-in-place joint of precast concrete slabs reinforced by CFRP. A lot of specimens were conducted for the fundamental experiment. Final, one method was proposed to apply CFRP in precast concrete slabs and the joint position that can enhance the durability of joint and reduce the width of joint. This study encourages the development and application of CFRP in precast concrete slabs.

Chapter 5 is the summary for this study. Several conclusions were given to apply CFRP in bridge structures. In addition, recommendations for future work is considered.

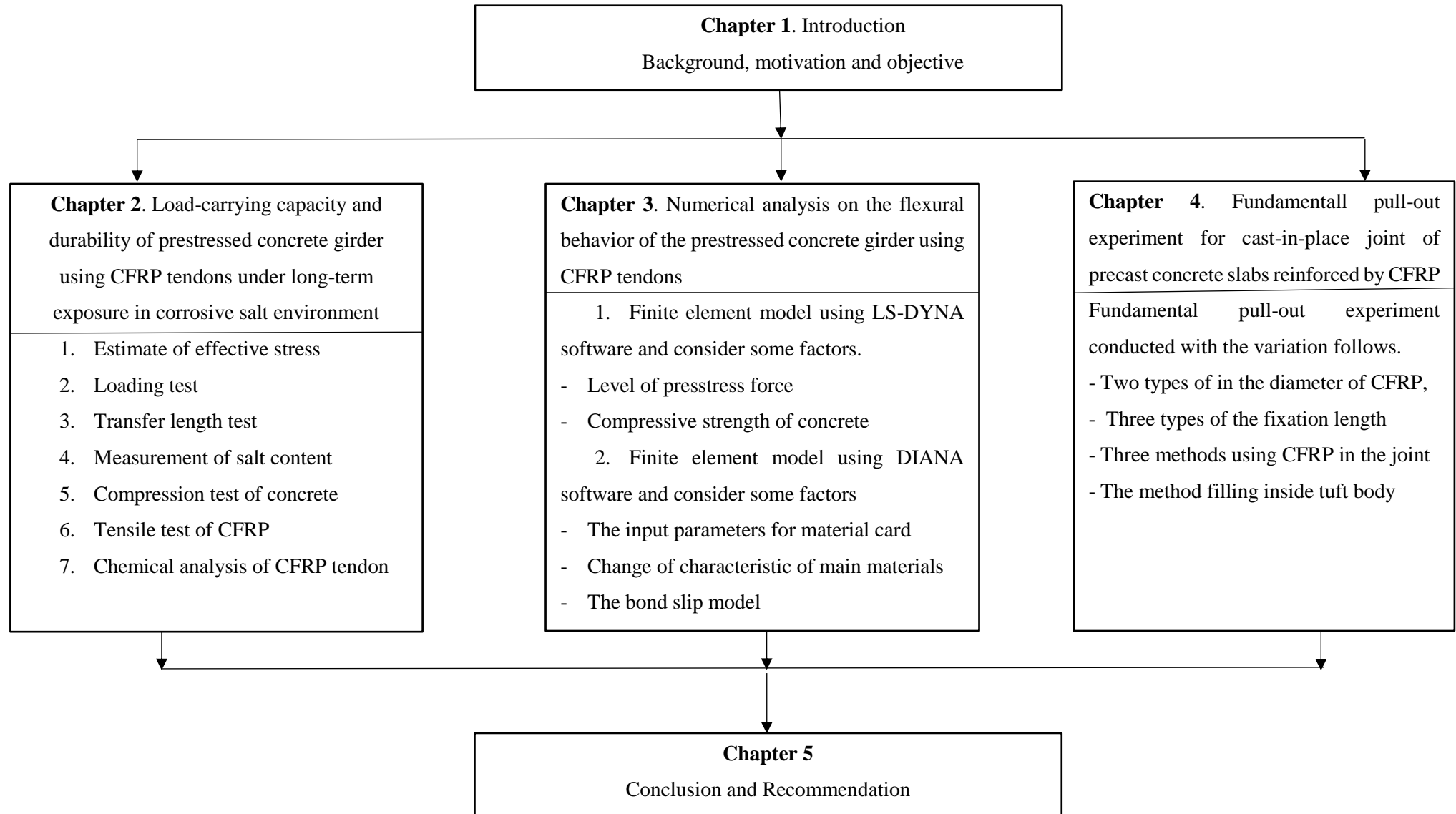


Figure 1.5 Structure of this dissertation

References

- [1] A. R. Emparanza, R. Kampmann, and F. De CasoBasalo, “State-of-The-practice of frp rebar global manufacturing,” *CAMX 2017 - Compos. Adv. Mater. Expo*, vol. 2017-Decem, no. September 2018, 2017.
- [2] C. Tuakta, “Use of Fiber Reinforced Polymer Composite in Bridge Structures ,” *Thesis*, Engineering at the Massachusetts institute of technology, 2005.
- [3] M. A. Erki and S. Rizkalla, “FRP Reinforcement For Concrete Structures,” *ACI Concrete International*, vol. 15 (6), pp. 48–53, 1993.
- [4] M. F.Green, “Long-term applications of CFRP prestressing in Canada,” *Fourth Conference on Smart Monitoring. Assessment and Rehabilitation of Civil Structures*, 2017.
- [5] H. T. Nguyen *et al.*, “Long-term Application of Carbon Fiber Composite Cable Tendon in the Prestressed Concrete Bridge - Shinmiya Bridge in Japan,” *MATEC web Conference 206*, vol. 02011, 2018.
- [6] P. B. Potyrała, “Use of Fibre Reinforced Polymer Composites in Bridge Construction. State of the Art in Hybrid and All-Composite Structures,” 2011.
- [7] JSCE, “Recommendation for design and construction of concrte stuctures using continuous fiber reinforcing materials,” 1998.
- [8] A. E Refai, “Durability and fatigue of basalt fiber-reinforced polymer bars gripped with steel wedge anchors,” *Journal of Composites for Construction*, vol. 17, no. 6, pp. 1–11, 2013.
- [9] R. Joven, “Study of Thermal Expansion in Carbon Fiber Reinforced Polymer composites,” Conference paper, January 2012.
- [10] T. Enomoto, “Use of CFCC Tendons and Reinforcements in concrete structures for durability,” in *APFIS 2012, Hokkaido University, Japan*, 2012.
- [11] N. Santoh, H. Kimura, T. Enomoto, T. Kiuchi, and Y. Kuzuba, “Report on the Use of CFCC in Prestressed Concrete Bridge in Japan,” *Fiber-Reinforced-Plastic (FRP) Reinforcement Concrete Structure Proceeding Intenational Symposium. ACI, SP-138*, pp. 895–911, 1993 (in Japanese).
- [12] S. H. Rizkalla and G. Tadros, “A smart highway bridge in Canada,” *Concrete International*, vol. 6, no. 4, pp. 37–42, 1994.

- [13] A. A. Abdelrahman and S. H. Rizkalla, "Serviceability of Concrete Beams Prestressed by Carbon Fiber-Reinforced-Plastic Bars," *ACI Structure Journal*, no. 94, pp. 447–454, 1998.
- [14] N. F. Grace, F. C. Navarre, R. B. Nacey, W. Bonus, and L. Collavino, "Design - Construction of Bridge Street Bridge - First CFRP Bridge in the United States," *PCI Journal*, 47 5, pp. 20-35., 2002.
- [15] W. D. Corte and P. Van Bogaert, "Evaluation of an experimental CFRP pre-stressed beam and slab road bridge," *Composite Part B Engineering*, vol. 36, no. 2, pp. 91–98, 2005.
- [16] T. Enomoto, N. F. Grace, and T. Harada, "Life Extension of Prestressed Concrete Bridges Using CFCC Tendons and Reinforcements," *Proceeding, Conference on FRP Composites in Civil Engineering*, vol. Rome Italy, 2012.
- [17] N. F. Grace, E. Jensen, C. Eamon, T. Enomoto, and X. Shi, "Life cycle cost analysis of prestressed concrete bridges using CFRP reinforcement," *Proceeding. CICE 2012 6th International Conference on FRP Composites in Civil Engineering*, pp. 1–8, 2012.
- [18] A. C. 440, M. Farmington Hills, and A. C. Institute, "State-of-the-Art Report on Fiber Reinforced Plastic (FRP) Reinforcement for Concrete Structures (ACI 440 R-96)," 1996.
- [19] R. Katarzyna and Z. Łukasz, "Prestressing Concrete Structures with CFRP Composite Tendons," *Emerging Technology Series Prestressing*, pp. 1–35, 2015.
- [20] T. S. Yaman, "Behaviour of precast concrete beams prestressed with CFRP strands," *Journal of Croatian Assoc. Civ. Eng.*, vol. 68, no. 10, pp. 775–786, 2016.
- [21] T. Yamashita, T. Kiuchi, H. Inukai, and T. Iwasaki, "PC Bridge with New Material - Construction of Shinmiya Bridge," *Prestress. Concr. Vol. 31, No.2*, pp. 71-78, 1989 (in Japanese).
- [22] T. Futakuchi, S. Komada, T. Kiuchi, and K. Matsumoto, "Actual Bridge Loading Test of New Material PC Bridge," *Proc. 2nd Symp. Prestress. Concr. Tech. Assoc.* pp. 307-310, 1991 (in Japanese).
- [23] H. Kanda, T. Kiuchi, and K. Matsumoto, "Loading test report of actual bridge test girder of new material PC Bridge," *Proc. 5th Symp. Prestress. Concr. Tech. Assoc.*, pp. 529–532, 1995 (in Japanese).

Chapter 2. Load-carrying capacity and durability of prestressed concrete girder using CFRP tendons under long-term exposure in corrosive salt environment

2.1 Introduction

The Hokuriku region, which is along the coastline of the Sea of Japan, is highly affected by seasonal-wind-based airborne salinity from the Northwest. Reinforced concrete structures are corroded by salt penetration, and thus the serviceability and durability of the structures are decreased. This problem has become a challenge for civil engineering works, especially for bridges. The old Shinmiya Bridge in Ishikawa located on the coast of Ishikawa Prefecture was a reinforced concrete bridge that had been damaged by salt corrosion. It was necessary to build a new bridge after 12 years in service [1].

The appearance of FRP brought another approach to solve the problem of structural deterioration caused by steel corrosion. The use of Carbon-Fiber-Reinforced Plastic (CFRP) as an alternative to ordinary steel has increased rapidly since the 1980s in Japan. In October 1988, CFRP was selected as the tensioning material for the main girders of the new Shinmiya Bridge. This is the first prestressed concrete bridge in Japan and the world to utilize CFRP tendons against salt damage [2].

After 30 years of Shinmiya Bridge construction, the technical of CFRP application in the bridge construction was developed strongly in other countries such as the United State, Canada, Belgium, Germany [3]–[5]. However, the uncertain of long-term durability is a barrier for application expansion of CFRP in the world. Therefore, this problem becomes the research topic for sciences. Many studies were conducted both of in laboratory and in outside with the various in the shape and form of structures using CFRP. It is difficult that CFRP is a new material and the design life of a civil engineering structure is between 50 to 100 years. Hence, the long-term serviceability and long-term quality of CFRP and structure using CFRP are lack of data. Only several studies of the bridge structure using CFRP under a real of corrosion environment were recorded.

From the time of Shimmiya Bridge construction, the long-term observation and study were performed by the three full-scale girders. These girders were fabricated the same of main girders and two girders placed next to the main girders under the same environment in two directions including seaside and mountainside. The other one was subjected for loading test to determine the ultimate behavior and load-carrying capacity of the prestressed concrete (PC) girder [6] as well the deflection and the strain behavior of the CFRP [7] in 1989. In 1994 (six years after the construction time), the seaside girder was remove form site and conducted a destructive test, the load-carrying capacity of the seaside girder was compared with the result of the first girder, and the durability of the CFRP tendons was confirmed [8].

In this study, the load-carrying capacity and durability of prestressed concrete girder using CFRP tendons affected by an actual corrosive salt environment for nearly 30 years were investigated. A series of experiment were conducted for the girder exposed at mountainside of Shinmiya Bridge. The destructive bending experiment was performed on the girder to clarify the flexural capacity. The ultimate load and crack initiation load were compared with those values at the time of construction and six years after the time of construction. In addition, after the bending test, a larger number of concrete cores were



Figure 2.1 Shinmiya Bridge - October 2017

taken from the girder to estimate the mechanical properties of concrete such as compression strength, static elastic modulus. Amount of salt in the girder was measured to evaluate and discuss from the cores collected. The mechanical and chemical tests were conducted on CFRP tendons removed from the main girder. From the experimental results, the mechanical properties and durability of prestressed girder as well CFRP were confirmed.

2.2 Description of Shinmiya Bridge

The Shimiya Bridge was built at the Shika town, Hakui district, Ishikawa Prefecture, Japan in October 1988. Originally, the bridge was a reinforced-concrete-slab bridge, but under the corrosive environment of the building site, the steel material significantly corroded and the concrete surface was broken within 12 years after the original construction. Therefore, CFRP was selected to reinforce the main girders in the new bridge in October 1988. *Figure 2.1* shows the Shinmiya Bridge on October in 2017.

Figure 2.2 and 2.3 respectively show the side view and cross-section of the Shinmiya Bridge. The bridge length was 6100 mm and the effective width was 7000 mm. As shown in *Figure 2.3*, the main bridge has a structure in which 24 main girders with an I-shaped cross-section (JIS A 5313, S106-325). Regarding countermeasures against salt damage to the main girders, a D6 epoxy-coated rebar and eight CFRPs of $\varnothing 12.5$ mm with seven strands were selected. On both sides of the bridge, two full-scale test girders at mountainside and seaside were fabricated and transversely tightened together with the main girders of the bridge in the same environment to confirm their long-term robustness. When six years passed (1994) after construction, the test girder at the seaside was removed and the bending fracture experiment was conducted using this girder. In addition, the transmission length test, salinity measurement, tensile test and chemical composition test of the CFRP tendons removed were performed. In this research, other test girder on the mountainside was removed from the main bridge and subjected to the same tests as mentioned above.

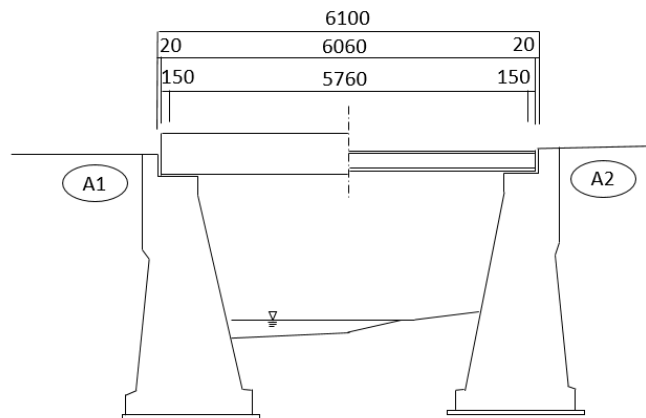


Figure 2.2 Side view (mountainside) of Shinmiya Bridge

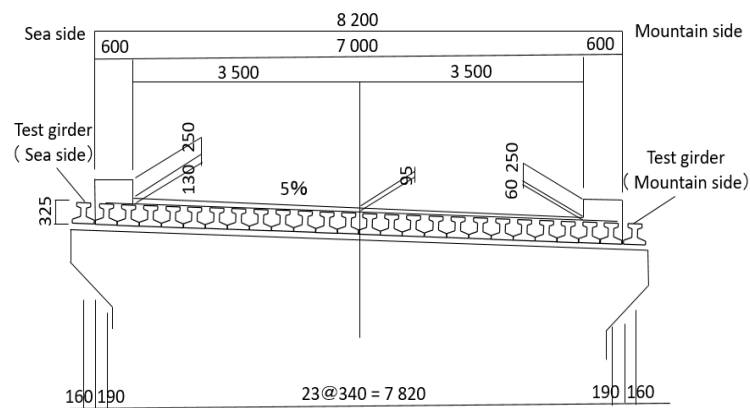


Figure 2.3 Cross-section of Shinmiya Bridge (unit: mm)

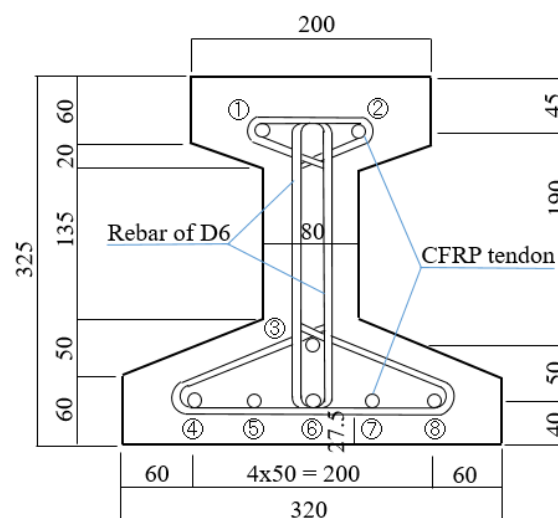


Figure 2.4 Cross-section of main girder (unit: mm)

Figure 2.4 shows the I-shaped cross-section of the mountainside girders. The length, height, and width of upper flange, width of lower flange are 6060 mm, 325 mm, 200 mm, and 320 mm respectively. The girder was reinforced with eight CFRPs with \varnothing 12.5 mm and seven strands, in which six CFRPs was used for the tensile zone and two CFRPs located in the compression zone. The space between CFRPs in upper flange was 80 mm while this number was 50 mm of five CFRPs in the lower flange. The number three of CFRPs in the tensile zone was located at the center of the lower flange and at a height of 90 mm from the bottom of the girder (seen in *Figure 2.4*). Epoxy coated rebar of D6 was set up for stirrups and the compressive strength of 59.8 N/mm² for concrete



(a)



(b)

Figure 2.5 The mountain girder after removing from the site

was recorded in 1988. *Figure 2.5 (a)-(b)* show the condition of the mountainside girder after removing from the site and moving to the laboratory.

2.3 Experimental method

The experimental process followed in this research is shown in *Figure 2.6*. First, after removing the test girder from the bridge site, it was brought into the laboratory; the effective stress was estimated using the stress release technique with a core incision, and the obtained value was compared with the design value. Next, a flexural experiment by applying a bending load was carried out, and the difference from the ultimate load obtained in the same test conducted six years after construction was considered. The transfer length of the prestressed girder, which obtained by recording a relationship between strains on the concrete girder surface versus the distance to the end of the girder before and after cutting the upper and lower flanges, was examined by using half of the girder after the flexural experiment. Furthermore, the concrete cores were collected, the compressive strength test was conducted and salt content was measured. Finally, the mechanical and chemical characteristics of the CFRP removed from the main girder were determined.

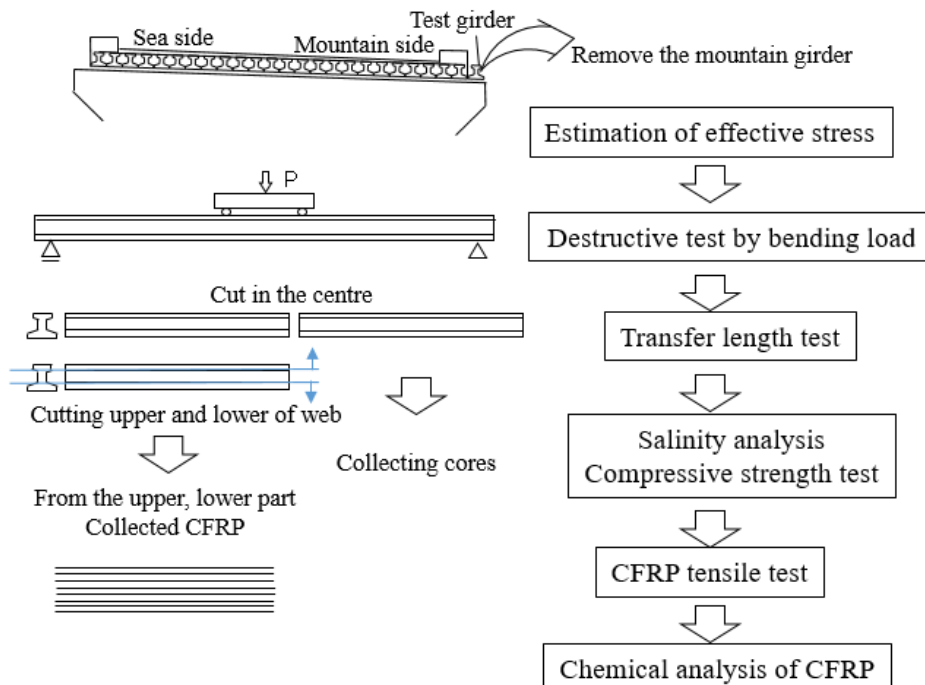


Figure 2.6 The flow chart of research

2.4 Estimate of effective stress

2.4.1 Test method

Regarding the use of CFRP, it was considered that the effective stress might decrease owing to material fatigue caused by repeated live loading and relaxation caused by material deterioration under exposure to an actual service environment over a long period. Therefore, to determine whether the effective stress of the prestressed concrete girder using CFRP tendons was still in the design stress state after nearly 30 years, the effective stress estimation method based on the stress release technique [9] was used. The effective stress was estimated by the release of the working stress and measuring the strain.

The measurement procedure divided 7 steps. First, three survey positions were selected for this test. This test girder was a pre-tensioned beam, and a transfer length existed at the end of the girder. The stress was stabilized in the cross-section at the center of the span, and the bottom flange with a large stress was selected as the measurement position. Although no noticeable deterioration was observed in the appearance of the test specimen, the stress might vary along the width of the bottom flange. Hence, the positions deviated from the center of the cross-section to the left and right at 160 mm from the center and 60 mm from the edge, and the distance between the two positions was 1000 mm. Three positions considered in this experiment can see in *Figure 2.7*.

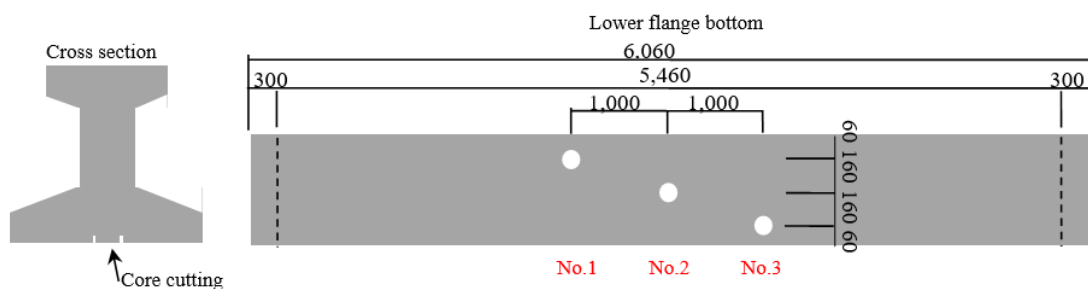


Figure 2.7 Measurement position

Next, strain gauges were pasted on the survey positions as shown in *Figure 2.8 (a)*. A gauge for concrete with a gauge length of 30 mm was attached to the measurement position in two directions perpendicular to the prestress direction. In order to make a note by the core drill around the gauge, a type that lead wire can be attached and detached with solder was used. Initial of strain was recorded with a static strain gauge as the initial value before the release of core incision.

In term of the stress decreased by core incision, the core incision was made to a depth of 18 mm using a drilled core of $\varnothing 50$ mm,. *Figure 2.8 (b)* show core cut condition.

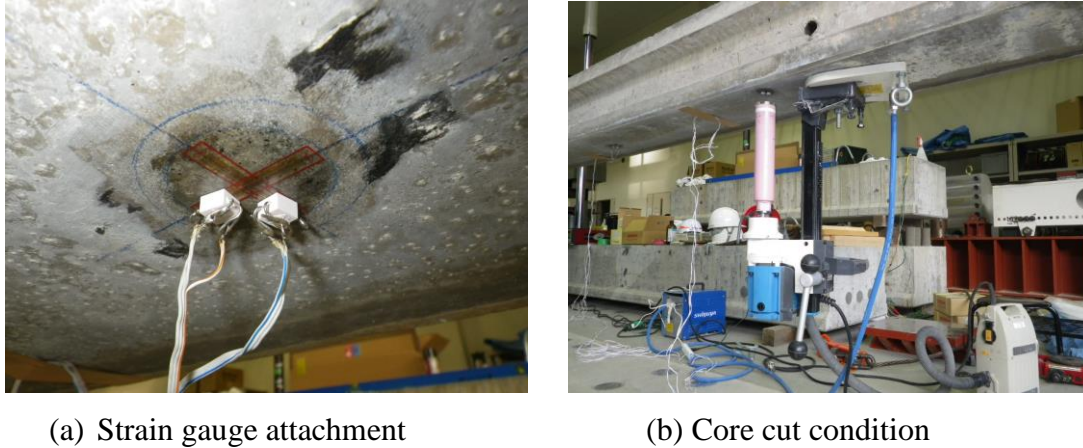


Figure 2.8 The setup of experiment

After cutting, gauge lead wires were wired and measured at intervals of 150 second intervals. Then, the stability of the strain value was confirmed and the measurement was terminated. The Young modulus required for stress conversion, the measured value by the core sample was adopted. From the measured values, the present prestress was estimated and calculated from the estimation equation of effective stress [9].

2.4.2 Estimation results

By applying the effective stress estimation method based on the stress release technique, the effective stress on the main girders was estimated and compared to the design value of the effective stress to evaluate the durability of the CFRP tendons. *Table 2.1* compares the design value of the effective stress with the estimated values (these values did not consider stress due to dead load). The estimated values at each measurement sample almost approximated to the design value. In comparison with sample 2 (No.2), the value of sample 3 (No.3) was slightly higher by 0.3 N/mm^2 and the value of sample 1 (No.1) was lower by about 1 N/mm^2 . This result was consistent with the deformation behavior of the warp due to the increase and decrease in the tensile force. The average of the three positions (11.51 N/mm^2) was higher than the design value by 0.43 N/mm^2 , and the ratio between the average value and the design value was 104%. It

appeared that there was no significant difference between the effective stress in this study and the design value.

*Table 2.1 Comparison of effective stress of design value and estimated value
(Did not consider stress due to dead load)*

No.	Design value (N/mm ²)	Estimated value (N/mm ²)	Ratio	Difference
1	11.08	10.76	97%	-0.32
2	11.08	11.72	106%	0.64
3	11.08	12.05	109%	0.97
Average	11.08	11.51	104%	0.43

2.5 Loading test

2.5.1 Test method

The loading test was conducted using the same method that was used in 1988 and six years after the construction (1994). The loading method is shown in *Figure 2.9*, and the arrangement of measurement points is shown in *Figure 2.10*. In the destructive bending experiment, the static bending load was applied at two points in the middle of the span with a distance of 1000 mm. Measurement items included the displacement at the support positions, at the center of the main girder, embedded strain gauge, and concrete surface strain gauge.

The loading procedure was the same as that used in the flexural experiment, which was conducted in 1988 and 1994. First, the load was applied up to 35.4 kN (design load 35.3 kN) and returned to 0 kN. Second, the sample was loaded to crack initiation load and returned to 0 kN again. Finally, the sample was loaded to the ultimate load as the final stage.

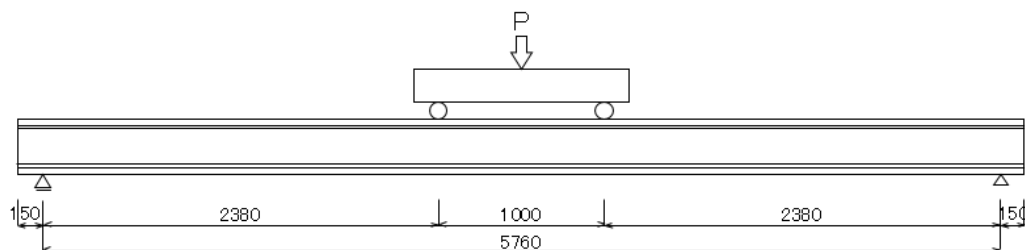


Figure 2.9 The setup of loading test

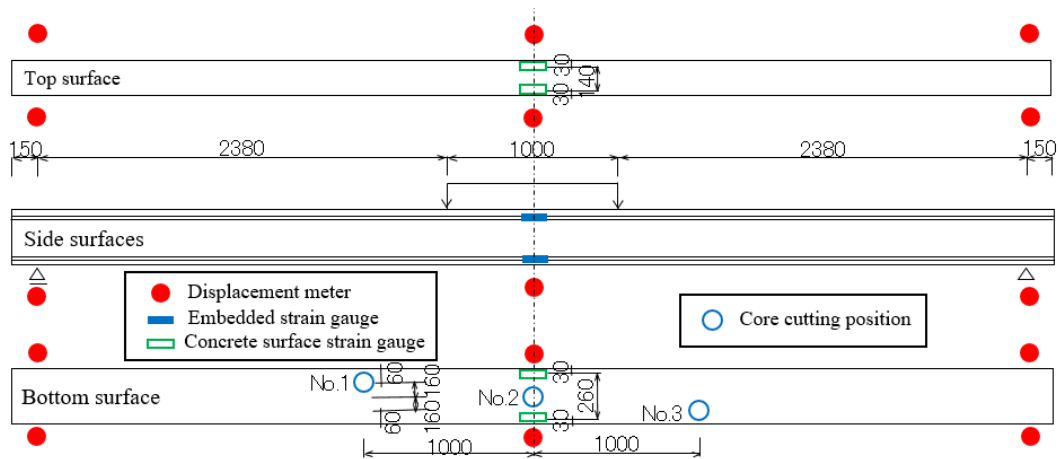


Figure 2.10 Measurement positions (unit: mm)



Figure 2.11 Girder specimen before test

2.5.2 Results and discussion

Figure 2.11 and Figure 2.12 show the situations of the girder before the test and at the failure, respectively. The crack pattern after loading test is shown in Figure 2.13 and the load-displacement relationship obtained by the loading test is shown in Figure 2.14. In addition to the results of this flexural experiment, the crack initiation load, load-carrying capacity at the time of construction and six years after construction, and design values are summarized in Table 2.2.



Figure 2.12 Girder specimen at failure



Figure 2.13 Crack pattern after loading test

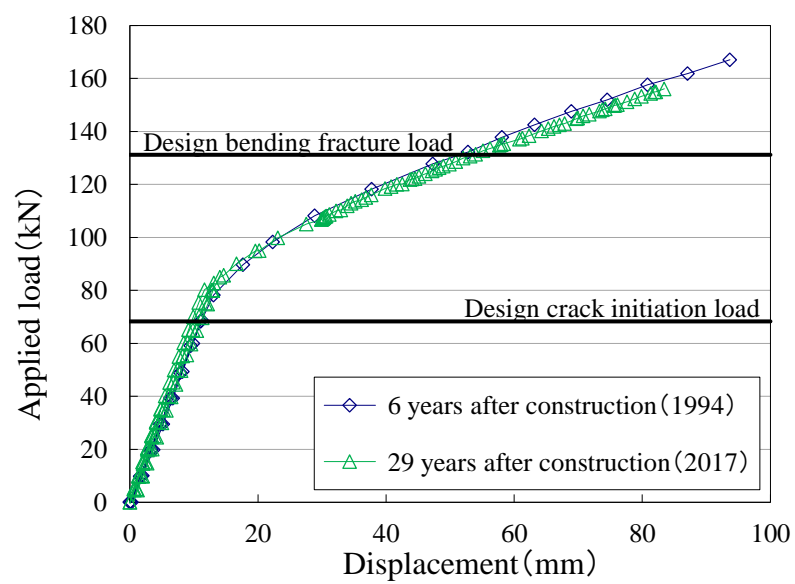


Figure 2.14 Load-displacement relationship at the center of the girder

Table 2.2 Comparison of crack initiation load and ultimate load

		In 1988	In 1994	In 2017
	Design value	At the time of construction	After 6 years	After 29 years
Crack initiation load (kN)	68.3	70.6	98.3	82.8
Ultimate load (kN)	131.2	132.3	167.1	157

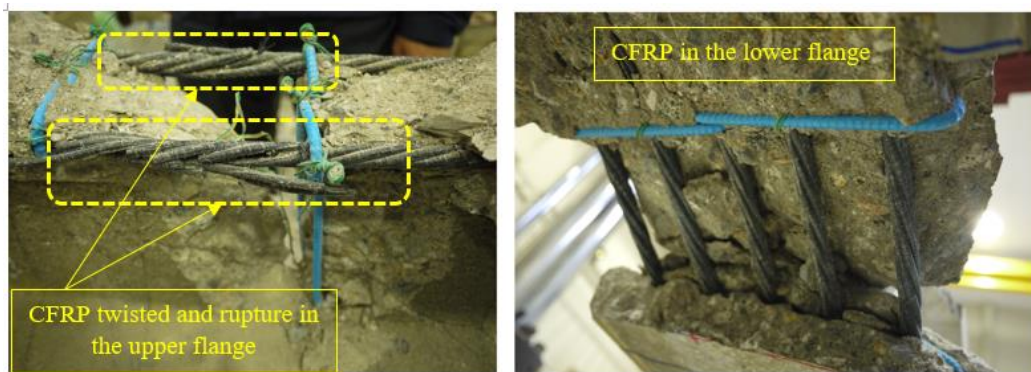


Figure 2.15 Status of CFRP in compression and tension zone at failure

The failure mode imposed in this loading test was the crushing of concrete in the compressive area after the bending crack propagation. This failure mode occurred because two reasons. Firstly, CFRP is linear elastic and has no yield phenomenon. Secondly, the girder was calculated and designed to be a destructive form, in which the concrete in the compressive zone collapsed before the CFRP in the tensile zone ruptured. This destruction was similar to that observed on test girders in the experiments at the time of construction and six years after construction.

Figure 2.15 shows the condition of the prestressed concrete girder surface after the concrete collapse with detailed CFRP observations. It was found that the CFRP in the upper side was twisted and broken after crushing of the concrete. The situation of CFRP in the upper side was shown on the yellow dash-line areas on Figure 2.15. However, failure due to tension could not be confirmed at the CFRP on the lower side.

The design crack initiation load (68.3 kN) and design bending fracture load (131.2 kN) are mentioned in Figure 2.14. From the load-displacement relationship, when the load was removed after loading up to design load and crack initiation load, almost no residual displacement could be confirmed. Although the results of the loading test of the

mountainside girder at this time and of the seaside girder at six years after construction time were almost overlapped, the ultimate load is lower around 6% as compared with the result obtained at six years after construction. However, crack initiation load and ultimate load in both 1994 and 2017 respectively exceeds the value at the time of construction and design value as shown in *Table 2.2*. Therefore, it can be judged that the load-carrying capacity of the girder has been still in good condition.

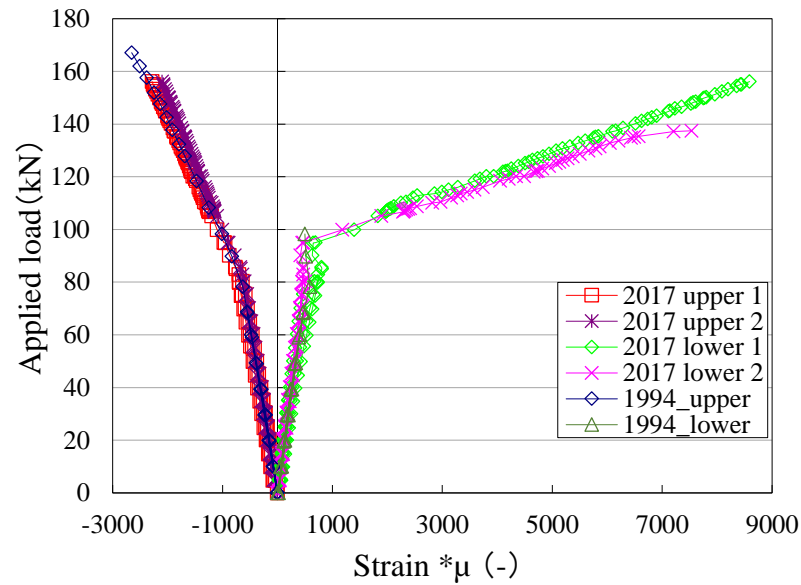


Figure 2.16 Load-strain relationship of concrete

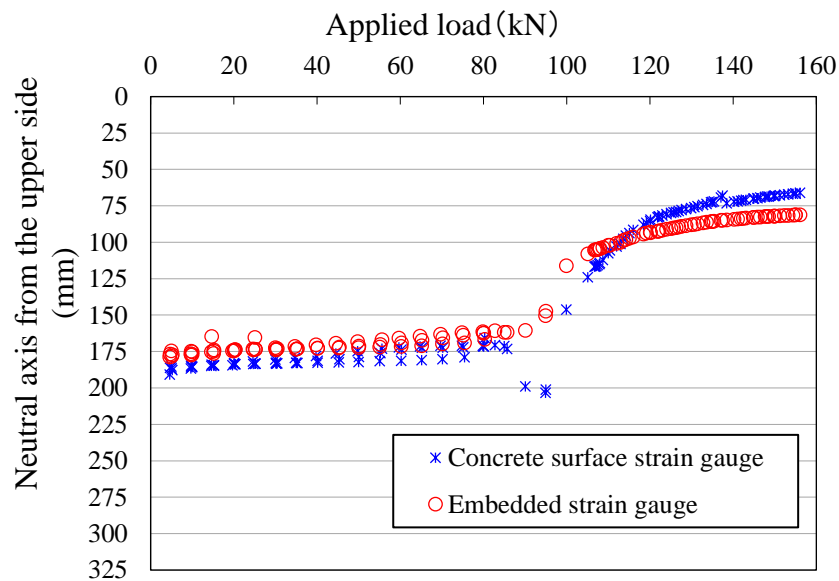


Figure 2.17 The neutral axis depth

The load-strain relationships of concrete on the top and bottom surfaces at the span center are presented in *Figure 2.16*. The result obtained from the bending experiment in 1994 was added to compare. As can be seen from *Figure 2.16*, the relationship between applied load and strain obtained by this experiment was close to the results in 1994. The neutral axis depth from the top edge was calculated from the concrete surface strain gauge and embedded strain gauge (see *Figure 2.17*). It assumed the linear distribution of strain in the cross-section for the neutral axis calculation. In the elastic stage, the neutral axis depth was almost similar between two results. After reached the crack initiation load of 82.8 kN, the values of the neutral axis were a slight difference. However, both of them had the trend toward the compression zone with an increase of the applied load. This difference may be due to one of the concrete surface strain gauges on the lower side that was broken before ultimate load and the strain distribution on the cross-section was not linear. In term of the result calculated, the neutral axis depth of test girder was approximately 81 mm at 156.2 kN.

2.6 Transfer length test

2.6.1 Test method

In pre-tensioning concrete members, the steel strands has an initial stress following the required force, then concrete is cast around strands. When the concrete reaches a sufficient compressive strength, the prestress force is transferred to the concrete due to the bond between the strands and the surrounding concrete through the release of prestress. After this release, there is a variability in the prestressed force from zero in the end of structure to the constant maximum value (effective prestressing force) in the center zone. The length required to achieve the effective prestressing force is defined as transmission length or transfer length [10].

After long-term service of the girder, to investigate whether the bond between the CFRPs and concrete was decreased or not and the transmission length changed or not, a transfer length test was conducted.

In this test, the technique of concrete surface strain, which recorded a relationship between strains on the concrete girder surface versus the distance to the end of the girder, was used to determine the transfer length. After the flexural test, the main girder was cut at the center of the span and one of two half girders was used. First, 40 strain gauges were

attached on the neutral axis in an interval of 2000 mm from the end of the girder. *Figure 2.18* shows an arrangement of strain gauges following the zigzag because the size of the

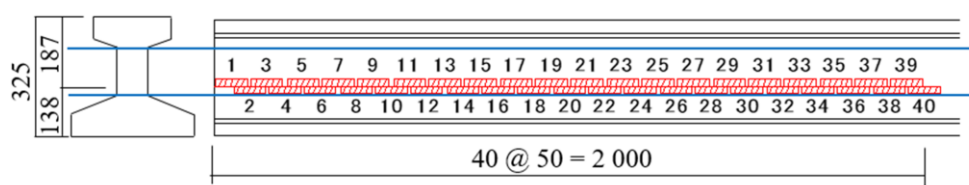


Figure 2.18 Setup of transfer length test



Figure 2.19 The 1/2 girder before and after cutting flanges

strain gauge (WFLM-60-11) for this test was large. Next, the web where tendons were not present was removed from the main girder by concrete cutting machine (see *Figure 2.19*). The blue line in *Figure 2.18* indicates the boundary among the web, lower flange, and upper flange. The strains were measured at the time of cutting and the transmission length was determined by observing the variation of strains.

2.6.2 Results and discussions

Figure 2.20 shows the measurement values of strain in three cases. The blue circles are used to show the measured strains after the lower flange was completely cut. The orange triangles indicate the results measured immediately after both of the upper and lower flanges were cut off. And the green squares serve to illustrate values of strain on the concrete surface measured after 16 hours since both of the upper and lower flanges were cut off.

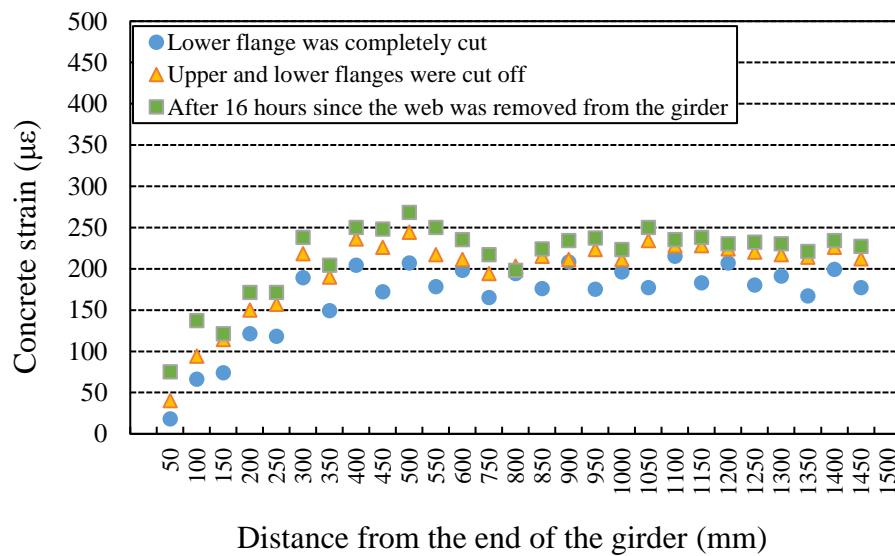


Figure 2.20 Changes in transfer length in web

The transmission length according to the road bridge specification is defined as 65ϕ [11] hence it was 812.5 mm in the case of this main girder. However, from the results of this test shown in *Figure 2.20*, the transmission length was considered 500 mm, which was smaller than 65ϕ . The same result was obtained in the test conducted six years after construction [8], and it became clear that both of the transfer length and the bond between the CFRP and concrete had not changed.

2.7 Measurement of salt content

2.7.1 Test method

After the flexural test, four drilled cores were collected on the web side and bottom surface of the girder as shown in *Figure 2.21*. Three cores were on the web side and one core was on the bottom surface of the girder. Then, the salt content was measured on these samples.



Figure 2.21 The method collecting the cores

On the web side, three concrete cores with a diameter $\varnothing 40$ mm and length of $L = 80$ mm were collected at positions of 1080 mm, 1150 mm and 1280 mm from the end of the girder. One core with a length of $L = 30$ mm from the concrete surface to the stirrup position at the position 920 mm from the end of the girder was collected on the bottom surface of the girder. The concrete cores were sliced to a 10-mm-thick layer, and the total chloride ion concentration in each slice was measured according to JIS A 1154 [12]. From the measurement results of the chloride ion concentration, the total chloride ion concentration at each depth was calculated using the Fick's diffusion coefficient of chloride ions and surface chloride ion concentration as following equation.

$$C(x, t) = C_0 \left(1 - \operatorname{erf} \left(\frac{x}{2\sqrt{D * t}} \right) \right)$$

In here, $C(x, t)$: chloride concentration at depth x (cm) and time t (year)

C_0 : Surface chloride concentration (kg/m^3)

D : Fick's diffusion coefficient of chloride ions (cm^2/year)

2.7.2 Results and discussion

From the measured and calculated results, the total chloride ion concentration on the web side (three samples) and lower flange are shown in *Figure 2.22* and *Figure 2.23*, respectively. In *Figure 2.22*, the red circles, blue triangles and green squares show measurement results of cores at positions of 1080 mm, 1150 mm and 1280 mm on the web, respectively. These values were measured with 10 mm-thick layers of samples, hence they are plotted in the center of each slice. In addition, the red line, blue line and green line illustrate the calculated results of the total chloride ion concentration for each

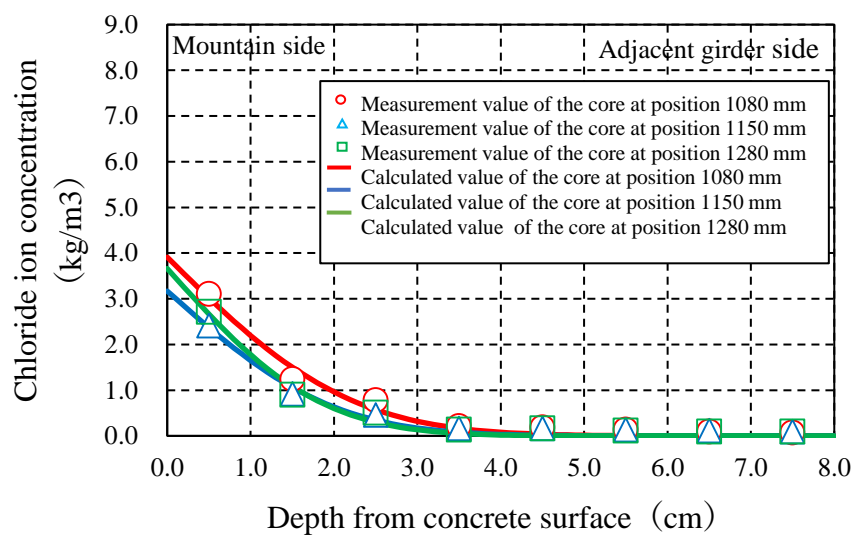


Figure 2.22 Chloride ion concentration on web of main girder

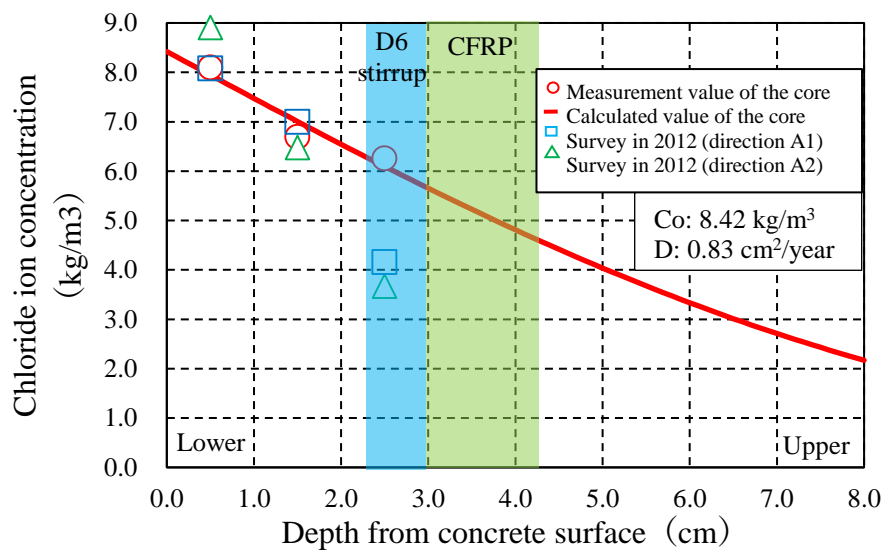


Figure 2.23 Chloride ion concentration on the lower flange of main girder

depth of cores corresponding to three positions (1080 mm, 1150 mm and 1280 mm). In the same way, the red circles are used to demonstrate measured results of the core in the bottom surface while the red line shows the calculated results of salt content at each depth of this core in *Figure 2.23*. Moreover, blue triangles and green squares, which indicate the results of the chloride concentration survey in 2012 by the drill method at positions located on the bottom surface of this girder on two directions (abutment A1 and abutment A2, as shown in *Figure 2.2*), were added on *Figure 2.23* for comparison.

First, in terms of comparing the results in *Figure 2.22* and *Figure 2.23* of two measurement sites, the bottom surface has a higher chloride ion concentration than the side surface. It was considered that this phenomenon was caused by rinsing of the salt on the concrete surface on the side by rainwater.

Second, considering the results for the web of the girder in *Figure 2.22*, there is a decrease of chloride ion concentration in the width of the web from the mountainside to the adjacent girder side. Salinity penetration from the mountainside was remarkable. In addition, the results chloride ion concentration on the adjacent girder side (the side that was face-to-face with the other girder) was quite lower. The average value of the surface chloride ion concentration (C_0) was 3.58 kg/m^3 , and the average value of the diffusion coefficient of chloride ions (D) was $0.04 \text{ cm}^2/\text{year}$.

However, from the results for the bottom surface of the girder, the surface chloride ion concentration (C_0) was 8.42 kg/m^3 , and the diffusion coefficient of chloride ions (D) was $0.83 \text{ cm}^2/\text{year}$. Compared to the chloride ion concentration on bottom surface measured in 2012, there was no significant increase in chloride ion concentration for the depths from 0.0 to 2.0 cm from the concrete surface in *Figure 2.23*, but the chloride ion concentration at a depth from 2.0 to 3.0 cm from the concrete surface has significant change. It was confirmed that the concentration increased, and it was estimated that the chloride ion concentration was nearly 6.0 kg/m^3 at the position of the stirrup rebar (reinforcement cover was 27.5 mm). It largely exceeded the corrosion occurrence limit of steel, 1.2 kg/m^3 ; the rebar could have been considered corroded if general steel materials were used.

2.8 Compression test of concrete

2.8.1 Collected the samples

After bending fracture experiment, two cores with a diameter of approximately $\varnothing 40$ mm was taken from the upper flange of the girder at 740 mm and 870 mm from the end of the span, and the compressive strength test was carried out. *Figure 2.24* shows the sample and the setup for the compressive test.



Figure 2.24 Setup the compressive experiment

2.8.2 Experimental result

The compressive strength, elastic modulus, and Poisson's ratio was calculated and summarized in *Table 2.3*. It seems that the average value of the compressive strength (75.1 N/mm^2) is higher than the value recorded (59.8 N/mm^2) in 1988, which is also given in *Table 2.3*.

Table 2.6 Results of compressive strength test of concrete

	Compressive strength (N/mm^2)	Elastic modulus (kN/mm^2)	Poisson's ratio
No. 1	79.8	39.8	0.2
No. 2	70.4	34.6	0.2
Average	75.1	37.2	0.2
In 1988	59.8	32.1	0.2

2.9 Tensile test of CFRP

2.9.1 Collected the samples

A concrete cutting machine removed CFRPs in the upper and lower flanges of the girder that were separated in the transfer length test. CFRPs were collected as samples for this test with the length of 2.2 m as shown in *Figure 2.25*. Subsequently, they were subjected to preparation for the tensile test (see *Figure 2.26*).



Figure 2.25 CFRP after removed from the girder and prepare for the tensile test



Figure 2.26 Setup the tensile experiment of CFRP

2.9.2 Experimental results

The ultimate tensile load and elastic modulus were determined. In addition to the ultimate tensile load and elastic modulus obtained in this study, the results at the time of the construction, the results at six years after construction, and the standard values are summarized in *Table 2.4*.

Table 2.9 Results of CFRP tensile test

	Rupture load			Elastic modulus (kN/mm ²)
	Average (kN)	Maximum (kN)	Minimum (kN)	
At the time of construction (in 1988)	156.8	165.1	148.0	139.2
After 6 years (in 1994)	155.8	165.4	148.8	142.1
After 29 years (in 2017)	156.8	161.0	148.6	132.5
Quality standard value		137.2		129.4~144.1

The elastic modulus decreased by approximately 7% from the value obtained six years after construction, but this value was still within the allowable variation range. In addition, the ultimate tensile load was comparable to that of past values and residual tension load capacity was confirmed.

2.10 Chemical analysis of CFRP tendon

2.10.1 FE-SEM observation

CFRPs were exposed to an alkaline environment in concrete and were affected by chloride ions and repeated loading due to the live load. Here, surface observation was carried out for CFRPs at positions ③, ④, and ⑧, shown in *Figure 2.4*. The CFRP (polyester, wrapping) surface was observed with an optical microscope; the surface of the carbon fiber removed from the CFRP surface coating and the epoxy resin were observed in detail by FE-SEM (field emission scanning electron microscopy). *Figure 2.27* shows the CFRP surface observed with an optical microscope (20 times) in the left side and the surface of the carbon fiber observed with FE-SEM (2000 times) in the right side.

Although some scratches were caused when CFRPs were collected from concrete, there was no part where the coatings and carbon fibers themselves seemed to have

deteriorated owing to the salt environment and live load. Therefore, it was confirmed that there was no problem in the CFRP surface and carbon fiber surface.

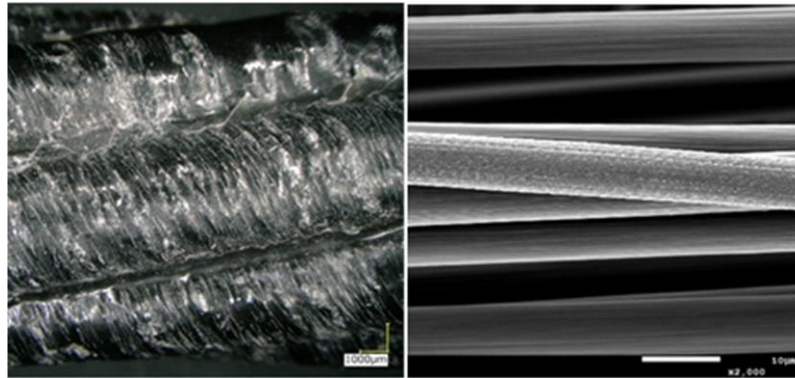


Figure 2.27 CFRP surface and carbon fiber surface

2.10.2 Fourier Transform Infrared Spectroscopy (FT-IR) Analysis

FT-IR (Fourier Transform Infrared Spectroscopy) analysis was conducted using CFRPs from positions ③, ④, and ⑧, shown in *Figure 2.4*. A total of nine core wires and two helical wires of each cable were used as samples to investigate the chemical structural changes that accompany deterioration. As an example of the analysis results obtained using FT-IR, *Figure 2.28* shows the comparison between the result of the core strand of the CFRP in position ④ and that obtained six years after construction. There was no major change in the result of this test compared with the FT-IR measurement result at six years after construction, but there was a position where a fine peak appeared.

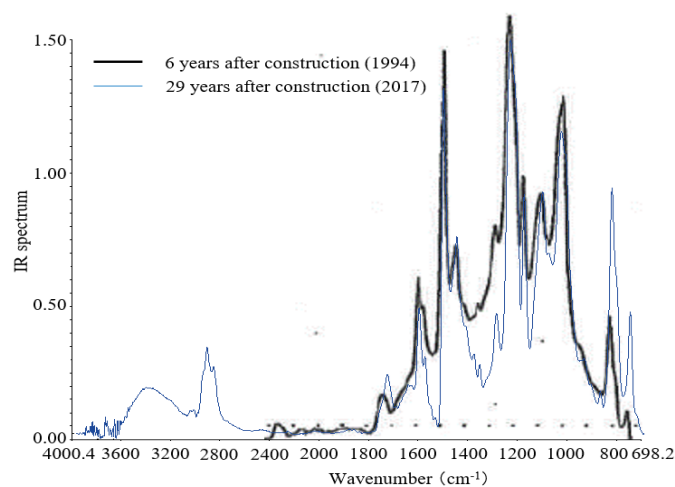


Figure 2.28 Analysis result by FT-IR

This may be because of the excellent accuracy of the current measuring machine. Therefore, it can be said that although several differences were observed, no deterioration attributed to chemical structural changes occurred because large changes, such as the disappearance of the main peak, could not be confirmed.

2.11 Conclusions

In this study, the series of experiments was conducted on the prestressed concrete girder using CFRP tendons, which was exposed to an actual corrosive environment for nearly 30 years. The measurement of effective stress, the transfer length test, compressive strength test of concrete, the destructive bending experiment were carried out on the main girder and the mechanical and chemical properties of CFRPs removed from the main girder after the flexural experiment were examined. From the results and discussions, the load-carrying capacity and the durability of the girder were confirmed. The remarkable conclusions in this research are as follows.

- (1) No significant difference between the effective stress in this study and the design value.
- (2) From the load-displacement relationship, the results of this test and the results at six years after the construction were almost overlapped, but the ultimate load in this study were approximately 6% lower than that at six years after construction. However, the results exceeded the design value and value at the time of construction. It could be considered that the load-carrying capacity of the girder has been still in good condition.
- (3) The transfer length of the specimen was determined to be 500 mm, which was smaller than 65ϕ . The same result was obtained in the test conducted six years after the original construction, and it became clear that the transfer length and the bond between CFRPs and concrete did not change.
- (4) From the analysis results of the salt content in the core collected from the lower surface of the main girder, chloride ion concentration in the bottom surface was higher than that in the side surface; the chloride ion concentration was estimated to be approximately 6.0 kg/m^3 at the position of the stirrup rebar (reinforcement cover was 27.5 mm).
- (5) The compressive strength of concrete (75.1 N/mm^2) is higher than the value recorded (59.8 N/mm^2) in 1988.
- (6) The tensile test of the CFRPs taken out after the flexural experiment was confirmed, the rupture load was comparable to the previous results and residual tension load capacity was observed. The elastic modulus of CFRP decreased by approximately 7% from the value in 1994.

(7) There was no position where the coatings and carbon fibers themselves seemed to be deteriorated, according to the FE-SEM observations of the CFRP tendons. It was confirmed that there was no problem in the CFRP surface and carbon fiber surface. In addition, from the FT-IR analysis results, no significant change, such as the disappearance of the main peak or appearance of a new peak, could be confirmed. Therefore, it was considered that deterioration caused by chemical structural change did not occur.

References

- [1] T. Enomoto, N. F. Grace, and T. Harada, "Life Extension of Prestressed Concrete Bridges Using CFCC Tendons and Reinforcements," *Proc., Conf. FRP Compos. Civ. Eng.*, vol. Rome Italy, 2012.
- [2] N. Santoh, H. Kimura, T. Enomoto, T. Kiuchi, and Y. Kuzuba, "Report on the Use of CFCC in Prestressed Concrete Bridge in Japan," *Fiber-Reinforced-Plastic (FRP) Reinforcement Concr. Struct. Proc. Int. Symp. ACI, SP-138*, pp. 895–911, 1993 (in Japanese).
- [3] S. H. Rizkalla and G. Tadros, "A smart highway bridge in Canada," *Concr. Int.*, vol. 6, no. 4, pp. 37–42, 1994.
- [4] N. F. Grace, F. C. Navarre, R. B. Nacey, W. Bonus, and L. Collavino, "Design - Construction of Bridge Street Bridge - First CFRP Bridge in the United States," *PCI Journal*, 47 5, pp. 20-35., 2002.
- [5] W. D. Corte and P. Van Bogaert, "Evaluation of an experimental CFRP prestressed beam and slab road bridge," *Compos. Part B Eng.*, vol. 36, no. 2, pp. 91–98, 2005.
- [6] T. Yamashita, T. Kiuchi, H. Inukai, and T. Iwasaki, "PC Bridge with New Material - Construction of Shinmiya Bridge," *Prestress. Concr. Vol. 31, No.2*, pp. 71-78, 1989 (in Japanese).
- [7] T. Futakuchi, S. Komada, T. Kiuchi, and K. Matsumoto, "Actual Bridge Loading Test of New Material PC Bridge," *Proc. 2nd Symp. Prestress. Concr. Tech. Assoc.* pp. 307-310, 1991 (in Japanese).
- [8] H. Kanda, T. Kiuchi, and K. Matsumoto, "Loading test report of actual bridge test girder of new material PC Bridge," *Proc. 5th Symp. Prestress. Concr. Tech. Assoc.*, pp. 529–532, 1995 (in Japanese).
- [9] K. Niitani, H. Watase, K. Sakata, and K. Ayano, "Study on Estimation Method of Effective Stress of Concrete Members," *Pap. Concr. Eng.*, vol. 20, No.2, pp. 27–37, 2009 (in Japanese).
- [10] J. R. Martí-Vargas, L. A. Caro, and P. Serna, "Experimental Technique for Measuring the Long-term Transfer Length in Prestressed Concrete," *Strain*, vol. 49, no. 2, pp. 125–134, Apr. 2013.
- [11] Japanese Road Association, "Road-Bridge standard specifications I Common bridge III Concretebridge," p. 200, 2002.
- [12] Japanese Industrial Standards, "Methods of test for Chloride ion content in hardened concrete.," *JIS A 1154*, 2012.

Chapter 3. Numerical analysis on the flexural behavior of the prestressed concrete girder using CFRP tendons

3.1 Introduction

The reduction in the lifespan of concrete structures in bridges due to steel corrosion has become a significant problem, especially with structures built on the coast area. Since the 1980s, Japanese engineers have used Carbon Fiber Reinforced Plastic (CFRP) in the research to replace the conventional steel, counteract corrosion and enhance durability because of superior CFRP characteristics.

The durability and serviceability of structure using CFRP have been investigated since 1988 when the Shinmiya Bridge was built. This was the first bridge using CFRP tendons (CFRP strand of Tokyo Seiko Rope Mfg. Co., Ltd) in main girders both in Japan and in the world. The Shinmiya Bridge was built near the coastal line at the Shika town, Hakui district, Ishikawa Prefecture. The maximum precipitation per day in this area fluctuated from 51 mm to 144 mm from 1988 to 2017, the highest temperature was 38.7°C in 1999 and the lowest temperature was -8 °C in 1988. This area is one of the areas affected significantly by salt damage in Japan. Therefore, CFRP tendons were applied in the main girders of the prestressed concrete bridge in order to counteract the salt damage. In Shinmiya Bridge, two test girders were fabricated, placed next to the main girders, and exposed to the actual corrosive environment. After six years of construction time (1994), one of the girders was subjected to the bending test. The durability of the girder and CFRP tendons were confirmed. After nearly 30 years (2017), the second girder was also removed from the main bridge and subjected to the flexural experiment. The results of the load-carrying capacity and durability have been evaluated. They have been already shown in Section 2.5 of Chapter 2.

Nowadays, the development of the science and technology provided commercial soft-wares for numerical simulation with finite element method. These commercial soft-wares are effective tools and can be more economical in comparing with the investment for conducting experiments. The finite element method can be used to model various

combinations of geometric and loading conditions. Therefore, utilize of them became popular in architectural engineering and civil engineering field. This chapter aims to use numerical analysis to predict the flexural behavior of the prestressed concrete girder of Shinmiya Bridge, which reinforced by CFRP tendons and exposed to the actual environment after nearly 30 years. CFRP has linear elastic behavior, the model will support to observe the flexural response of the girder until the failure. The properties of the material used in modelling the girder were based on the experimental tests in Chapter 2. The results obtained from the finite element method was firstly compared with the results of the experiment to evaluate the accuracy of the model. Then, the fundamental model was proposed to study factors that can be affected the behavior of the girder.

3.2 Finite element model using LS-DYNA software

3.2.1 Overview of analysis

To obtain a deeper understanding of the variations in the structural behavior of the girder, numerical simulations were performed using the finite element method (FEM). The three-dimensional analysis model was built in LS-DYNA as shown in *Figure 3.1*. In the numerical approach, the models were first verified by comparing the elicited results with those obtained in real-scale tests. The emphasis here is on the methodology, i.e., on the identification of ways to apply FEM analysis to the CFRP girder that possesses new characteristics. Because the destructive test, itself encompasses nonlinear structural features and is associated with significant deformation, modelling the behavior of the specimen until the final state requires the consideration of both high-order geometrical and nonlinear mechanical parameters, particularly for the selected nonlinear models. The developed model considered the nonlinear mechanical properties of the materials. This

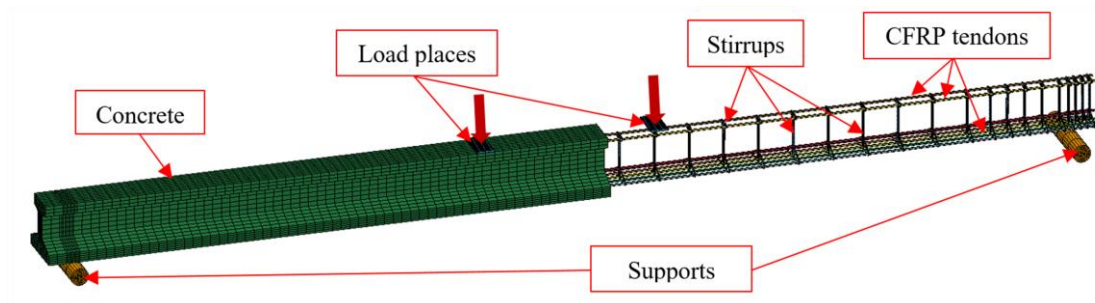


Figure 3.1 Three-dimensional analysis model for mountainside girder in LS-DYNA

model is closely as the experimental girder with five main part namely the supports, concrete beam, tendons, stirrups and the load plates.

3.2.2 Method for prestressed in tendon

Pre-stress can apply to the structure by many methods in LS-DYNA. In this study, applying a thermal gradient was employed for the tendons obtained the pre-stress. The decrease in the temperature in tendons causes shrinkage and tensile stress was creased in tendons. The material property of tendons with the variation of temperature was defined by using the material card *MAT_ELASTIC_PLASTIC_THERMAL (MAT 004) [1]. Following this card, the *LOAD_THERMAL_LOAD_CURVE card [1] was used for defining the relationship between time and temperature, two curves needed to add for this option. The dynamic relaxation phase was carried out by *DYNAMIC RELAXATION card [1] that required the first curve. This curve was a sudden decrease in temperature, it began from an initial temperature to a determined temperature and then the temperature kept constant. The second curve was used for an explicit phase; it was a constant temperature with time variation. The change in the temperature can be calculated from the following equation [2][3]:

$$\Delta T = \frac{f}{\alpha E_c A_c} + \frac{f}{\alpha E_t A_t} \quad (3.1)$$

Here, ΔT is the temperature change; E_c , E_t are respectively Young's modulus of concrete and tendons; A_c , A_t are respectively sectional area of concrete and tendons; α is the thermal expansion coefficient of the tendons. In this study, a temperature gradient of 1866.2°C was input for CFRP tendons to obtain the required pre-stress.

3.2.3 Material modelling

3.2.3.1 Constitutive model for concrete

Concrete was modelled by using solid eight-node element. The mesh size was considered the number of elements and the sensitivity analysis of mesh. In LS-DYNA software, there are various types of material for modelling concrete model, such as MAT_PSEUDO_TENSOR (MAT 016), MAT_CONCRETE_DAMAGE (MAT 072), MAT_CONCRETE_DAMAGE_REL3 (MAT 072R3), MAT_WINFRITH_CONCRETE (MAT 084/085) and

MAT_CONTINUOUS_SURFACE_CAP_MODEL (MAT 159) [1], each of these types has both of advantage and disadvantage. Concrete a pressure-dependent material, hence the general form of the yield function was be written as following.

$$Y(I_1, J_2, J_3) = 0 \quad (3.2)$$

In here, I_1 is the first invariant of stress tensor, which indicated volumetric responses; J_2 and J_3 are the second and third invariant of deviatoric stress tensor and they present for deviatoric responses. In general, the primary difference between concrete constitutive models is how the deviatoric and volumetric responses are mentioned.

In this study, *MAT 72R3_REL3 was employed for the simulation of concrete. The Karagozian & Case concrete model (KCC) - Release 3 is a plasticity, it has three independent strength surfaces including the maximum strength surface, yield strength surface and residual strength surface [1] (see *Figure 3.2*). The three surfaces denoted by $\Delta\sigma_y$, $\Delta\sigma_m$ and $\Delta\sigma_r$ represent the yield, maximum and residual stress difference, respectively, where $\Delta\sigma = \sqrt{3 \cdot J_2}$. The yield function is defined as:

$$Y(I_1, J_2, J_3, \lambda) = \sqrt{3 \cdot J_2} - \gamma(I_1, J_2, J_3, \lambda) \quad (3.3)$$

$$\text{where } \gamma = \begin{cases} r(J_3) \cdot [\eta(\lambda) \cdot (\Delta\sigma_m - \Delta\sigma_y) + \Delta\sigma_y] & \lambda \leq \lambda_m \\ r(J_3) \cdot [\eta(\lambda) \cdot (\Delta\sigma_m - \Delta\sigma_r) + \Delta\sigma_r] & \lambda > \lambda_m \end{cases} \quad (3.4)$$

where $\eta(\lambda)$ is nonlinear function that rangers from zero to unity for $\lambda \leq \lambda_m$ and from unity to zero when $\lambda > \lambda_m$ and λ is accumulated as a function of the effective plastic strain using three damage accumulation parameters: b_1 , b_2 , b_3 .

Three parameters a_{0i} , a_{1i} , and a_{2i} (9 parameters total for the three surfaces define each of failure surface as flowing equation.

$$F_i(p) = a_{0i} + \frac{p}{a_{1i} + a_{2i}p} \quad (3.5)$$

In here, p is the pressure-normal stress; F_i is the i^{th} of the three surface. For hardening, the plastic surface used in the model is interpolated between the yield and maximum surfaces based on the value of damage parameter, λ . For softening, a similar interpolation is performed between the maximum and residual surface. [4]

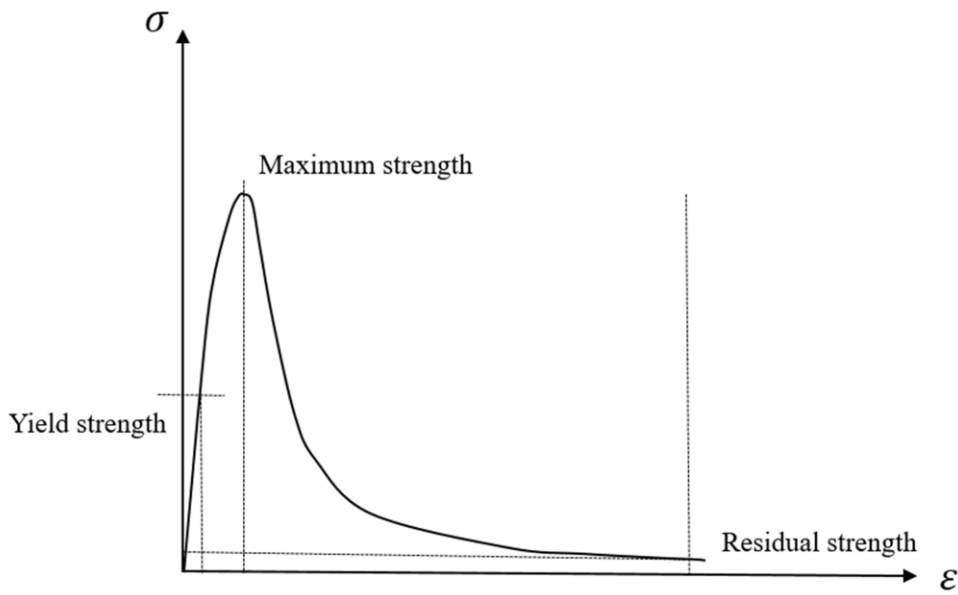


Figure 3.2 Stress-strain concrete behavior in LS-DYNA

To provide a simple users, this material card was developed, in which almost parameter can be generated automatically based on inputting only the unconfined compressive strength of concrete and density of concrete [4][5]. Moreover, this model obtained accurate results for analysing the concrete behavior in the prestressed concrete structure in the previous studies [6][3]. In this study, Young's modulus and unconfined compressive strength of concrete were collected from the results of the compressive test, which was carried out for specimens collected from the tested girder after the bending test as mentioned in Chapter 2. The parameters used in LS-DYNA to define concrete model shown in *Table 3.1*.

When the tensile stress in the concrete element reached the value that larger than the maximum initial tensile stress, the concrete element fails and removes from the model. *MAT_ADD_EROSION card [1] was used in this study to define the maximum initial tensile stress at failure.

3.2.3.2 Constitutive model for stirrup and CFRP tendons

The stirrups selected Hughes-Liu with 2x2 Gauss cross-section for beam elements and *MAT_PIECEWISE_LINEAR_PLASTICITY (MAT 003) [1] for the material. As while the CFRP tendons chose Hughes-Liu with 2x2 Gauss cross-section for beam elements with *MAT_ ELASTIC_PLASTIC_THERMAL (MAT 004) for material.

*MAT 004 was used to define the temperature-dependent material property for tendons and linked the keyword *LOAD_THERMAL_LOAD_CURVE to define the variation of temperature versus time. The parameters were input for stirrups and CFRP tendons as shown in *Table 3.1*.

3.2.3.3 Constitutive model for supports and plates

Solid element and *MAT_ELASTIC (MAT 001) [1] were employed for the support. This material model has the simple isotropic elastic behavior and can be used for any element type in LS-DYNA. The load plate used the shell element and *MAT_RIGID (MAT 020) card [1] was selected in numerical simulation. *Table 3.1* shows the input values for material properties of numerical model used to define these material models.

Table 3.1 Material properties of numerical model

Part	Material model card	Input parameter	Value	Unit
Concrete	*MAT 72R3 MAT_CONCRETE_DAMAGE_REL3	Mass density	2.30E-09	t/mm ³
		Unconfined strength	7.51E+01	N/mm ²
		Young's modulus	3.72E+04	N/mm ²
Tendon	*MAT 004 MAT_ELASTIC_PLASTIC_THERMAL	Mass density	1.99E-09	t/mm ³
		Young's modulus	1.33E+05	N/mm ²
		Poisson's ratio	0.3	
		Yield stress	2063	N/mm ²
		Plastic hardening modulus	1000	N/mm ²
		Thermal expansion coefficient	2.00E-06	
Stirrups	*MAT 003 MAT_PIECEWISE_LINEAR_PLASTICITY	Mass density	7.83E-09	t/mm ³
		Young's modulus	2.07E+05	N/mm ²
		Poisson's ratio	0.3	
		Yield stress	395	N/mm ²
		Tangent modulus	2000	N/mm ²
Support	*MAT 001 MAT_ELASTIC	Mass density	7.83E-09	t/mm ³
		Young's modulus	2.07E+05	N/mm ²
		Poisson's ratio	0.3	
Plate	*MAT 020 MAT_RIGID	Mass density	7.83E-09	t/mm ³
		Young's modulus	2.07E+05	N/mm ²
		Poisson's ratio	0.3	

3.2.4 Contact and boundary conditions

The bonding between the concrete, steel, and CFRP tendons was assumed a fully bond in this study. Because of the geometry characteristic, the node of concrete has not overlapped the node of reinforcement; shared nodes can be not modelled for the perfect bond in this case. Therefore, the card *CONSTRAINED_BEAM_IN_SOLID [8] was selected to couple beam element to solid elements. The slave nodes were defined for reinforcing beam nodes. Concrete nodes were indicated the master nodes. Coupling direction had defaulted on “0” which means the constraint along with all directions.

The interface for the contact between the supports and concrete, as well the load plates and concrete were defined by contact card *AUTOMATIC_SURFACE_TO_SURFACE [1]. This keyword allows creasing two surfaces that can connect the nodes on the surfaces during the duration of simulation. The compression load was transferred from the slave surface to the master surface. All directions of the supports were constrained moving and rotating.

3.2.5 The analysis method

Normally, the quasi-static problem was solved by the implicit finite element method. However, it is sometimes difficult to converge on the model of nonlinear and progressive damage failure [6]. Therefore, the explicit finite element method was chosen in this study. The stress and strain of nodes in the model was calculated in LS-DYNA at small time steps during the duration of the analysis. The number of time-step in explicit method was calculated from the theory of LS-DYNA depend on the stiffness, density of materials and element length in the model. If the model has two or more material, the LS-DYNA software will calculate the shortest time-step and use for analysis.

Control displacement was performed instead of control load or acceleration in this simulation. The analysis was carried out by applying incremental displacement via keyword *BOUNDARY_MOTION_RIGID [1].

3.2.6 Comparison between analytical and experimental results

The comparison between numerical and experimental results was done to evaluate the accuracy of the finite element method. Load-bearing capacity, the curve of applied load versus middle span deflection, and crack pattern were the objects in this evaluation.

Figure 3.3 shows the relationship between the applied load and middle-span deflection obtained from the experiment (EXP) and simulation (FEM). Overall, the trend of the analytical curve was similar to the experimental curve from the beginning to the failure. The value of yield load, which was the value transferred between the elastics stage and plastic stage, was modelled well. However, both of the ultimate load and middle-span deflection predicted from the numerical analysis slightly higher than these values in the experiment. The finite element model predicted the load-bearing capacity and middle span deflection at the failure of the tested prestressed concrete girder were 158 kN and 91 mm, respectively. In fact, these numbers in the results of the experiment were 157 kN of the ultimate load and 84 mm of the displacement in the central of the span.

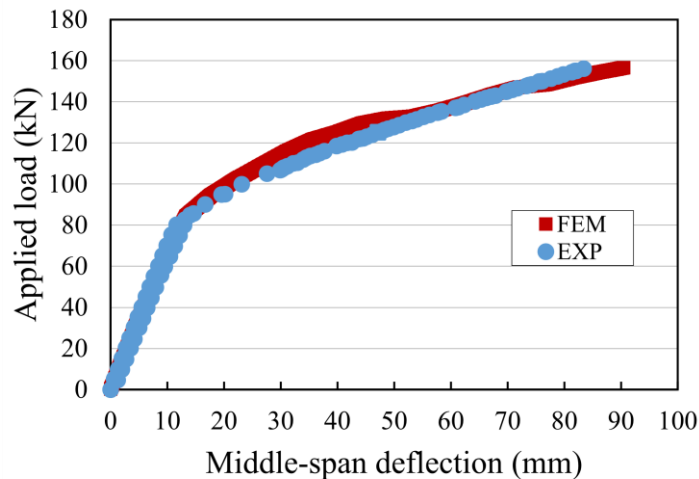


Figure 3.3 Relationship between applied load and displacement

Crack pattern of the prestressed concrete girder at the failure stage cannot be directly shown because concrete model KCC is unable to track cracks. However, the cracks can be equivalently illustrated by effective plastic strains. Deformation and strain situation in several stages of the simulation were shown in *Figure 3.4*. Firstly, the strain changed in the middle of the span in the tensile zone when load was applied. Then, these strain expanded and developed higher to the compressive zone. Finally, the failure model of the tested girder was crushing of concrete in the compressive zone as the observation in the experiment. It is seen that the area with the distribution of the change of deformation and strain agree well with the experiment ones, respectively.

In summary, the good agreement of numerical analysis and experiment results indicates the validity of the numerical model. The model is fundamental to investigate the effect of parameters.

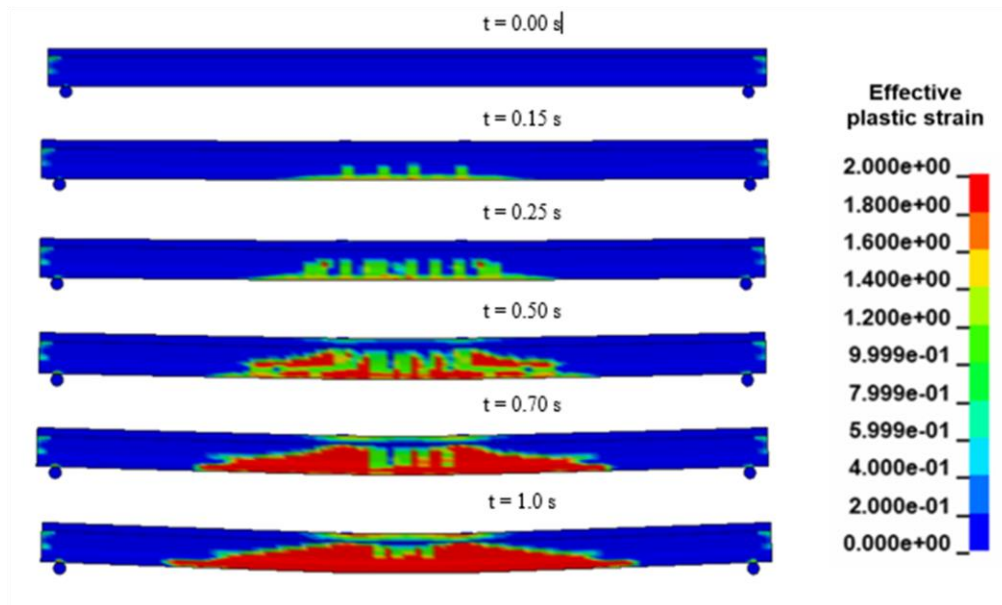


Figure 3.4 Deformation and strain situation in several stages of simulation

3.2.7 Parametric study

3.2.7.1 Overview

This section studied the effect of the prestressing force in tendons to the change of the behavior of the tested girder. The pre-stressing loss varied from 10% to 30% of the initial prestressing force of the girder. In addition, the influential parameter in the performance of concrete is compressive strength. In this section, a reduction of 10% and 30% in compressive concrete strength was studied to consider the effect on the behavior of the structure.

3.2.7.2 Effect of the pre-stressing force in tendons.

In Figure 3.5, the relationship between the load and deflection in the mid-span in case of the initial pre-stress is showed in the red curve. The yellow curve and green curve are those relationships when the pre-stress losses 10% and 30%, respectively. According to Figure 3.5, the deflections in the mid-span obtained from three studied cases are quite similar. However, the inclination angle in the plastic stage has a lower trend and the load-

bearing capacity of the girder decreases significantly when the pre-stress in the tendons was reduced. This difference in load-bearing capacity is small, which is just around 4% when the pre-stressing loss was 10%. Whereas, this change quickly climbed to 12.2% when the pre-stressing loss was 30%.

It can be confirmed that the level of pre-stress in the tendons significantly affects the behavior of the prestressed concrete girder, especially load-bearing capacity as shown above. The pre-stressing level is an important factor that needs to consider and record in future research.

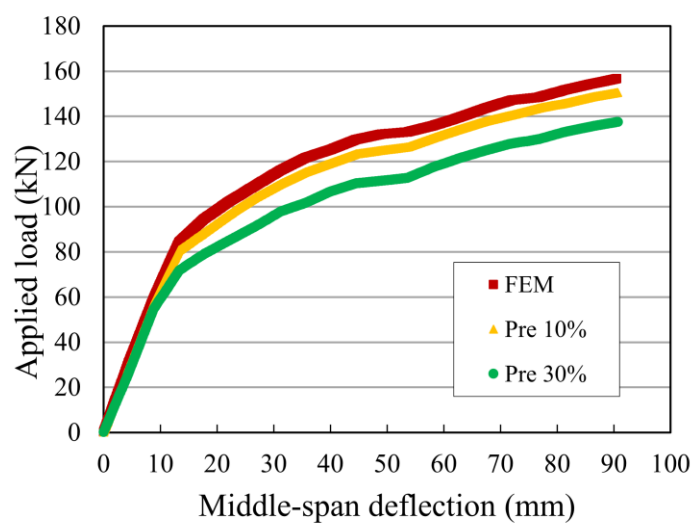


Figure 3.5 Relationship between applied load and middle-span deflection in case of prestressing decrease

3.2.7.3 .Effect of the reduction in compression concrete strength

According to *Figure 3.6*, the behavior of the experimental girder in the original simulation the red curve was compared with the case of the reduction of 10% in compressive concrete strength (the blue curve) and the case of the reduction of 30% in compressive concrete strength (the black curve). In LS-DYNA, the input parameters of concrete are interconnected. Therefore, when the compressive strength of concrete decreases, Young's modulus of concrete will also decrease. This is a reason for the phenomena that the angle of inclination in the elastic phase is different between the three relationship curves. These inclination angles tend to be smaller when the compressive strength of concrete decreases. This change is the starting point of changes in later stages

of girder behavior. The load-bearing capacity of the girder declined by 1.34% and 8.87% when the compressive concrete strength reduces by 10% and 30%, respectively.

Based on the above discussion, it can be seen that the reduction in the load-bearing capacity of the prestressed concrete girder in the cases of pre-stressing loss is higher than in the case of compressive strength reduction.

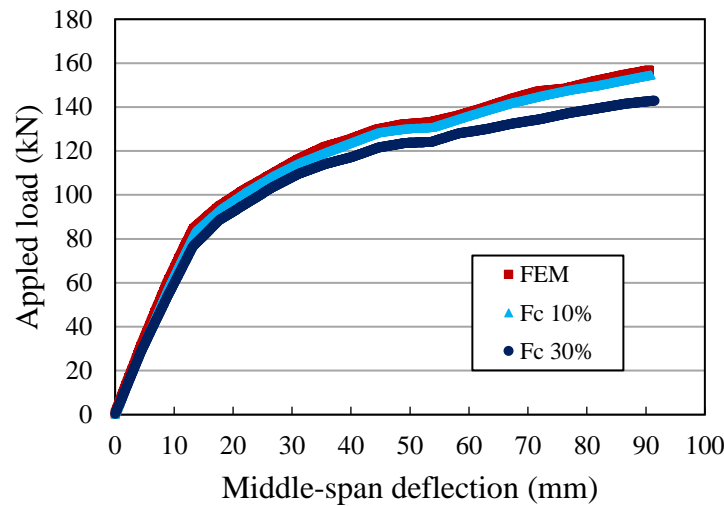


Figure 3.6 Relationship between applied load and middle-span deflection in case of middle-span deflection in case of decrease of concrete strength

3.3 Finite element model using DIANA software

3.3.1 Overview of this model

The flexural behavior of the prestressed concrete girder was investigated by LS-DYNA software in the first part of this chapter, the results show the good agreement between experiment and simulation. Furthermore, the model was the fundamental model for studying some factors namely prestressing force, compressive strength of concrete to the change in structural behavior. However, the final behavior of this girder continues to be performed by the second laboratory software in this part of the chapter with the other approach. The numerical model was developed using DIANA and validated by experimental result. Constitutive materials, contact between components were selected compatibly with this software. Instead of the pre-stressing load was assigned to CFRP by temperature variations included shrinkage in pre-stress strand in the first phase of analysis, the pre force was applied to pre-stress in this study. The force control changed to the

displacement control as another factor in analysis method. The constitutive models and element types were carefully selected to model the experimental behavior of the prestressed concrete girder

As shown in *Figure 3.7*, a three-dimensional (3D) numerical model is produced in accordance with the specifications of the actual specimen using FX+ in DIANA, which is a commercially available program used for nonlinear FE analyses.

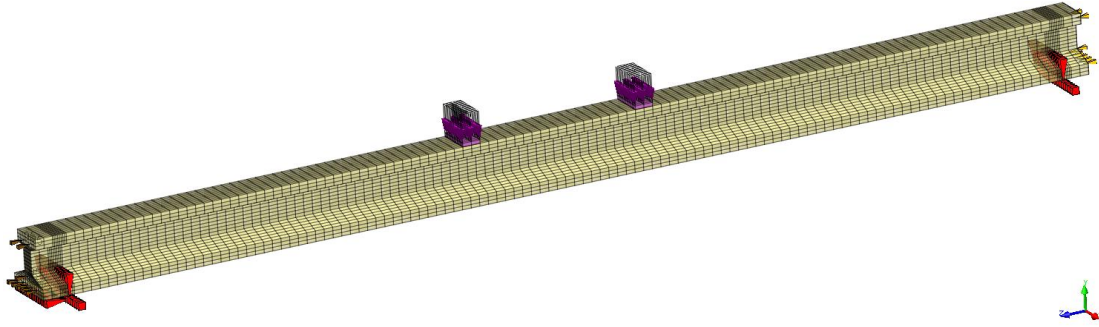


Figure 3.7 Three-dimensional (3D) analysis model for the CFRP girder in DIANA

3.3.2 Material properties of concrete and steel

3.3.2.1 Concrete

Concrete was modelled using solid element. The rotating total strain crack model for concrete [7] was employed in this study, which includes the JSCE tension softening model for tensile behavior, and the multilinear model for compressive behavior. The parameters of concrete for the rotating strain crack model are presented in *Table 3.2*. Specifically, the Young's modulus and compressive strength of concrete were obtained from compression tests on concrete cores collected from the test specimens. The multilinear model was utilized to reproduce the compression stress-strain relationship of the concrete, as shown in *Figure 3.8 (a)*. Moreover, the critical parameters governing the JSCE tension softening model for tensile behavior (see *Figure 3.8 (b)*) were the fracture energy and tensile strength of concrete. The fracture energy of concrete is the energy consumed to form cracks per unit area and is calculated based on equation (6) [8].

$$G_f = 10(d_{\max})^{(1/3)} f_{ck}^{(1/3)} \quad (3.6)$$

where G_f , d_{\max} , and f_{ck} are related to the fracture energy (N/mm), maximum aggregate size (mm), and compressive strength of concrete (N/mm²), respectively. In the

present study, the value of d_{\max} is assumed to be equal to 20 mm. Additionally, owing to the absence of experimental data, the estimation of the tensile strength of concrete f_{tk} can be performed using equation (7), based on the characteristic compressive strength f_{ck} [8]. The unit of strength is N/mm^2

$$f_{tk} = 0.23 f_{ck}^{(2/3)} \quad (3.7)$$

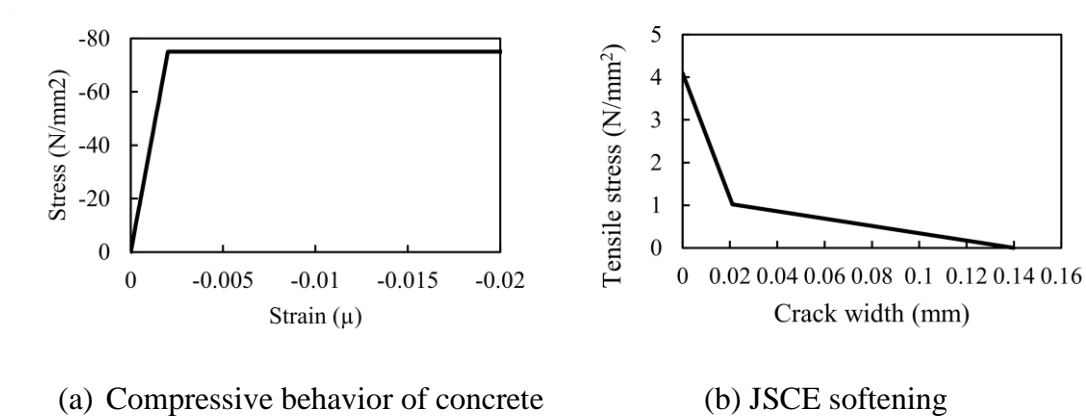


Figure 3.8 Stress-strain curve for concrete in DIANA

Table 3.2 Concrete properties for FE analyse

Young's modulus (kN/mm^2)	Poisson's ratio	Compressive strength (N/mm^2)	Tensile strength (N/mm^2)	Maximum size of coarse aggregate (mm)	Fracture energy (N/mm)
37.2	0.2	75.1	4.09	20	0.1145

3.3.2.2 Steel

The stirrups were assumed to have the same Young's modulus as the linear elastic material model, $E_s = 207000 \text{ N/mm}^2$, and the same Poisson's ratio, $\nu = 0.3$. The Von Mises that is an elastic-perfectly plasticity was employed to simulate the behaviors of CFRPs. Specifically, the CFRP was defined by a property with a Young's modulus of $E_s = 132500 \text{ N/mm}^2$ and Poisson's ratio of $\nu = 0.3$. The yield stress was defined as 2063 N/mm^2 based on results of the tensile test. Regarding the prestressing force, a value of 931 N/mm^2 was assigned to the CFRP. In addition, the prestress was applied to the numerical model as the initial stress at the execute start step.

Regarding the element types used in the analyses, the embedded steel reinforcement elements reproduced the stirrups and CFRP. Therefore, the bond between steel, CFRP and surrounding concrete was perfect.

3.3.3 The analytical method

The energy-controlled convergence norm and regular Newton–Raphson were selected as the iterative methods. The analysis was carried out by applying incremental load factors with specified sizes. To facilitate simulation, several simplifying assumptions for the mechanical properties of the materials and supports were adopted.

3.3.4 Comparison between analytical and experimental results

The evaluation of the accuracy of the simulation result was made by comparison with the experimental result, including the ultimate load, middle span deflection, and the failure mode, crack pattern. The relationships between the applied load and displacement of the girder predicted from the numerical simulation was compared with the results obtained from the experiment in *Figure 3.9*. There was a reasonable consistency between the experimental and simulation results. In the elastic stage, the load values increase linearly with the deflection. The predicted result of the FEM model was close to the experimental result in terms of both the load and deflection. In the plastic stage, the load-displacement curve in the FEM analysis showed a similar trend to that obtained in the experiment, which provided a slightly higher inclination angle compared to the numerical result. The experimental value reached the final load of 157 kN, and the value of the

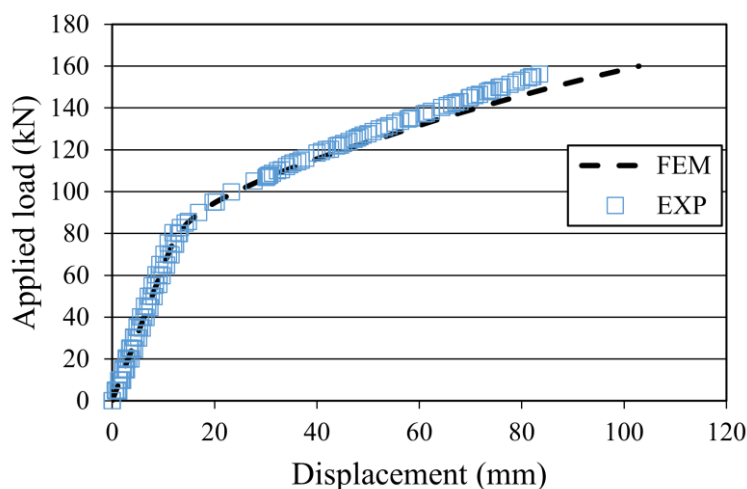


Figure 3.9 Load-displacement relationship at the middle of span

displacement in the center of girder was 84 mm. Regarding the numerical results, the applied load was estimated to be 160 kN at the corresponding the maximum displacement of 110 mm.

The failure mode in the simulation result was the compressive failure, which was similar to the experiment result. In addition, *Figure 3.10* shows the crack patterns of the girder from the DIANA analysis and bending test. The ranges of the appearance of bending cracks and shear cracks in the actual test was similar to results by the analysis. The first cracks were seen in the flexure area after new flexure and shear cracks occurred when the load increased. These cracks tended to expand the compression zone.

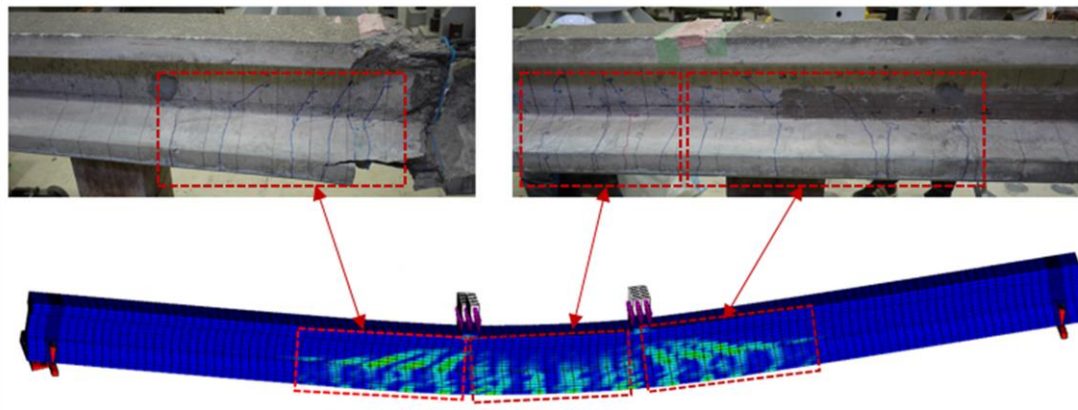


Figure 3.10 Crack pattern due to loading test and DIANA predicted

The numerical results agreed well with those obtained from the experiment. Therefore, the proposed model could provide a reasonable outcome. This work is a fundamental first step in the parametric analyses presented in the following section.

3.3.5 Parametric study

3.3.5.1 Overview

To deeply understand the results of the loading experiment in Chapter 2, the difference in the results obtained by the loading test in this study and the experiment conducted in 1994 and predict the behavior change of the girder in future. This section considers the factors influencing the results of the numerical simulation as well as the behavior of the structure by ten simulation models as shown in *Table 3.3*. First, the model was analyzed when different input data were set for parameters. Second, the behavior of

the structure was examined when the parameters of the main material were changed. Finally, the difference in the simulation was performed with or without the bond-slip

Table 3.3 Cases to parametric study

Case study	Material properties						Bond-slip behavior
	Concrete			CFRP			
	Compressive strength	Elastic modulus	Tensile strength	Fracture energy	Breaking load	Elastic modulus	
	(N/mm ²)	(kN/mm ²)	(N/mm ²)	(N/mm)	(kN)	(kN/mm ²)	
Reference case: Concrete average + CFRP average	75.1	37.2	4.1	0.1145	156.8	132.5	
Case 1: Concrete average + CFRP max	75.1	37.2	4.1	0.1145	161	132.6	-
Case 2: Concrete average + CFRP min	75.1	37.2	4.1	0.1145	148.6	130	-
Case 3: Concrete max + CFRP average	79.8	39.7	4.3	0.1168	156.8	132.5	-
Case 4: Concrete min + CFRP average	70.4	34.6	3.9	0.1121	156.8	132.5	-
Case 5: Concrete average + CFRP,E=0.8	75.1	37.2	4.1	0.1145	156.8	106	-
Case 6: Concrete E=0.8 + CFRP average	75.1	29.8	4.1	0.1145	156.8	132.5	-
Case 7: Concrete average + CFRP,T=0.8	75.1	37.2	4.1	0.1145	125.4	132.5	-
Case 8: Concrete C=0.8 + CFRP average	62	37.2	3.6	0.1074	156.8	132.5	-
Case 9: Concrete average + CFRP average, Bond-slip model 1	75.1	37.2	4.1	0.1145	156.8	132.5	DSSY=2 975220 N/mm ³ > DSSX=6 48.11 N/mm ³
Case 10: Concrete average + CFRP average, Bond-slip model 2	75.1	37.2	4.1	0.1145	156.8	132.5	DSSY= DSSX=2 975220 N/mm ³

model for the CFRP tendon.

In Chapter 2, to investigate the compressive strength of concrete, the samples were taken at two different positions on the girder. In addition, four samples were tested to determine the tensile strength of the CFRP. Each sample gave one data on the characteristic of the material. Thus, model cases 1, 2, 3, and 4 were used to study the change in the simulation results when the difference of material characteristic was selected for input parameters. Case 1 used the average result for concrete and the largest data in the CFRP parameters. Case 2 was the combination of the average data set of concrete and the smallest CFRP data set. The largest and smallest data sets for concrete were combined with the average data of CFRP set in cases 3 and 4, respectively.

For clarifying the behavior of the girder, cases 5, 6, 7, and 8 were conducted with a modification of the strengths and moduli of the materials. Specifically, in cases 5 and 6, the simulation model used the input data with a 20% modulus reduction in the CFRP and concrete, respectively. In contrast, when the modulus was unchanged, the tensile strength of the CFRP was only 80% of the average tensile strength in case 7. Regarding the concrete in case 8, the modulus was maintained, the compressive strength decreased by 20%, and the tensile strength and fracture energy decreased.

Another highlight of this study is the implementation of a bond-slip reinforcement instead of the regular embedded model. Cases 9 and 10 were added to study the bond-slip model in DIANA. The difference in the ultimate behavior in the cases where the CFRP tendons were produced with and without bond-slip properties was investigated. Bond is the expression used to express the interaction and transfer of force between reinforcement and concrete. An excellent bond no longer exists between the concrete and reinforcement bars. Therefore, the bond-slip reinforcement models are valid when there is a relative displacement between the concrete and reinforcement nodes. Bond slip was introduced to the numerical model by defining a bond-slip material. The bond-slip reinforcement elements reproduced the stirrups and CFRPs [7]. Regarding the bond-slip interface failure model, this study applied the cubic function according to Dörr (Dörr 1980) to describe the relations between shear traction and slip. In particular, Dörr proposed a polynomial relationship between shear traction and slip, which shows a limit if the slip is larger than a specific value, Δu_t^0 . This bond-slip law is given by a cubic function:

$$t_t = \begin{cases} c(5(\frac{\Delta u_t}{\Delta u_t^0}) - 4.5(\frac{\Delta u_t}{\Delta u_t^0})^2 + 1.4(\frac{\Delta u_t}{\Delta u_t^0})^3) & 0 \leq \Delta u_t < \Delta u_t^0 \\ 1.9c & \Delta u_t > \Delta u_t^0 \end{cases} \quad (3.8)$$

where t_t denotes the bond stress, value c is the parameter c , and value Δu_t^0 is the shear slip Δu_t^0 at which the curve reaches a plateau. DIANA recommends using $c = f_{tk}$; thereby, the maximum value for the shear traction t_t equals $c = f_{tk}$, in which f_t is the tensile strength of the concrete (N/mm²). Moreover, the recommended value for Δu_t^0 is 0.06 mm. *Figure 3.11* shows the cubic bond-slip curve employed for the bond-slip interface failure model in this study.

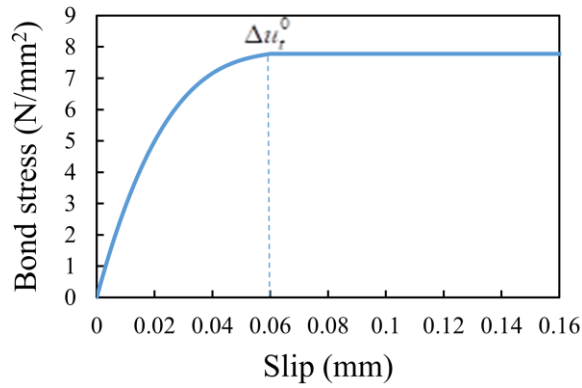


Figure 3.11 Bond stress-slip relationship

In addition, interface elements in bond-slip models require the input of the linear stiffness parameters, which are the shear stiffness, DSSX, and the normal stiffness, DSNY. In particular, DSSX sets the relation between the shear traction and the relative shear displacement in the x-direction of the reinforcement [10]. The relationship between the normal traction and normal relative movement in the y-direction reinforcement was described by DSNY [10]. The dimension of the stiffness moduli is force per area per length, i.e., stress per length, e.g., N/mm³. Regarding the cubic bond-slip formulation, the shear stiffness is calculated at the plateau of bond-slip curve, which corresponds to a slip of 0.06 mm. The formula for DSSX calculation for the cubic bond-slip formulation was proposed by DIANA [10] as the following.

$$DXXS = 5 \frac{1.9 * f_{tk}}{\Delta u_t^0} \quad (3.9)$$

where $DXXS$, f_{tk} , and Δu_t^0 stand for the shear stiffness (N/mm³), tensile strength (N/mm²), and shear slip at which the curve reaches a plateau (mm), respectively.

Regarding the normal stiffness calculation, this study employs an approach proposed by Eriksen and Kolstad [11], which assumed that $DSNY$ is the concrete resistance of the reinforcement penetrating and crushing the concrete. $DSNY$ was obtained for each CFRP tendons using equation (10).

$$DSNY = \frac{E_c}{2R} \cdot 10^3 \quad (3.10)$$

where $DSNY$, E_c and R are related to the normal stiffness (N/mm³), Young's modulus (N/mm²), and the radius of each tendon (mm), respectively. In the case 9, $DSNY$ was higher than $DXXS$ while $DXXS$ and $DSNY$ were almost equal in case 10.

To compare the different simulation scenarios, the results of the original model described in Section 3.3.2 to 3.3.4 were employed as the reference values, and the results obtained when the concrete reaches its extreme concrete compression fiber strain of 0.0035 were the comparison values [12].

3.3.5.2 Results and discussion

Compressive failure mode was observed in ten cases of simulation and all of them were similar to the result obtained from the experiment. The following paragraphs discuss the ultimate load and displacement between simulation cases and the reference case.

Figure 3.12 (a) serves to compare the simulation results of the reference case and case 1, case 2 that the input data of CFRPs included the ultimate load and elastic modulus were changed corresponding to the tensile specimens of CFRPs obtained the maximum and minimum breaking force values. Overall, there was no change in the simulation result among the three cases. The result of case 1 was similar to the results of case 2 and close to the reference case. The ultimate load of the girder was 160 kN and 159kN in case 1 and case 2, respectively. These results may be due to the small difference between the parameters of the three studied cases.

Regarding cases 3 and 4, the input data was based on the results of the concrete compression test after the bending test. For each sample, the compressive strength, elastic modulus, and Poisson's ratio were used as the properties of concrete in DIANA, and the results are shown in *Figure 3.12 (b)*. It can be seen that these parameters almost affected

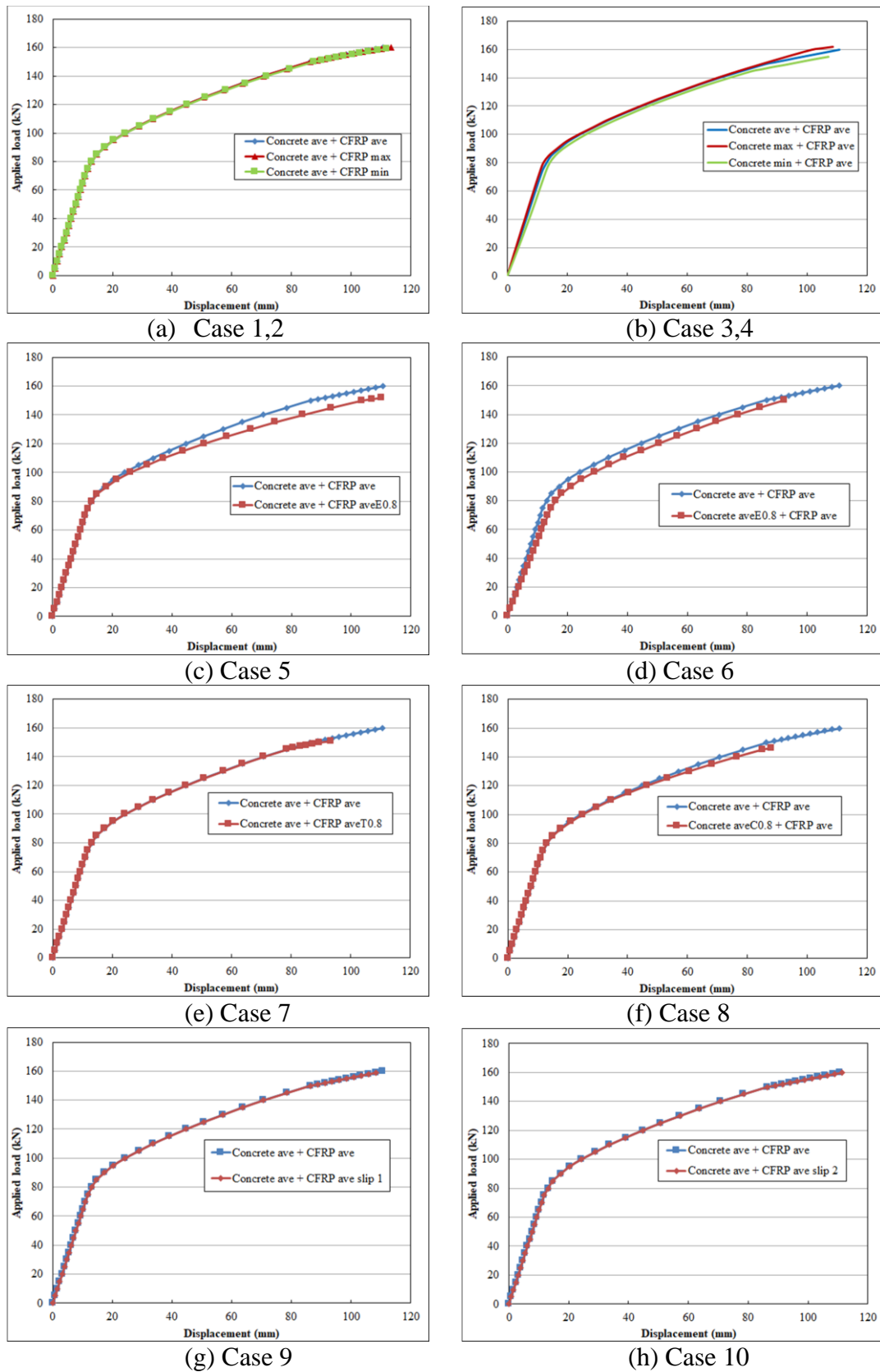


Figure 3.12 FE-predicted the load-displacement relationships

the simulation scenarios, but this difference was small at the inclination angle of the elastic stage and the ultimate load of the girder compared to the reference model. The ultimate loads in case 3 and case 4 were 161 kN and 155 kN, respectively.

From the above analysis, it can be concluded that the position of the samples and sample experiments, which provide input data to the model, as well as the accuracy of the numerical simulation method, play an important role in generating the results.

Figure 3.12 (c) and *Figure 3.12 (d)* show the simulated results when the elastic moduli of the CFRP and concrete decreased by 20% in case 5 and case 6, respectively. In addition, *Figure 3.12 (e)* and *Figure 3.12 (f)* show the simulation results of cases 7 and 8, in which the breaking force of the CFRP decreased by 20% and the concrete compressive strength reduced by 20%, respectively. In *Figure 3.12 (c)*, no significant change was observed in the elastic stage after changing the CFRP parameters. However, in the plastic stage, there was a significant difference between the load-displacement relationships. The inclination angle in case 5 was lower than that in the reference case. In contrast, in *Figure 3.12 (d)*, when the modulus of concrete decreased, there was a significant change in the load-displacement relationship in both stages. As the modulus of the concrete decreased, the initial stiffness of concrete reduced, thereby the inclination angle in the elastic stage of the load-displacement curve decreased. The final load of the girder in this case at 150 kN was also lower than the value in the reference case.

In case 7, the decrease in the CFRP breaking force caused the load-carrying capacity to decrease to 152 kN, as shown in *Figure 3.12 (e)*. However, the displacement in this case (98 mm) was lower compared to case 5. *Figure 3.12 (f)* also shows the change in the relationship between the load and displacement of the girder in case 8. The decrease in the concrete compressive strength caused a corresponding decrease in the tensile strength of the concrete and fracture energy. The change in the shape of the load-displacement curve occurred significantly in the plastic stage. In addition, the ultimate load of the girder was predicted to be 145 kN; this number was 9% lower than that in the reference model.

Based on the above discussion, the change in the modulus and strength of the concrete and CFRP have a significant impact on structural behavior.

Figure 3.12 (g) and *Figure 3.12 (h)* depict the load-displacement relationship of the reference case and bond-slip models 1 and 2, respectively. There was a slight

difference in case 9 when the ultimate load was lower than that in the reference case. However, when shear stiffness increased highly, equal to the value of normal stiffness, this difference became quite small. The result in case 10 with bond-slip of was similar to the numerical result with the embedded model. The initial crack occurred in the load step from 80–85 kN in both cases while the load value in the experiment was 82.8 kN. Therefore, the model, which was selected for simulation namely bond-slip of Dörr model or embedded model, also have affected to the results of numerical simulation.

3.4 Conclusion

In this chapter, the flexural behavior of the prestressed concrete girder reinforced by CFRP tendons was clarified and deeply understood by numerical models. The outcomes of the research are summarized as follows:

(1) The proposed modelling method using LD-DYNA and DIANA software were effectively employed to predict the structural behavior of the girder. Each software has the advantage to help to observe the behavior and failure mode of the girder clearly. In comparing with the experimental results regarding load-bearing capacity, relationship between applied load and middle span deflection, and crack pattern, the results from the numerical analysis have a consistency with the results from the experiment. The model by finite element method can be used to understand the overview of the complex behavior and phenomena appeared in the test girder.

(2) The fundamental model proposed by LS-DYNA predicted the behavior of the girder using CFRP tendons when the prestressing force in the tendons and compressive strength of concrete reducing of 10% and 30%. The analysis results were shown that the load-bearing capacity would reduce significantly, when the pre-stressing loss occurs. These values are lower in case of the concrete strength decreases. This study can be used to guide for future research regarding the behavior of the girder

(3) From the results of the parametric studies by a model built-in DIANA, the position of the samples for fundamental test namely tensile and compressive experiments affected the results and the accuracy of the numerical simulation. These factors provided directly the input data for the numerical simulation. Unlike the model in LS-DYNA, the model built in DIANA can consider the change of each property in each material. Therefore, the model in this study have the changes, in which the modulus, the strength of concrete or CFRP was set to reduce

in a sequence. The FEM result showed that the final load of the girder decreased, and the relationship between the load and displacement changes in above cases. The models in these cases are an effective basis to predict the robustness of the main girders in the future. The model of the bond-slip case also studied in this part. The result from numerical simulation indicated that having a slight difference between the perfect bond model and bond-slip model in this study.

3.5 References

- [1] LS-DYNA, “Keyword user’s manual.” Livermore Software Technology Corporation, 2016.
- [2] H. Jiang and M. G. Chorzepa, “An effective numerical simulation methodology to predict the impact response of pre-stressed concrete members,” *Eng. Fail. Anal.*, vol. 55, pp. 63–78, 2015.
- [3] T. V. Do, T. M. Pham, and H. Hao, “Numerical investigation of the behavior of precast concrete segmental columns subjected to vehicle collision,” *Eng. Struct.*, vol. 156, pp. 375–393, Feb. 2018.
- [4] Y. Wu, J. E. Crawford, and J. M. Magallanes, “Performance of LS-DYNA Concrete Constitutive Models,” *12th Int. LS-DYNA Users Conf.*, no. 1, pp. 1–14, 2012.
- [5] J. M. Magallanes, Y. Wu, L. J. Malvar, and J. E. Crawford, “Recent improvements to release III of the K&C concrete model,” in *11th International LS-DYNA User Conference*, 2010, no. 1, pp. 37–48.
- [6] F. A. Tavarez, L. C. Bank, and M. E. Plesha, “Analysis of fiber-reinforced polymer composite grid reinforced concrete beams,” *ACI Struct. J.*, vol. 100, no. 2, pp. 250–258, 2003.
- [7] DIANA, “User’s manual of FX+ for DIANA version 9.6.” April 2017, 2017.
- [8] JSCE, “Japan Society of Civil Engineers Concrete Committee, Standard specifications for concrete structures: design code,” *Concr. Comm.*, 2012.
- [9] K. DÖRR, “Ein Beitrag zur Berechnung von Stahlbetonscheiben unter besonderer Berücksichtigung des Verbundverhaltens,” University of Darmstadt, 1980.
- [10] DIANA FEA BV, “User’s Manual. Release 10.2.” 2017.
- [11] M. Eriksen and M. Kolstad, “Investigation of Cracking Behavior in Reinforced Concrete Panels with Bond-slip Reinforcement,” 2016.
- [12] Japanese Road Association, “Road-Bridge standard specifications I Common bridge III Concretebridge,” p. 200, 2002.

Chapter 4. Fundamental pull-out experiment for cast-in-place joint of precast concrete slabs reinforced by CFRP

4.1 Introduction

Reinforced concrete structure is a combination of concrete and reinforcement to enhance a bearing capacity of the structure through the advantages of two materials. These structures are widely used in construction field. However, the fact has shown that concrete structures in the natural environment increasingly appear of damages and their early degradation, especially the attack of corrosion phenomenon in the reinforcement in the salt damage environment as shown in *Figure 4.1*.



Figure 4.1 Salt damage due to flying salinity in Hokuriku region

New methods and materials such as epoxy-coated steel, stainless steel and cathode protection have been studied and proposed to overcome this problem. However, they still have disadvantages in terms of efficiency, complexity and long-term durability. At the same time, the development of composite materials has given a new answer for this difficult problem. FRP is known as a new material to replace reinforcement in concrete structures, which can significantly increase the service life of structures by reducing

concrete deterioration due to corrosion [1]. Researchers have found that Carbon Fiber Reinforced Plastic (CFRP) has outstanding characteristics in comparing to conventional reinforcement as high corrosion resistance, lightweight, and high tensile strength [1].

With advantages in characteristics, CFRP has been applied in the precast concrete components. Using CFRP for precast concrete slabs not only mitigate resists the steel corrosion improves the durability and serviceability of the structures but also reduces structural weight. The weight of CFRP is about 1/5 weight of conventional steel [2]. In addition, the amount of concrete that covers of slabs will reduce significantly when CFRP applies in precast slabs. The change in the structural weight leads to the difference request for structures foundation, the shape and architecture. Hence, using CFRP in precast slabs brings a great benefit for construction including technical, cost. The first bridge in Canada applied CFRP into part of concrete desk slabs in 1997 [3]. K.Charlesson et al. were conducted the experiment with full-scale model (7200 mm x 2950 mm x 200 mm) of the concrete desk slab reinforced with CFRP (Leadline) in replacement of the conventional steel. The result of the research of T.Hassan el al in 1999 also recommend the suitable of using CFRP and GFRP for bridge desk slabs [4].

However, as in the conventional reinforced concrete, the wet joints (cast-in-place joints) of these precast structures are always a matter that needs concern. The joint was expected that the shortest possible width, the high durability of structure, saving the time, and saving the cost of labor.

To develop the precast concrete slabs using CFRP, this study focuses on investigating the method to enhance the durability of the joint and reducing the width of the joint as short as possible by increasing the bond between CFRP and concrete in the joints as shown in *Figure 4.2*. A series of fundamental pull-out experiments were

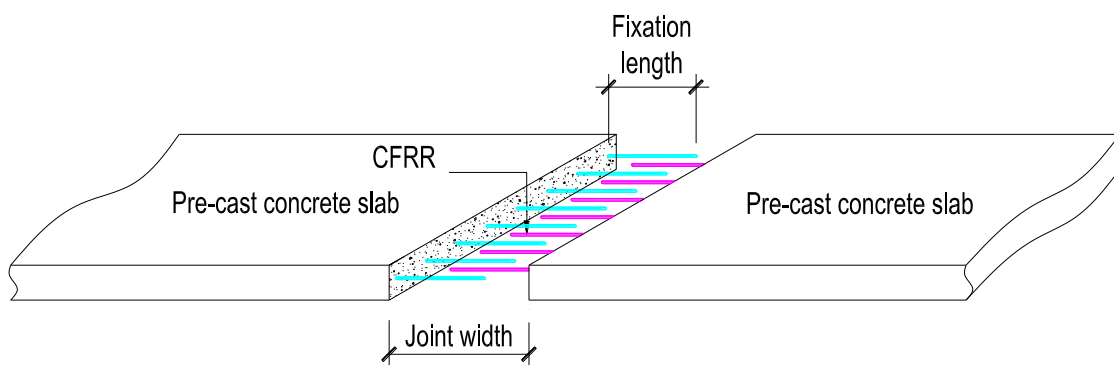


Figure 4.2 The cast- in-situ joint of precast concrete slabs reinforced by CFRP

conducted for the cast-in-place joint with the variation in the diameter of CFRP, the fixation length, and the method using CFRP in the joint. The results were discussed, the outcome was found, and the final proposal was showed.

4.2 The outline of fundamental pull-out experiment

The pull-out experiment was conducted following the method in JSCE-G503-2013. The universal test machine-Shimadzu corporation UH-1000kN was set up for this experiment as shown in *Figure 4.3*. The specimen was prepared with CFRP in the centre of concrete block. One at the end of CFRP was covered by steel pipe, which has the diameter and the length belongs to the specimen (see in *Table 4.4*). This steel pipe protected the CFRP from the gripping force of the machine. The other end of CFRP was attached a displacement meter (CDP5) to record the displacement of the tip of CFRP. Loading force was measured by a load cell (Tokyo Sokki Kenkuyjo Co., Ltd CLC-300KNA) during the time of the experiment.

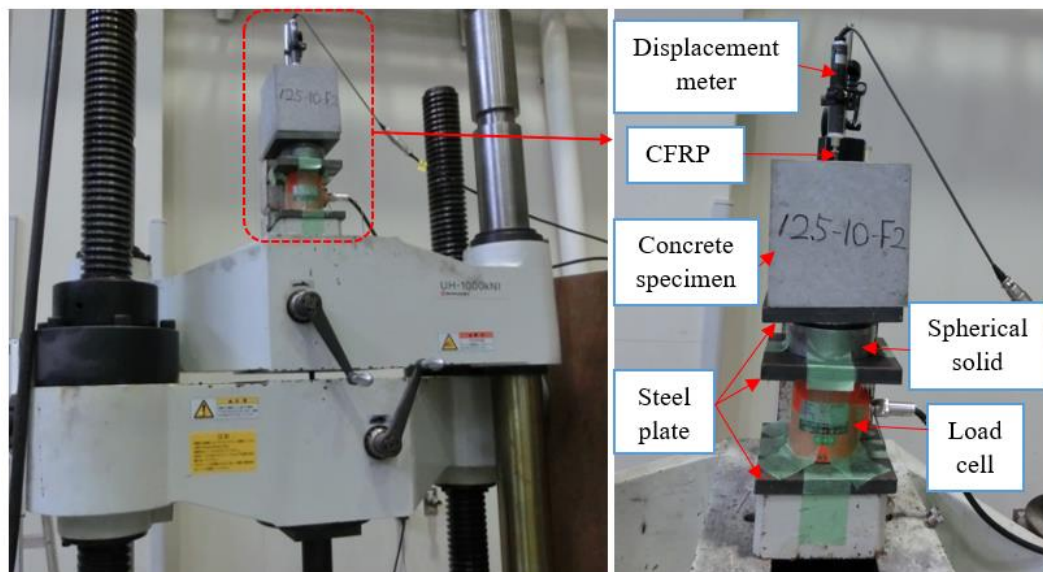


Figure 4.3 The set-up of pull-out experiment

4.3 The material of experiment

Specimens was prepared for the fundamental experiment with two main materials including concrete and CFRP. The difference in these specimens was CFRP diameter, the fixation length, and the method using CFRP in the joint.

4.3.1 Concrete

Concrete was mixed with fly ash, and designed for standard compressive strength of 50 N/mm^2 . The detail of compounding of concrete was shown in *Table 4.1*. In here,

- G_{\max} is maximum aggregate size;
- W/B is water-binder ratio;
- W is water;
- B is powder amount, and it was calculated as the following equation $B=C+EX+FA$; EX is expansion agent;
- C is early-strength Portland cement;
- FA15 is fly ash from Hokuriku Electric Power Nanao with rate 15%;
- s/A is fine aggregate percentage; S (fine aggregate) and G (coarse aggregate) are respectively crushed sand and crushed stone, they were from Sakurawaga, Ibaraki Prefecture;
- AE is high-performance AE water reducing agent.

Table 4.1 Standard specification of compounding of concrete

Slump (cm)	Air content (%)	G_{\max} (mm)	W/B (%)	W (kg)	B (kg)	EX (kg)
18	4.5	13	35	165	471.4	20
C (kg)	FA 15 (kg)	s/A	S (kg)	G (kg)	AE (kg)	Anti- foaming Agent (kg)
383.7	67.7	0.41	736.9	1060.5	3.3	14.1

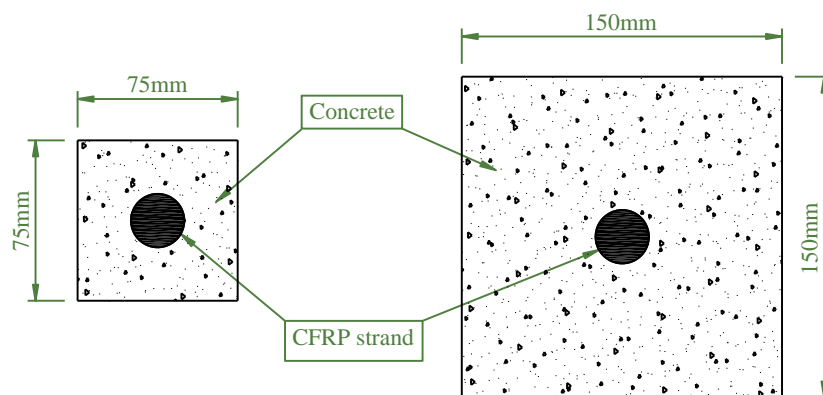


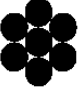
Figure 4.4 Cross-section size of the first, second, and third experiment

Two cross-sections were set for concrete block. Cross-section of 75mm x 75mm was cast in the first experiment and 150mm x 150mm was chosen for the second and third experiment as shown in *Figure 4.4*.

4.3.2 CFRP diameter

CFRP was used to replace the regular steel in precast concrete slabs in this study. A normal slab was reinforced by steel having a diameter of D16 or D19 corresponding with $\varnothing 10.5$ mm of CFRP because the tensile strength of CFRP has about five times that of ordinary steel reinforcement. However, to escape the excessive crack width in the high strength region, $\varnothing 12.5$ mm and $\varnothing 15.2$ mm of CFRP were selected and investigated in this study. *Table 4.2* summarizes the mechanical properties of CFRP from the manufacturer (Tokyo Rope).

Table 4.2 Standard specification of CFRP

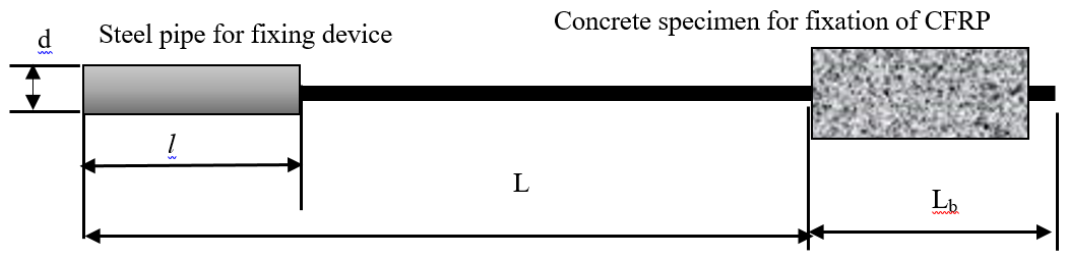
Cross-section of CFRP	Designations	Diameter (mm)	Effective cross-sectional area (mm ²)	Guaranteed capacity (kN)	Nominal mass density (g/m)	Tensile elastic modulus (kN/mm ²)
	7 strands	12.5	76	184	145	155
	7 strands	15.2	115.6	270	221	155

4.3.3 The fixation length

The fixation length means the part of CFRP inside of concrete specimen and it has the relationship with the width of the joint (see *Figure 4.2*). Normally, the width of the cast-in-place joint of the precast concrete slabs was roughly 600 mm when the conventional steel of D19 was used and the lap-splice method was chosen. If the width of the joint was shortened, the durability of the structure is still guaranteed, this work will save a lot of costs on materials, labour and construction time for a project. Furthermore, in previous studies show that the bond between CFRP and concrete was 7.32 MPa, which was two times larger than the value of the conventional steel [5]. Therefore, the fixation length in this study was designed to be CFRP diameter multiples of 10, 15 and 20 (10 \varnothing , 15 \varnothing and 20 \varnothing) (see *Table 4.3*) to investigate the reduction of the joint width.

Table 4.3 Size of specimens

	Fixation length (mm)	d (mm)	ℓ (mm)	L (mm)	L_b (mm)	Total length (mm)
CFRP $\varnothing 12.5$	10 \varnothing	$\varnothing 27.2$	250	940	167	1107
	15 \varnothing				230	1170
	20 \varnothing				292	1232
CFRP $\varnothing 15.2$	10 \varnothing	$\varnothing 31.8$	350	993	194	1187
	15 \varnothing				270	1263
	20 \varnothing				346	1339



4.3.4 The method using CFRP in joint part

CFRP was set up in a joint with three different methods to find the most effective method, which can enhance the durability of the structure. Firstly, CFRP was used with the ordinary type, which was the straight type like in precast concrete slabs, and called S-type. Then, non-twisted CFRP type has been investigated and it divided two different types. First non-twisted CFRP type was put inside the tuft body by the polyurethane foam.

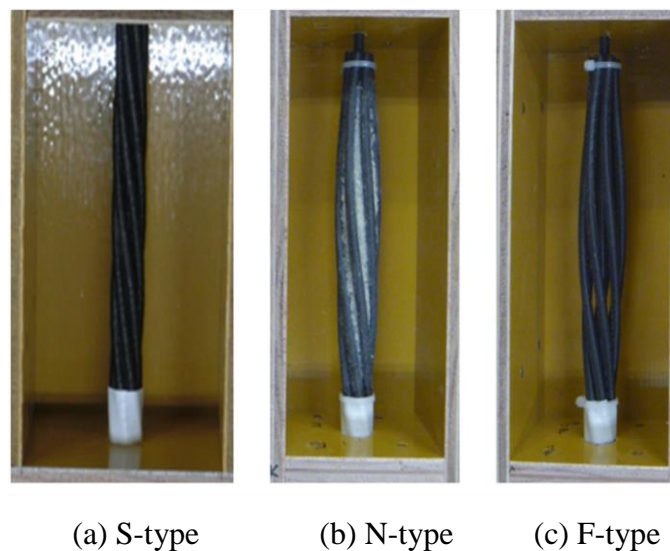


Figure 4.5 Three types of CFRP used at joint

Consequently, concrete cannot be completely filled and the diameter of the CFRP tuft body could be narrowed. It' name was N-type or no filling inside tuft body. Second non-twisted CFRP type, in which tuft body was freedom and concrete can filling inside, was called F-type or filling inside type. *Figure 4.5 (a), (b) and (c)* show three methods mentioned above. The detail of the set-up for specimens was shown in *Table 4.3*.

4.4 The first experiment

4.4.1 The set-up of experiment

In the first experiment, 18 specimens were designed with cross-section of concrete block of 75 mm x 75 mm (see in *Figure 4.4*) and the detail of specimens for experiment was shown in *Table 4.4*.

Table 4.4 List of specimen number

Diameter (mm)	Fixation length (mm)	The number of specimens				Total number of the first test	Total number of the second test
		S- type	N- type	F-type in first test	F-type in second test		
Ø12.5	125mm(10Ø)	1	1	1	2	3	4
	188mm(15Ø)	1	1	1	2	3	4
	250mm(20Ø)	1	1	1	2	3	4
	Total number of test	3	3	3	6	9	12
Ø15.2	152mm(10Ø)	1	1	1	2	3	4
	228mm(15Ø)	1	1	1	2	3	4
	304mm(20Ø)	1	1	1	2	3	4
	Total number of test	3	3	3	6	9	12

4.4.2 The result of the first experiment

Figure 4.6 shows the failure situation of specimens in the first experiment. Here, the name “12.5-10-S” means the CFRP diameter of 12.5 mm - the fixation length (10Ø) - method of using CFRP in the joint part was S-type. Most of the failure of the specimens

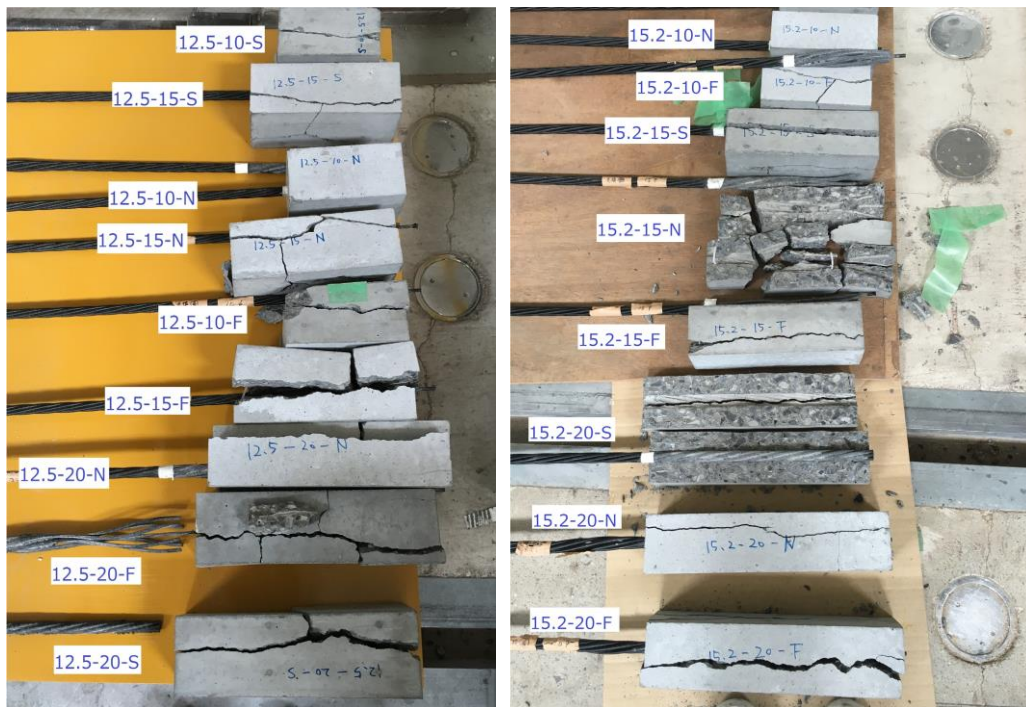


Figure 4.6 Situation of specimens after the first experiment

due to concrete splitting. Only the specimen of $\varnothing 15.2$ mm, 10 \varnothing and N-type pulled out and specimen $\varnothing 12.5$ -10 \varnothing -N was re-loading by setting miss. Therefore, it was impossible to judge which shape of CFRP in joint part has the stronger adhesive strength.

Figure 4.7, Figure 4.8, and Figure 4.9 show the relationship between load and displacement corresponding to two types of CFRP diameters, fixation lengths and CFRP types. The maximum load of all experimental cases of the experiment were smaller than

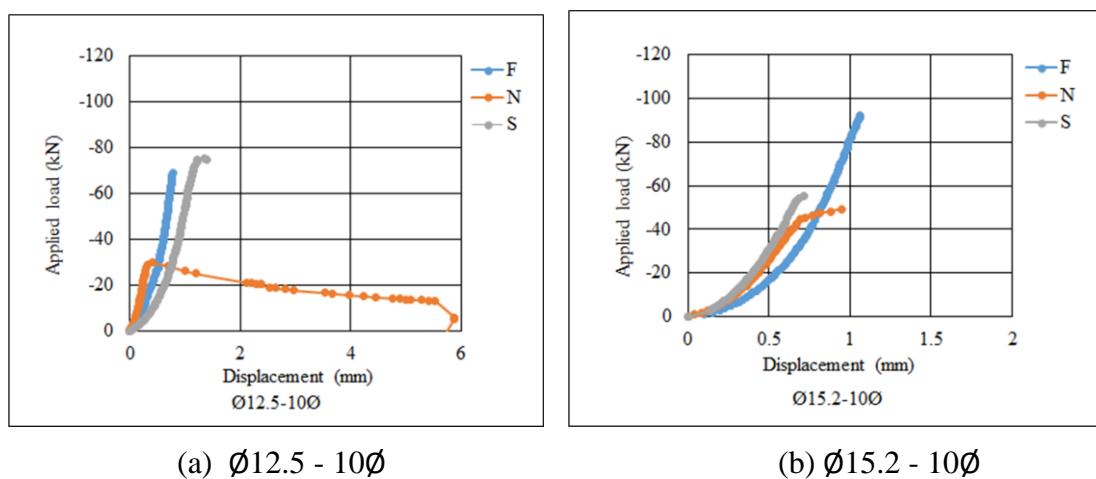


Figure 4.7 Relationship between load and displacement of 10 \varnothing group in the first experiment

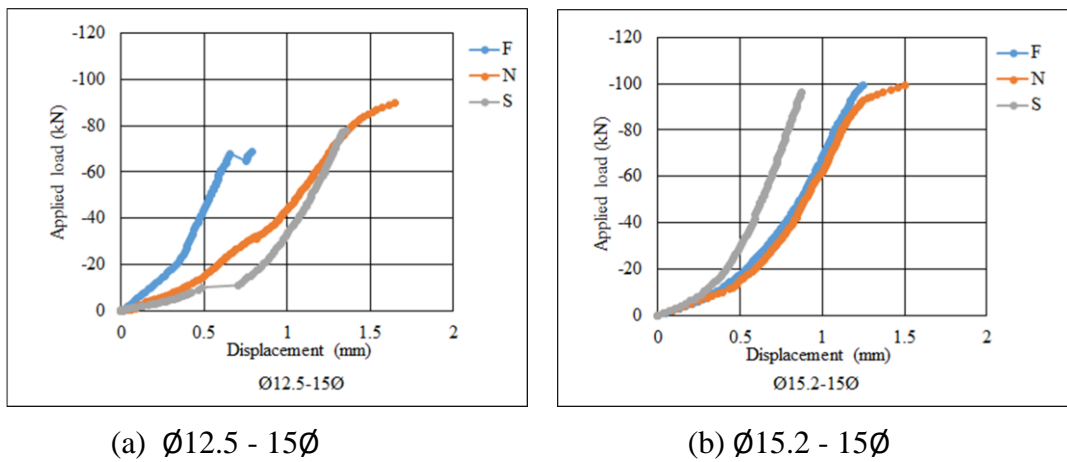


Figure 4.8 Relationship between load and displacement of 15Ø group in the first experiment

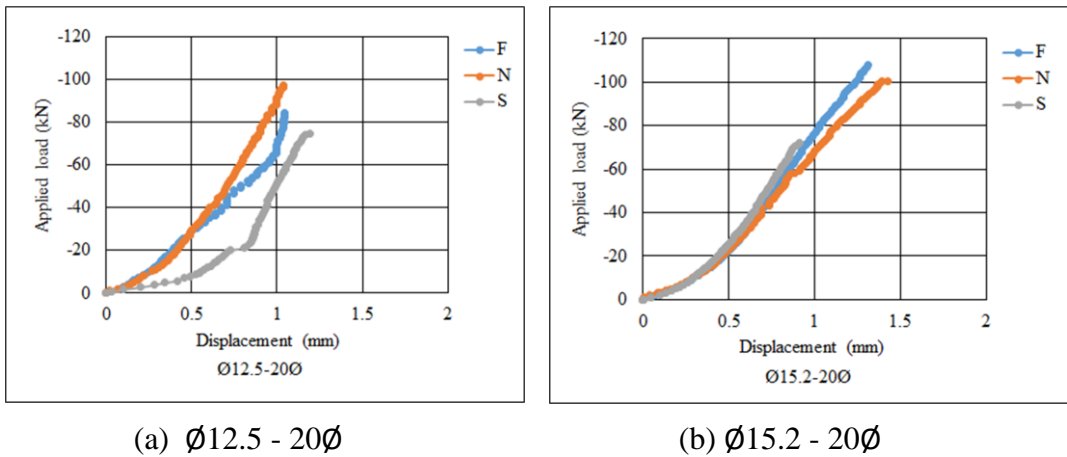


Figure 4.9 Relationship between load and displacement of 20Ø group in the first experiment

110kN. This value was significantly lower than the guaranteed capacity of CFRP with diameter 12.5 mm (184kN). It seems that concrete was damaged sooner than the pull-out of CFRP and the accurate of the adhesive strength could not be measured. From the results, it was judged the cross-section of concrete unsuitable for the purpose of the experiment.

4.5 The second experiment

4.5.1 The set-up of experiment

After the first experiment, the second series of experiment was conducted by considering the effect of the cross-section of concrete block to the bond-failure mode of

joint. In this series, the cross-section specimens was changed to 150mm x 150mm as shown in *Figure 4.4*. When CFRP reinforced for precast concrete slabs, concern regarding corrosion was limited, the concrete cover can be thinned. Therefore, this dimension was chosen for concrete block to expect the reduction of structural weight. It was expected that the specimens of F series could have the highest bond capacity so the number of specimens in the second test was two pieces (F1 and F2) for each diameter and each fixation length respectively to improve the accuracy of the data. (See *Table 4.4*)

4.5.2 The result of the second experiment

Figure 4.10 shows the situation of specimens after the second experiment was carried out and *Figure 4.11*, *Figure 4.12*, and *Figure 4.13* show the relationship between load and displacement of the experimental specimens. The failure mode of this series test in S-type and N-type was the pull-out mode of CFRP. In the series of F-type, the failure mode was concrete splitting.



(a) Group of 10Ø

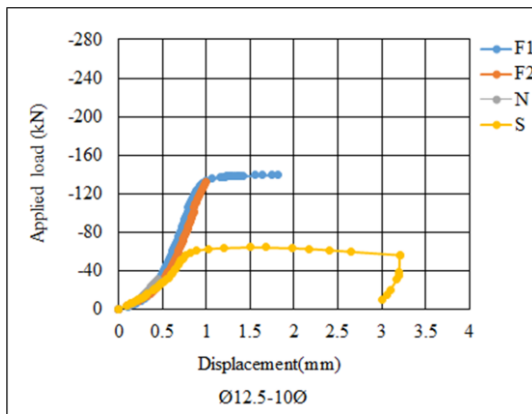


(b) Group of 15Ø

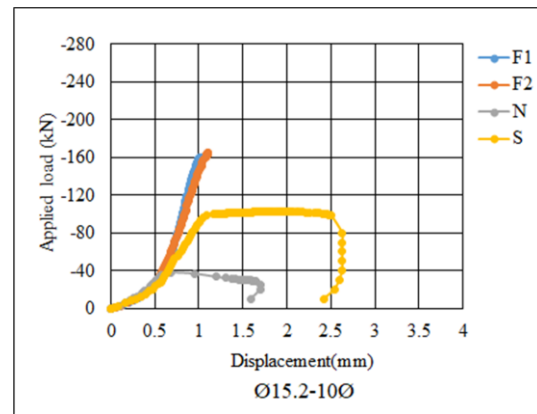


(c) Group of 20Ø

Figure 4.10 Situation of specimens after the second experiment

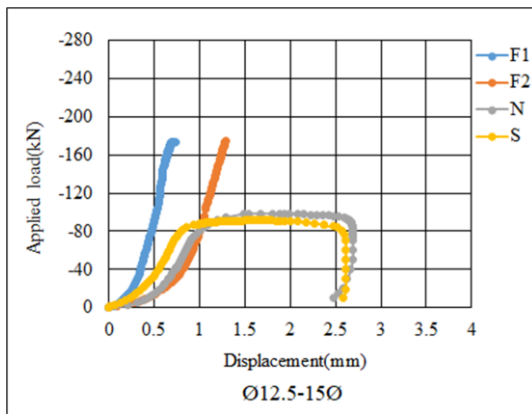


(a) Ø12.5 - 10Ø

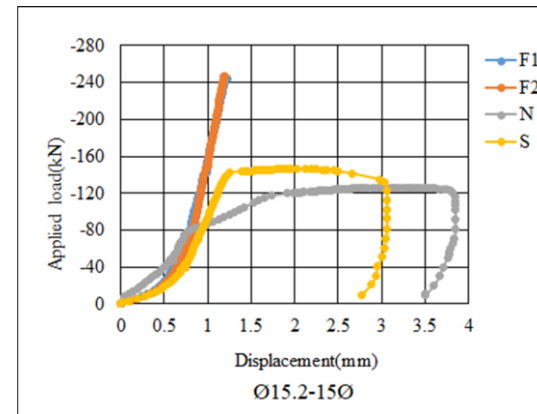


(b) Ø15.2 - 10Ø

Figure 4.11 Relationship between load and displacement of 10Ø group in the second experiment

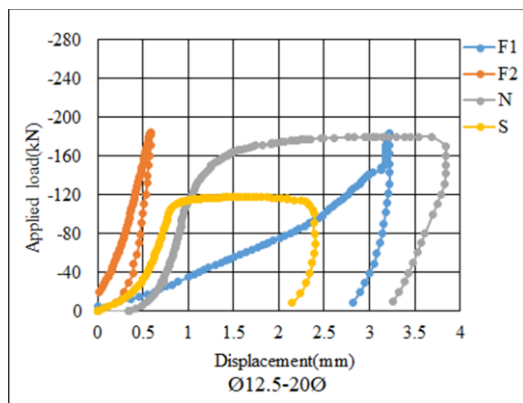


(a) Ø12.5 - 15Ø

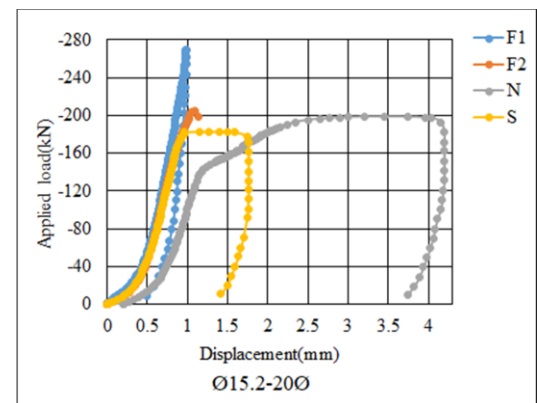


(b) Ø15.2 - 15Ø

Figure 4.12 Relationship between load and displacement of 15Ø group in the second experiment



(a) Ø12.5 - 20Ø



(b) Ø15.2 - 20Ø

Figure 4.13 Relationship between load and displacement of 20Ø group in the second experiment

Table 4.5 summarised the experimental results of the second experiment. Firstly, the results were evaluated between two groups of CFRP diameter. As shown in Figure 4.11, Figure 4.12, Figure 4.13, and Table 4.5, the diameter of CFRP in the specimens was larger, the pull-out load was higher. Secondly, the pull-out load was considered in specimens having different fixation length. Experimental results indicated that the fixation length increased, the pull-out load also increased accordingly. Finally, when the results were compared among three types of CFRP, F-type achieved the highest-maximum load in the group having the same diameter and fixation length as expected. In

Table 4.5 Summary of experimental results of the second experiment

STT	Name	Maximum load P_{max} (kN)	Maximum displacement d_{max} (mm)	Ratio of P_{max} to guaranteed break force	Ratio of P_{max} to P_{max} of straight type	Bond stress (N/mm ²)
1	Ø12.5-10Ø-S	64.3	1.508	35%	100%	13.10
2	Ø12.5-10Ø-N	30.6	0.458	17%	48%	6.23
3	Ø12.5-10Ø-F1	139.5	1.818	76%	217%	28.42
4	Ø12.5-10Ø-F2	134	1.032	73%	208%	27.30
5	Ø12.5-15Ø-S	91.5	1.708	50%	100%	12.39
6	Ø12.5-15Ø-N	98.1	1.942	53%	107%	13.29
7	Ø12.5-15Ø-F1	174.1	0.712	95%	190%	23.58
8	Ø12.5-15Ø-F2	174.9	1.288	95%	191%	23.69
9	Ø12.5-20Ø-S	118	1.756	64%	100%	12.02
10	Ø12.5-20Ø-N	98.1	3.684	53%	83%	9.99
11	Ø12.5-20Ø-F1	184.2	1.086	100%	156%	18.76
12	Ø12.5-20Ø-F2	184.8	0.582	100%	157%	18.82
13	Ø15.2-10Ø-S	102	1.998	38%	100%	14.05
14	Ø15.2-10Ø-N	38.1	0.686	14%	37%	5.25
15	Ø15.2-10Ø-F1	160.1	1.04	59%	157%	22.06
16	Ø15.2-10Ø-F2	165.3	1.108	61%	162%	22.77
17	Ø12.5-15Ø-S	146.6	2.032	54%	100%	13.46
18	Ø15.2-15Ø-N	126	3.2	47%	86%	11.57
19	Ø15.2-15Ø-F1	243.7	1.218	90%	166%	22.38
20	Ø15.2-15Ø-F2	247.1	1.194	92%	169%	22.70
21	Ø15.2-20Ø-S	182.8	1.148	68%	100%	12.59
22	Ø15.2-20Ø-N	198.7	3.452	74%	109%	13.69
23	Ø15.2-20Ø-F1	270	0.984	100%	148%	18.60
24	Ø15.2-20Ø-F2	204.7	1.092	76%	112%	14.10

F-type, the ratio of the maximum pull-out load to CFRP guaranteed break force reached from 60% to 76% in group having fixation length of 10ϕ and from 90% to 95% in the group having fixation length of 15ϕ . Regarding the group having fixation length of 20ϕ of F-type, this number was over 100% in three specimens.

On the other hand, it was necessary to concern the ($\phi 15.2$ - 20ϕ -F2) specimen, which was destroyed due to the concrete splitting at 204.7 kN. This value was lower than the guaranteed break force of CFRP. The status of specimens after the test was shown in *Figure 4.14*, some reasons were given to discuss and explain for this phenomenon. Final, the third experiment was planned to consider two factors including the length of the tuft body in the fixation length and the effect of the presence or absence of filling material inside the tuft body.



Figure 4.14 Specimen of ($\phi 15.2$ - 20ϕ -F2) after test

4.5.3 Bond stress

To investigate and evaluate the influence of some factors on the bond stress, this section was added to study based on the results of the second experiment.

The bond stress was generally calculated by the following equation and the results shown in *Table 4.5* and *Figure 4.15*.

$$\tau = \frac{F}{\pi \phi L} \quad (4.1)$$

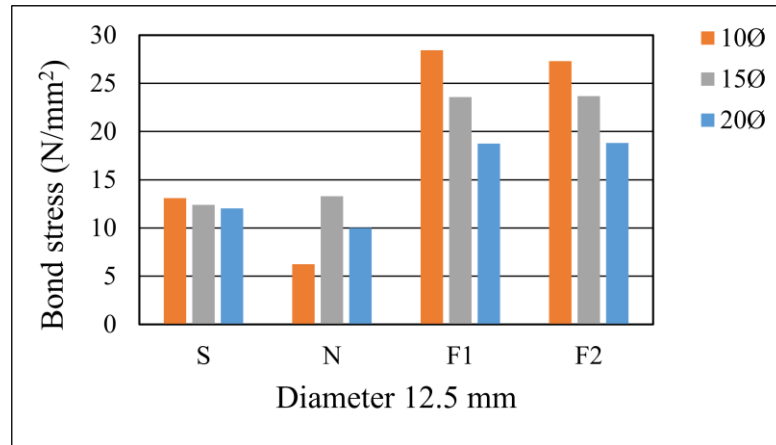
where,

τ is average bond stress (MPa),

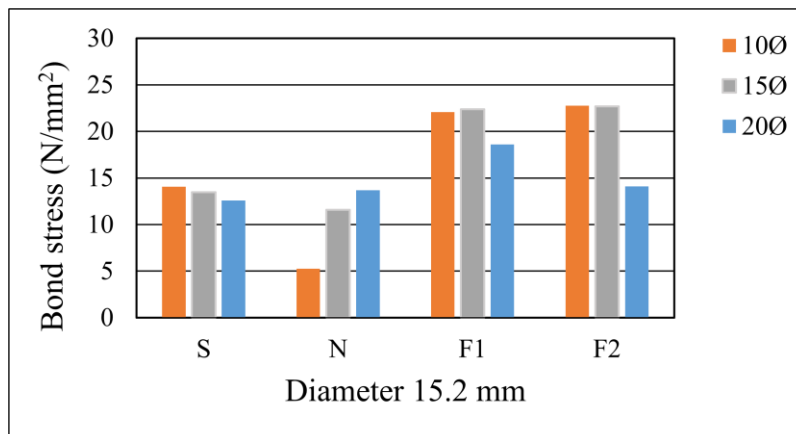
F is pull-out load (N),

\emptyset is CFRP diameter (m),

L is the fixation length (m)



(a) Group of Ø 12.5 mm



(b) Group of Ø 15.2 mm

Figure 4.15 Bond stress of specimens in the second experiment

4.5.3.1 The effect of diameter of CFRP strand

In previous studies, average bond stress between concrete and FRP decreases when the diameter of rebar increases. Several reasons are considered. The bleeding of the water in the concrete would be made contact force between concrete and FRP bar lower [7]. The fixation length requires longer suiting with larger diameter but greater fixation length reduces the bond strength. Sometimes, the Poisson ratio and shear stiffness are also influencing factors [8].

The results of the second experiment from *Figure 4.15 (a) and (b)* indicates that the average bond stress in the group of F-type decreased while the diameter of CFRP was changed from 12.5 mm to the 15.2 mm. The bond stress of specimens in the group of S-type different slightly between two diameters. In the case of N-type, the specimens gave an unclear result, in which 2/3 specimens were close and 1/3 specimens were not close with the results of F-type.

4.5.3.2 The effect of CFRP fixation length

The fixation length plays an important role in bond stress of FRP bar and concrete. The bond stress reduces when fixation length rises [6], [7]. The results of the specimens using CFRP with S-type and F-type in the same diameter group agreed with the previous studies. In contrast to those, the specimens of N-type also gave an unclear result, which the higher bond stress was indicated in the case longer fixation length.

4.5.3.3 The effect of method using CFRP strand in joint part

The outer surface has a remarkable influence on bond stress when the failures did not occur in the concrete. Some authors had worked with the straight outer surface (S-type). In 1989, it was reported that the bond stress of experiment with CFRP having a diameter of 12.5 mm and concrete strength 47.6 MPa was 7.23MPa [10]. This value was 9.5 MPa and 13 MPa in the research of Tepfers in 1992 corresponding to 12.5 mm in CFRP diameter, 47.3 MPa and 44.4 MPa of concrete strength, respectively [11]. Likewise, the bond stress of S-type in this study fluctuated from 12.02 MPa to 14.05 MPa depending on CFRP diameter and the fixation length. It is not much different in the bond stress between two groups namely S-type and N-type. However, the method using CFRP with F-type, the bond stress was high. The values of bond stress in F-type were nearly two-fold that of S-type. Although the failure mode of F-type was split and fractured, the accuracy of bond strength was not obtained this time, but the bond strength still exceeded 20 N/mm².

4.6 The third experiment

4.6.1 The set-up of experiment

Based on the consideration the results of the second experiment, an additional test-the third experiment was conducted to focus on the F-type in order to pursue a more

efficient shape in term of function and cost. In addition, the experiment also investigated the influence of the length of the tuft body and the method to fill inside the tuft body of CFRP on the adhesive strength.

To focus on F-type and consider the efficiency, the diameter of 15.2 mm, the fixation length of 15 ϕ and cross-section size of 150 mm x 150 mm were selected for the specimens in this experiment. Three lengths of tuft body in the fixation length (9 ϕ , 10 ϕ , and 11 ϕ) were investigated, they were shown in *Figure 4.16*. In addition, F-type in this experiment was divided into two types. Fa-type was the non-twisted type but the tuft body was freedom and concrete can filling inside as mentioned in the second experiment. Incidentally, Fb-type used the polymer cement mortar to fill inside the tuft body (see in *Figure 4.17*).

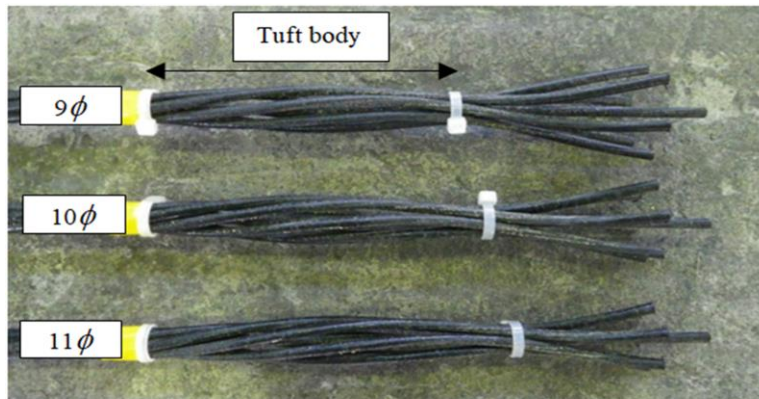


Figure 4.16 Three lengths of tuft body

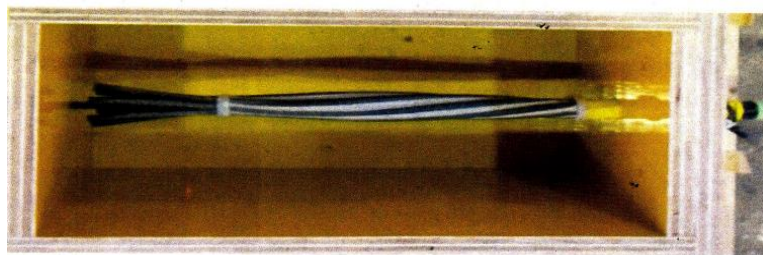


Figure 4.17 Polymer cement mortar filled inside tuft body (Fb-type)

4.6.2 The result of the third experiment

Table 4.6 Summary of experimental results of the third experiment

STT	Name	Maximum load P_{max} (kN)	Maximum displacement d_{max} (mm)	Ratio of P_{max} to guaranteed break force	Bond stress (N/mm ²)
1	Ø15.2-15Ø-9Ø-Fa1	216.1	0.016	80%	19.9
2	Ø15.2-15Ø-9Ø-Fa2	209	0.01	77%	19.2
3	Ø15.2-15Ø-9Ø-Fa3	202.8	0.01	75%	18.6
4	Ø15.2-15Ø-9Ø-Fb1	218	0.492	81%	20.0
5	Ø15.2-15Ø-9Ø-Fb2	216.1	1.018	80%	19.9
6	Ø15.2-15Ø-9Ø-Fb3	217.9	0.212	81%	20.0
7	Ø15.2-15Ø-10Ø-Fa1	221.7	0.026	82%	20.4
8	Ø15.2-15Ø-10Ø-Fa2	196.2	0.018	73%	18.0
9	Ø15.2-15Ø-10Ø-Fa3	208.3	0.026	77%	19.1
10	Ø15.2-15Ø-10Ø-Fb1	213.9	0.186	79%	19.7
11	Ø15.2-15Ø-10Ø-Fb2	152.8	0.018	57%	14.0
12	Ø15.2-15Ø-10Ø-Fb3	218.1	0.182	81%	20.0
13	Ø15.2-15Ø-11Ø-Fa1	205	0.002	76%	18.8
14	Ø15.2-15Ø-11Ø-Fa2	235.4	0.006	87%	21.6
15	Ø15.2-15Ø-11Ø-Fa3	197.6	0.024	73%	18.2
16	Ø15.2-15Ø-11Ø-Fb1	197.4	0.1	73%	18.1
17	Ø15.2-15Ø-11Ø-Fb2	203.5	0.244	75%	18.7
18	Ø15.2-15Ø-11Ø-Fb3	192.4	0.214	71%	17.7

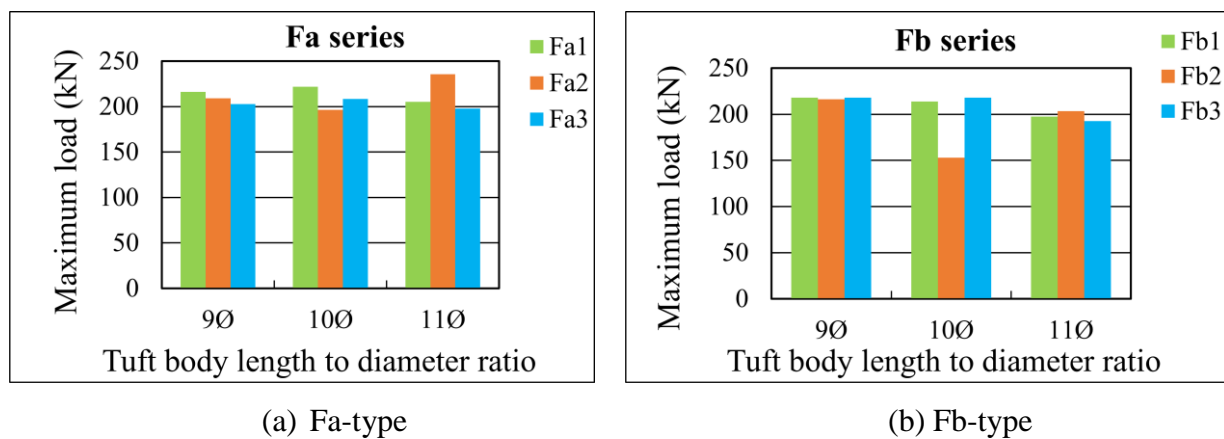


Figure 4.18 The relationship between the pull-out load and the length of tuft body corresponding with Fa-type and Fb-type

The results of 18 specimens after the third experiments are shown in *Table 4.6*, *Figure 4.18 (a)* and *(b)*. The variation of the pull-out load among specimens was slight, the average value stands roughly 210 kN. In addition, the bond stress of specimens also calculated following the *Equation (4.1)* and added in *Table 4.6*. The difference in the values of bond stress is small; it is around 20 N/mm². It seems that the pull-out load and bond stress did not depend on the length of the tuft body in this study.

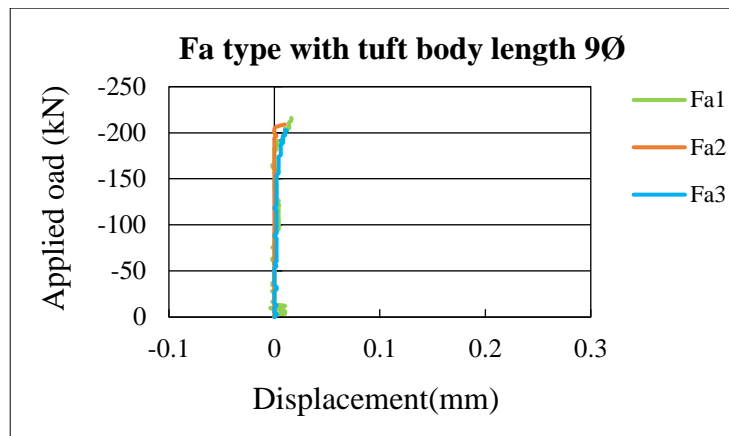
However, the group having the tuft body length of 10Ø in Fb-type had a significant difference. The second specimen in this group achieved the pull-out load at 152.8 kN. This value was to differ from two values in the same group. This consequence may come from the quality of filling inside the tuft body. Polymer cement mortar was remained with a large amount in the second specimen, whereas only a small amount was found in other specimens (see *Figure 4.19*). It may be the part of polymer cement mortar did not break because the contact surface between polymer cement mortar, CFRP and concrete was not good.



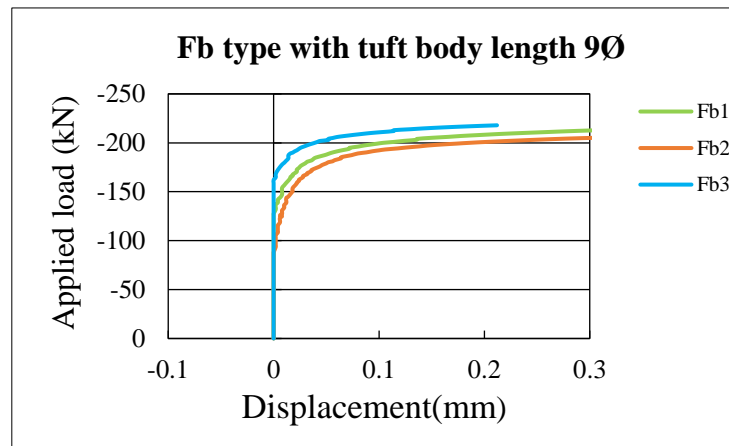
Figure 4.19 Three lengths of tuft body

Figure 4.20 shows the relationship between the pull-out load and the length of tuft body corresponding with Fa-type and Fb-type. These figures show that the applied load did not have a significant difference between two types but the displacement of Fb-type at the failure time is larger than that of Fa-type. It seems that the polymer cement mortar in the tuft body of the CFRP broken slowly and made the pull-out process slower. This phenomenon may be due to the tuft body pre-filled with cement mortar, which was more certain and the tuft body's stiffness was also higher than in the case filling by concrete. Therefore, the adhesion between the surface of the concrete and the CFRP strand in the joint was better. Furthermore, the stiffness of tuft body pre-filled with

cement mortar was reduced by the shrinkage of CFRP so this method made the pull-out of CFRP strand slowly.



(a) Fa-type



(b) Fb-type

Figure 4.20 The relationship between the pull-out load and displacement corresponding with Fa-type and Fb-type

4.7 Conclusions

From the above results and discussions, the conclusions are summarized as follows.

(1) The outcome of the method using three types of CFRP in joint part was shown. As expected, the method using F-type (filling inside tuft body) was provided the highest pull-out load and the highest bond stress among three types of CFRP at joint with the same conditions. In the second experiment, the applied load of specimens having fixation length of 20Ø in F series reached the value which higher than ultimate load of CFRP

standard. From these results, it is necessary to study with more investment for the method using F-type for joint part in design, manufacture, and application.

(2) F-type achieved the highest pull-out load and bond strength in comparing with N-type and S-type. When the specimen using CFRP with diameter 15.2 mm, the pull-out load achieved the higher value than that using CFRP with diameter 12.5 mm. The force in the case using the fixation length of 20Ø was the highest among three types of the fixation length. Therefore, the specimen of F-type, Ø15.2 mm, and 20Ø would be a great combination for the actual bridge. However, after considering the ultimate load, bond strength, the ratio of ultimate load to the breaking force of CFRP, and the fixation length; the method using CFRP with a diameter of 15.2 mm, the fixation length of 15Ø, and F-type (filling inside tuft body) was proposed to apply in the precast concrete slabs

(3) One of the purposes of the experiment was to clarify the minimum possible width of the joint. It was confirmed that when slabs using CFRP with the diameter of 15.2 mm, the fixation length of CFRP in joint of 15Ø and F-type was selected, the joint width was improved. Furthermore, the weight of slabs reduced significantly.

(4) From the result of the series in third test, no remarkable change was observed in the bond capacity with whatever the length of the tuft body. However, the bond capacity may be depended on the method and material to fill in the tuft body of CFRP, which should be considered more.

4.8 References

- [1] M. A. Erki and S. Rizkalla, "FRP Reinforcement For Concrete Structures," *ACI Concr. Int.*, vol. 15 (6), pp. 48–53, 1993.
- [2] T. Enomoto, "Use of CFCC Tendons and Reinforcements in concrete structures for durability," in *APFIS 2012, Hokkaido University, Japan*, 2012.
- [3] K. Charieson, R. Hutchinson, A. Abdelrahman, and S. Rizkuaa, "Full scale testing of a bridge deck slab reinforced with CFRP," in *the International Conference on Rehabilitation and Development of Lebanon*, p. June 1997.
- [4] T. Hassan, A. Abdelrahman, G. Tadros, and S. Rizkalla, "Fibre reinforced polymer reinforcing bars for bridge decks," *Can. J. Civ. Eng.*, vol. 27, no. 5, pp. 839–849, 2000.
- [5] M. Honma, T. Maruyama, T. Enomoto, and H. Shima, "Experimental research on

- CFCC adhesion: stress-slip relationship,” *Proc. Japan Concr. Inst.*, pp. 823–826, 1991 (Japanese).
- [6] A. Zenon and P. Kypros, “Bond behavior of FRP Bars under direct pullout conditions,” vol. 8, pp. 173–181, 2004.
- [7] B. Tighiouart, B. Benmokrane, and D. Gao, “Investigation of bond in concrete member with fibre reinforced polymer (FRP) bars,” *Constr. Build. Mater.*, vol. 12, no. 8, pp. 453–462, Dec. 1998.

Chapter 5. Conclusion and Recommendations

5.1 Introduction

Among difference approaches developed to enhance strength, durability and serviceability of bridge structures, against the corrosion phenomenon of steel reinforcement, especially those structures located in aggressive environments, using CFRP reinforcement as an alternative method to conventional steel has shown efficient and durable construction regarding cost, technical, serviceable life and long-term performance. With the purpose of contributing more evidence of the effectiveness to develop this method, this study focused on the experiments and numerical simulation for using CFRP in the girder and precast concrete slabs. Specifically, the girder using CFRP tendon, which have been subjected in this study, has been exposed for nearly 30 years in the corrosion environment. This girder was placed next to the main girders of Shinmiya Bridge – the first bridge in Japan and the world using CFRP tendons in the main girders against the steel corrosion.

This chapter presents a summary of this study; conclusions based on the results of the experiments, analyses, and give the recommendation for future works. The first section will summarize the works that have been done in this study. The second section shows the conclusions, the significant findings and observations that can be made based on this research. The last section will give some recommendations for future research.

5.2 Summary

One prestressed concrete girder using CFRP tendon was fabricated with a full-scale in 1989 and placed next to the main girders of Shinmiya Bridge in the mountainside in Hakusan, Ishikawa, Japan. This girder has I-shaped cross-section. The length of the girder was 6060 mm whereas the height, the width of the upper flange and width of lower flange were 325 mm, 200 mm, and 320 mm respectively. The girder was reinforced with eight CFRP tendons with $\varnothing 12.5$ mm and seven strands, in which six CFRPs was used for the tensile zone and two CFRPs located in the compression zone. Epoxy coated rebar of

D6 was set up for stirrups and the compressive strength of 59.8 N/mm^2 was recorded from 1988 for concrete. In October in 2017, this girder was brought to the structural laboratory of Kanazawa University to evaluate the quality, durability and serviceability of this girder as well as CFRP tendons after nearly 30 years exposed in the corrosion environment. A series of experiments were performed on this girder. First, the effective stress was estimated using the stress release technique with a core incision, and the obtained value was compared with the design value. Next, a loading test was carried out on the girder; the load-bearing capacity, the relationship between applied load and displacement, failure model, strain distribution and crack pattern were considered and evaluated. The transfer length of the prestressed girder, which obtained by recording a relationship between strains on the concrete girder surface versus the distance to the end of the girder before and after cutting the upper and lower flanges, was examined by using half of the girder after the flexural experiment. On the other half of the girder, the concrete cores were collected, the compressive strength test was conducted and salt content was measured. Finally, the mechanical and chemical characteristics of the CFRP removed from the main girder were determined.

To deep understand the flexural of the behavior of the prestressed concrete girder using CFRP tendons in the loading test, the three-dimensional model was developed by the finite element method based on the result of the investigation mentioned above. First, the model was built in LS-DYNA software. The accuracy of the model was evaluated by comparing the analysis result and experimental result including the load-bearing capacity, the relationship between applied load and displacement, and crack pattern. Then, a parametric study considered the loss of prestress force and the decrease of the compressive concrete strength to the change of structural behavior. The second approach is to build the model by the commercial finite element software, DIANA. The method, which creased directly the prestress force, and load control were used in this model to surmise the behavior of a prestressed concrete girder using the CFRP tendons. Moreover, parametric studies were conducted with the following objectives: To investigate the influence of the input data from the results of the CFRP tensile test and concrete compressive test on the results on the accuracy of the simulation; to determine the change in structural behavior with the modification of the material properties; and finally to study the model with or without the bond-slip model for contact between the CFRP and concrete.

The final work of this study is conducted three series of fundamental pull-out test. The aim of this work is to investigate the method for using CFRP in the cast-in-place joint of precast concrete slabs reinforced by CFRP to enhance the durability and reducing the width of the joint as short as possible. Sixty specimens were fabricated with the difference in the setup. Two diameters of CFRP were selected including $\varnothing 12.5$ mm and $\varnothing 15.2$ mm. Three types of fixation length were chosen in the relationship with CFRP diameter namely 10 \varnothing , 15 \varnothing , and 20 \varnothing . In addition, straight type (S-type), no filling inside tuft body in non-twisted type (N-type) and filling inside tuft body in non-twisted type (F-type) also known as three methods using CFRP in joint. Furthermore, to study the effect of the method filling inside tuft body to the adhesive strength, F-type divided into two group types. Fa-type having tuft body was freedom and concrete can filling inside and Fb-type used the polymer cement mortar to fill inside the tuft body.

5.3 Conclusions and Observations

Based on the results of the experimental and analytical investigation of the structures reinforced by CFRP, the main findings can be made follows.

For investigation by experiments conducted on the girder using CFRP tendons exposed in the corrosive environment for nearly 30 years

- (1) The effective stress of the prestressed concrete girder was estimated by the release of the working stress and measuring the strain. The results of the test confirmed that there was no significant difference between the effective stress in this study and the design value.
- (2) The load-carrying capacity of the girder using CFRP tendons exposed in the corrosive environment for nearly 30 years was confirmed after the loading test. The relationship between applied load and displacement in this study was almost overlapped with the result obtained from the girder conducted in 1994. Although the ultimate load in this study was approximately 6% lower than that at six years after construction (1994), this value exceeded the design value at the time of construction and it was judged that the load-carrying capacity of the girder has been still in good condition.
- (3) The transfer length of the specimen obtained in this test was the same with the results in this test conducted six years after the original construction. It was

determined to be 500 mm, which was smaller than 65 ϕ . It was confirmed that the transfer length and the bond between CFRPs and concrete did not change.

(4) The chloride ion concentration in the bottom flange of the girder was higher than that in the side surface. The chloride ion concentration at the position of the stirrup rebar (reinforcement cover was 27.5 mm) was estimated to be approximately 6.0 kg/m³ based on the analysis results of the salt content in the core collected from the lower surface of the main girder. This value largely exceeded the corrosion occurrence limit of steel of 1.2 kg/m³.

(5) The compressive strength of concrete from the test samples collected on the girder was 75.1 N/mm², this value was higher than the value recorded in 1988(59.8 N/mm²).

(6) CFRP was removed from the girder and subjected for the tensile test, the rupture load was compared with to the previous results and residual tension load capacity was confirmed. The elastic modulus of CFRP decreased by approximately 7% in comparing with the value in 1994.

(7) According to the FE-SEM observations of the CFRP tendons, there was no position where the coatings and carbon fibers themselves seemed to be deteriorated,. It was confirmed that there was no problem in the CFRP surface and carbon fiber surface. In addition, from the FT-IR analysis results, no significant change, such as the disappearance of the main peak or appearance of a new peak, could be confirmed. Therefore, it was considered that deterioration caused by chemical structural change did not occur.

For investigation by numerical analysis on flexural behavior of the girder using CFRP tendons

(1) The good agreement between the numerical result and experimental result was proposed a three dimensional model of the girder using CFRP tendons in commercial software such as LS-DYNA and DIANA. This model can be help to observe clearly the complex behavior and failure mode of the girder.

(2) The parametric study shows that the load-bearing capacity will reduce when the loss of pre-stressing loss or reducing of compressive strength of concrete occurs. However, the decrease of the load-carrying capacity of the girder in case of pre-stressing

loss was higher than that in case of reducing of compressive strength of concrete in the same rate.

(3) The location of the samples selected for fundamental tests such as tensile test and compressive concrete strength was important for the simulation, which provided the characteristics of main materials, and affects the accuracy of the numerical results. These parameters were input data for the software to predict the behavior of structure so that any change in the property of material will lead to differences in the behavior of the girder. In addition, the model that considered bond-slip mode for the contact between concrete and steel shows a slight difference with the result obtained from the perfect bond model.

For investigation by fundamental full-out test on joints of precast concrete slabs in bridges reinforced by CFRP

(1) The method using F-type (filling inside tuft body) was provided the highest pull-out load and the highest bond stress among three types of CFRP at joint with the same conditions. Some specimens of F series reached a higher value than the ultimate load of CFRP standard.

(2) The method using CFRP with a diameter of 15.2 mm, the fixation length of 15ϕ , and F-type (filling inside tuft body) was proposed to apply in the precast concrete slabs and the cast-in-place joint in real to enhance the durability and shortest the width of joint.

(3) This method needs to pay attention with the material and the method filling inside tuft body.

5.4 Recommendations for future work

For future work, the author wants to be done to develop the model for fundamental pull-out test between concrete and the straight type (S-type) mentioned in Chapter 4 by the finite element method. To investigate the bond-slip model for contact between concrete and CFRP, stirrups in this pull-out experiment via LS-DYNA software.

The second step, the author wants to use the bond-slip model that get the good agreement in the first step to applying for the three-dimensional model of the prestressed concrete girder using CFRP tendons mentioned in Chapter 3. Then, to evaluate the difference between two bond model including perfect bond and bond-slip.

In addition, based on published design guides, codes and specifications for FRP reinforcing bars and tendons, the bending moment under ultimate load will be calculate and compare with experimental results and analysis results.

Further work is recommended to investigate the loading test and fatigue test on the full-scale of precast concrete slabs that use the proposed method for joint in Chapter 4.

ACKNOWLEDGEMENTS

The author wishes to thank people who directly or not directly contributed to this dissertation. First, I would like to express my most sincere gratitude appreciation from the bottom of my heart to my supervisor, Professor Hiroshi MASUYA of Faculty of Geosciences and Civil Engineering. The professor has given dedicated guidance, spent a lot of time to do research with me, shared his knowledge, and given motivation for me during my graduate studying time in Kanazawa University. Furthermore, my family has received the great support from Professor Hiroshi MASUYA and his wife from the first days coming to Japan. With his invaluable advice and his encouragement, I overcame obstacles, reached the outcome of a doctoral course and finished my dissertation. I always remember the first letter of him to give me an opportunity to become a student in Structural Lab. Thank you very much, my sensei!

Second, I would like to send my special thanks to Professor Saiji FUKADA, who believed me, given me a chance to join a project of CFRP. The advice, suggestion and support of him are essential to achieve the results of my research.

Third, I also would like to thank the Ministry of Education and Training-Vietnam International Education Development for a full doctoral scholarship (Vietnamese Government Scholarship –VIED) and ThuyLoi University for the permission to continue my doctoral study.

Next, I am very grateful for all Cooperation Company and the Structural Laboratory members, present and past members, for helping me during study and experiment. Especially, Mr Ha Minh Tuan for the co-operation, discussion and advice in my publications; Mr Takafumi Yamaguchi, Mr Tran Le Hoang Trung, Mr Nguyen The Duc, Mr Masayuki Kadodera for working together during specimen preparation and testing.

Then, I wish to express my thanks to Ms Ihara-the secretary of Structural Lab and Ms Katayama-the secretary SIP Project for their support in administrative matters.

In addition, I want to thank the Vietnamese friends in Kanazawa-who give me the nice memories in the life in Kanazawa besides study, and the friends in Vietnam-who given me the encouragement.

Final, I am sincerely grateful to my family. My husband–the most wonderful husband. He gave up his work in Vietnam to study with me in Japan. He has always been with me, encouraging me when I had difficulties in the study, sharing the work of taking care of our daughter as well as housework. My daughter, my father, my mother, my father in law, my mother in law, my younger sister and my younger brother who always support me unconditionally.

Thank you very much!